Understanding and Measurement of Secondary Nucleation

Andrew Cashmore

Department of Chemical and Process Engineering

Thesis submitted to the Department of Chemical and Process Engineering at the University of Strathclyde in accordance with the requirements for the degree of Doctor of Philosophy.

August 2022

Declarations

This thesis is the result of the author's original research. It has been composed by the author and has not been previously submitted for examination which has led to the award of a degree.

Signed:

Date:

Abstract

Secondary nucleation is widely present in crystallisation processes, and it is often relied upon to attain desirable critical quality attributes of crystalline products, such as polymorphic form and crystal size distribution. This is particularly the case in continuous crystallisation, where secondary nucleation can be crucial to achieve and maintain steady state operation, and by relying on secondary nuclei, the stochasticity and hence inherent lack of control in primary nucleation is avoided. However, fundamental understanding of secondary nucleation is limited and its quantification and scale up remains elusive.

Solubility is the most important physical property in crystallisation as it is needed for the selection of the required supersaturation, the driving force for nucleation and growth. However, obtaining accurate solubility values, especially at higher concentrations and temperatures is not a simple task. A critical evaluation of three experimental techniques for determination of the solubility of glycine in water is presented, aiming to provide more accurate solubilities of α-glycine at elevated temperatures.

A rapid, small-scale workflow was developed utilising agitated vials, combined with in-situ imaging for crystal counting and sizing. The induction time distributions, crystal size distributions and number densities are used to quantify primary and secondary nucleation and crystal growth kinetics of α-glycine across a range of supersaturations in aqueous solutions under isothermal conditions. Both seeded and unseeded crystallisation experiments were conducted and a classification system for the crystallisation behaviour

was presented. Using this approach some fundamental insights into relationships between crystal growth, primary and secondary nucleation behaviour have been extracted.

A Couette flow cell was developed with in-line imaging enabling the quantification of nucleation and crystal growth kinetics under laminar fluid shear across a range of shear rates and supersaturations. The results indicated that laminar fluid shear alone can induce secondary nucleation at shear rates relevant for both laboratory and industrial scale stirred tanks.

This work aims to improve the fundamental understanding and quantification of secondary nucleation and introduce new approaches to assess and quantify nucleation and growth kinetics using small amounts of materials. It is hoped that this will facilitate more efficient development, design, and optimisation of crystallisation processes.

Acknowledgements

I would like to begin by thanking my three supervisors, Prof. Jan Sefcik, Dr. Mark Haw, and Dr. Mei Lee for their endless support and guidance throughout this project. I would also like to thank everyone in the EPSRC CMAC Future Manufacturing Research Hub for allowing me to use the incredible facilities, for the informal chats, encouragement, help and advice.

I would like to thank the team at GlaxoSmithKline for the hospitality during the time I spent working on site and offering valuable advice.

Finally, I would like to thank my family and friends for their unending support, encouragement, and motivation before and during this PhD project. Thank you.

Table of Contents

Chapter. 2. Materials and Methods

Chapter. 3. An Experimental Evaluation of α-glycine Solubility Using Multiple Experimental Techniques

Chapter. 6. Conclusions and Future Work

List of Figures

List of Tables

Chapter. 1. Introduction and Background

An Introduction to Industrial Crystallisation

Crystallisation defines the phase transformation from a liquid or gas state to a crystalline solid state[1]. Often, it is described as a highly efficient separation[2] and purification process[3] which is employed in the manufacture of chemical and pharmaceutical ingredients to achieve certain desired properties including, solid form, purity, particle size distribution and shape. As most pharmaceutical and chemical products must conform to tight regulatory guidelines in relation to the crystalline properties, selecting the 'correct' conditions for a process is essential to achieve a desired, quality product.

Unfortunately, despite decades of research there still seems to be a genuine, lack of understanding in regard to the fundamental mechanisms taking place in industrial crystallisation[4]. Recent developments in process analytical technology, small-scale specialised equipment and computational modelling provide a remarkable opportunity to unravel these phenomena. Only with an understanding of the complex relationships between different mechanisms such as primary and secondary nucleation, crystal growth and agglomeration can a process be designed and operated in a thoroughly controlled manner.

With conscious implementation of sustainability and waste reduction targets being employed across many industries, the chemical and pharmaceutical industry is shifting towards continuous manufacturing in an attempt to boost efficiency and lower costs[5]. Traditionally, the primary method for the manufacture of crystalline APIs would be in stirred tank reactors (STR's) under batch operation, but from a product perspective, it is thought that continuous

manufacturing, for example using continuous STRs, can reduce batch to batch variability and enhance the product quality. Secondary nucleation and/or external seeding is crucial, as it controls desired solid form and crystal size and enables steady state operation of continuous STRs. Therefore, understanding of secondary nucleation remains essential in the move from traditional batch to more sustainable and economical continuous manufacturing processes.

The primary aim of this thesis was to develop a fundamental understanding of secondary nucleation by constructing experiments and tools which enable the quantification of kinetics and assessment of the mechanisms under well controlled conditions. Secondary nucleation is a key mechanism in industrial crystallisation and this work should enable more facile development of crystallisation processes paving the way for greater control of the final crystalline properties.

1.1 Background

This chapter aims to outline the challenges which have been identified following a review of the literature, beginning with an introduction to the fundamentals of crystallisation including an overview of the standard terminology.

1.2 Solubility, Supersaturation, and the Metastable Zone

1.2.1 Solubility

Solubility may be defined as the point when solid-liquid equilibrium is reached following addition of solute to solvent. As a solute is added to a solvent, the chemical potential of the system is adjusted from its balanced state, and it then aims to regain that balance by allowing dissolution of a limited amount of solid (solute) until the point in which equilibrium is reached. The point at which this occurs is known as the solubility or saturation concentration and is a thermodynamic property dependent on temperature and pressure.

In the design of robust crystallisation processes, solubility is one of the most important parameters which must be determined to calculate accurate supersaturation (1.2.2), the driving force for nucleation and crystal growth. Therefore, if the solubility recorded is incorrect, the kinetics of crystallisation will be impacted potentially affecting the crystal size distribution. Decisions must therefore be made on the application of an appropriate technique in relation to consumption of material, time available, polymorphic form and precision of the technique[6].

Although one would assume that measuring solubility is a straightforward task, a review of the literature will highlight some significant questions. Here, in Figure 1.1. the glycine in water system is presented with some selected literature values. There is a considerable variation presented for the same system and it is clear that accurate solubility cannot be obtained from previously published literature data. As the temperature is increased it seems that the challenges only grow.

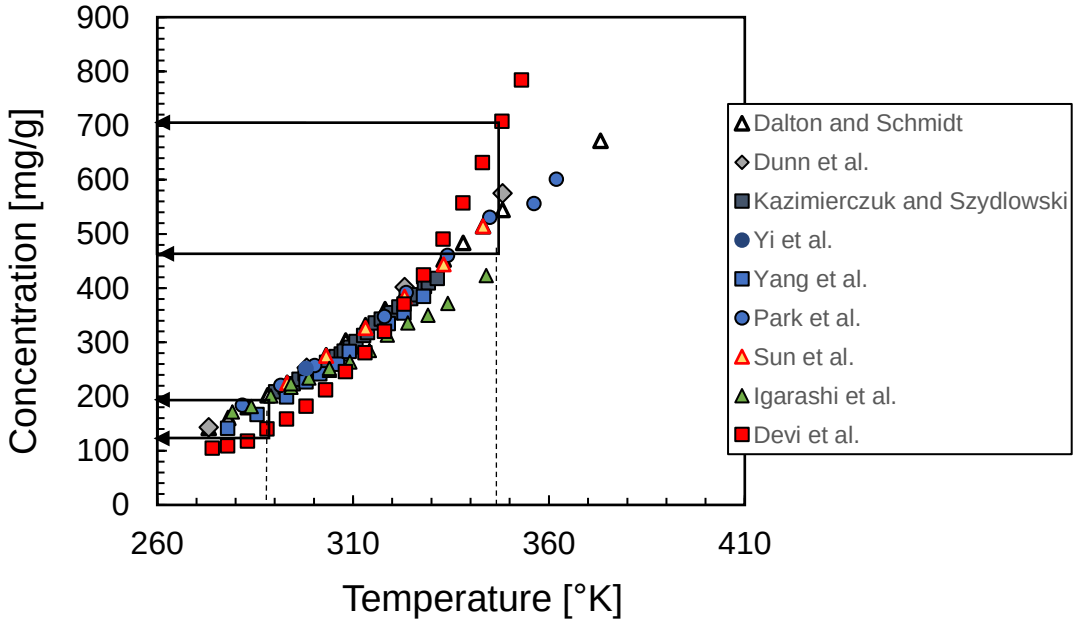

Figure. 1.1. A number of literature values for the solubility of glycine in water are presented[7, 8, 9, 10, 11, 12, 13, 14, 15] which were recorded using a range of different experimental techniques and show a significant variability. A full overview of the thermodynamic properties of the glycine water system has been previously presented in literature[16].

1.2.2 Supersaturation

Once the saturation concentration (solubility) of a given system has been determined, the supersaturation may be calculated. Supersaturation (*S*) is the

driving force for both nucleation and crystal growth and the degree to which a solution is supersaturated will dictate the kinetics. Therefore, to generate supersaturation and ultimately induce nucleation, the system must be manipulated to reduce the saturation concentration i.e., reduce the temperature or adjust the solvent composition.

There are several ways to define supersaturation and the two used throughout this thesis are shown in equations 1.1 and 1.2. Here, C is the working concentration and C* is the saturation concentration under the same conditions. The saturation concentration is consequently the point at which C=C*.

$$\text{Supersaturation Ratio } S = C/C^* \quad \textbf{(Eq. 1.1)}$$

$$\text{Relative Supersaturation } \sigma = (C-C^*)/C^* \quad \textbf{(Eq. 1.2)}$$

1.2.3 The Metastable Zone

At a certain concentration, the metastable zone width (MSZW) is defined by the difference in temperature between the saturation concentration (point of dissolution on heating) and metastable limit (point of rapid crystallisation due to spontaneous primary nucleation on cooling). Although this simple definition of the metastable zone suggests that there is a straightforward pathway to crystal proliferation, where at a very basic level nucleation is followed by crystal growth, the behaviour of metastable systems is much more complex. It has been proposed that within the metastable zone there are a series of further

boundaries which define areas in which specific mechanisms can be inhibited or induced.

Over the past decades there has been a gradual attempt to grasp an understanding of these sub-regions (Figure 1.2.) within the metastable zone which would enable probing and manipulating of the conditions within the metastable zone to achieve control over a crystallisation process and reach desired properties such as solid form and desired size distributions.

As an overview of the metastable zone width, starting at the saturation concentration and increasing supersaturation gradually, we would firstly pass into the 'dead zone'[17], this is a region laying on or close to the solubility curve implying nothing happens, neither nucleation, crystal growth or dissolution. As supersaturation is increased further, the 'growth only region'[18] is reached, this suggests that there is a region free from nucleation where only crystal growth takes place, often probed in continuous crystallisation processes following seed addition. Next, the secondary nucleation threshold[19] is reached and it is here that seed proliferation takes place, often exploited in both continuous and batch processes to control the solid form and the crystal size distribution. Finally, the metastable limit defines the upper limit of the metastable zone and indicates the point of spontaneous primary nucleation. However, such defined boundaries within the MSZW, although well studied, are unlikely to be mechanistically accurate and possibly result from limitations of experimental detection of slow growth and nuclei kinetics at low supersaturations.

The following sections of this chapter aim to give a more detailed overview of the mechanisms occurring throughout the crystallisation under metastable conditions. To control a crystallisation process, it is essential that both nucleation and growth mechanisms and kinetics are well understood in relation to supersaturation and processing conditions.

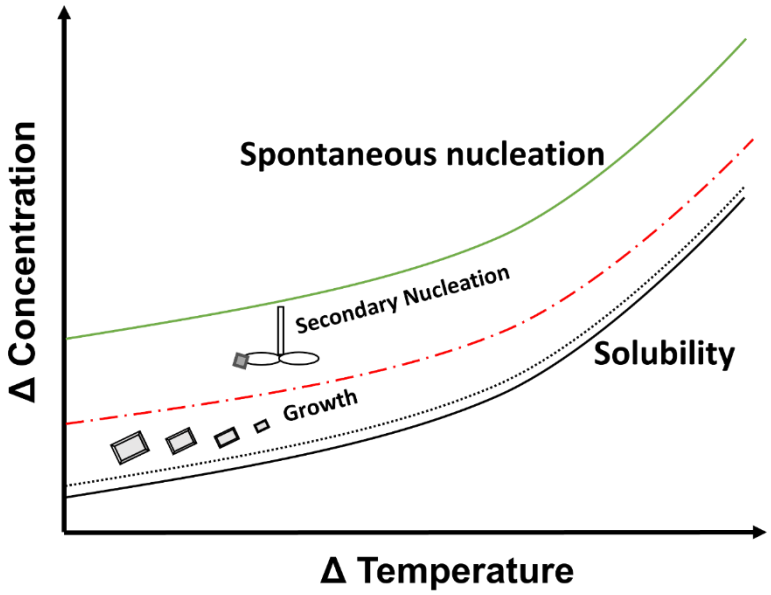

Figure. 1.2. The metastable zone width with the boundaries proposed in the literature. The solubility is depicted by the filled black line, the dead-zone by the dashed black line just above. This is followed by the growth only region before reaching the secondary nucleation threshold (red dashed line). Beyond this point secondary nucleation takes place and as the concentration is increased further the metastable limit is reached (green line). Beyond this point spontaneous primary nucleation takes place.

1.3 Primary Nucleation

Primary nucleation is the initial formation of a crystalline entity (i.e., birth of a new crystal) from a disordered state in a supersaturated solution, either directly within a bulk solution (homogeneous) or on a surface (heterogenous). Through

both pathways, an energy barrier must firstly be overcome. This energy barrier is reduced when a surface is involved and therefore it has been suggested that heterogenous nucleation is likely the source of most primary nucleation events in industrial crystallisation. As nucleation dictates many crystalline properties such as the solid form and crystal size distribution, understanding the underlying mechanisms is essential. Homogenous primary nucleation has been explained by the classical nucleation theory and more recently by the two-step nucleation theory.

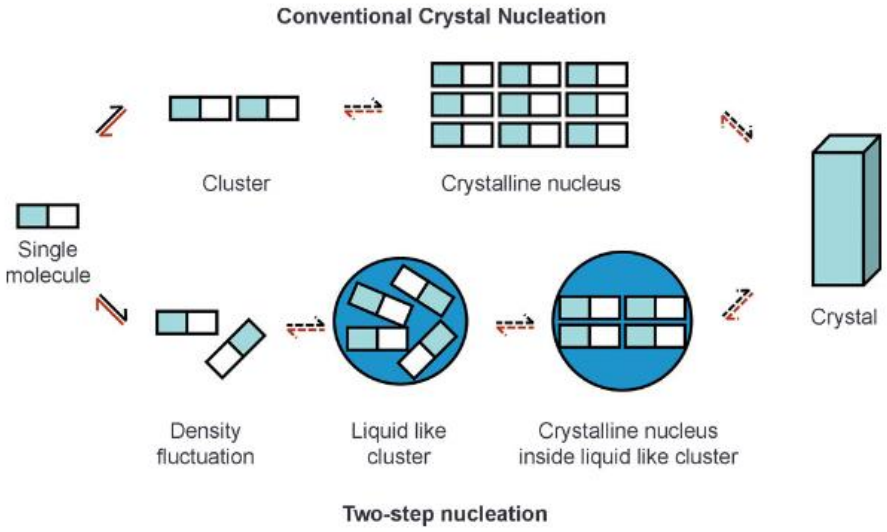

Figure. 1.3. Two routes of primary nucleation describing the conventional nucleation theories and the two step nucleation theory (Taken from ref 21[20]).

1.3.1 Classical Nucleation Theory

The most popular and widespread theory used to explain homogeneous primary nucleation is the classical nucleation theory. This implies that clusters form following local fluctuations in supersaturation within a solution, some of

these clusters then dissolve but some survive and grow beyond a critical stable size. With an increasing supersaturation the energy barrier required to be overcome is reduced and so the probability of nucleation occurring increases.

The direct, classical nucleation pathway can be described by equation 1.3 where J is the nucleation rate, k is the Boltzmann constant, v_m is the molecular volume and γ is the interfacial free energy[1,21].

$$J = AS\exp[-\frac{-16\pi\gamma^3 v_m^2}{3k^3T^3ln^2(S)}] \quad \textbf{(Eq. 1.3)}$$

1.3.2 Two-step Nucleation Theory

The classical nucleation theory does have some limitations and it has been seen that the values predicted by the model do not necessarily represent experimental data recorded.

The two-step nucleation mechanism proposes that nucleation is preceded by the formation of firstly a dense, liquid-like droplet followed by the re-organisation (once a critical size is reached) and nucleation within the dense droplet, Figure 1.3. outlines this pathway which has been supported with experimental data recorded using various techniques. This indication that nucleation occurs within intermediate droplets suggests that the nucleation pathway might be more complex than previous description with the classical nucleation theory. Here, two energy barriers must be overcome. Firstly, the formation of the disordered liquid-like droplet and secondly the re-organisation of the molecules within the droplet into nuclei.

Equation 1.4 shows the analogous equation to equation 1.3 defining the nucleation rate following the two-step pathway. Here *J* is the nucleation rate as a function of solute concentration, K_2 scales the nucleation rate of crystal inside of the clusters, C_1 is the solute concentration inside the clusters , ΔG_2^* is the barrier for nucleation inside of the clusters, ΔG_C^* is the standard free energy of a molecule inside the cluster in excess to that in the solution, η is the viscosity inside the cluster and U_1 and U_0 are the effective rates of decay and formation of clusters at temperature, *T*[22,23].

$$J = \frac{K_2 C_1 \mathrm{T} \exp(-\Delta G_2^*/k_B T)}{\eta(C_1,T)\left[1+\frac{U_1}{U_2}\exp\left(\frac{\Delta G_C^*}{K_B T}\right)\right]} \quad \textbf{(Eq. 1.4)}$$

1.3.3 Heterogeneous Nucleation

It is widely believed that the most common type of primary nucleation is not homogeneous nucleation from solution but rather heterogeneous nucleation. Heterogeneous nucleation is initiated by the existence of a surface i.e., dust particle, impurity or probe which acts as a site for nucleation. This reduces the energy barrier for nucleation essentially reducing the level of supersaturation required.

1.3.4 Measuring Primary Nucleation

Due to the stochastic nature by which nanosized clusters and nuclei spontaneously form from a supersaturated solution, experimentally measuring the creation of the first nucleus is something which remains intangible.

Therefore, many indirect measurements have been developed which attempt to determine the likelihood of nucleation taking place under a given set of conditions providing opportunity to uncover primary nucleation kinetics and fundamental behaviour. To determine probabilities, screening is usually conducted at small-scale where data can be generated rapidly under isothermal conditions (induction time distributions), or polythermal conditions[24] under temperature cycling (metastable limit). By utilising new technologies such as the Crystal 16 and Crystalline by Technobis (Chapter. 2), large data sets can be collected rapidly, improving the significance of the data, and with the application of more than one method to detect nucleation, there is a greater likelihood of capturing nucleation at an early stage[25].

Figure 1.4. displays typical temperature profiles which are used to detect the onset of unseeded nucleation. Here, the term ‘unseeded nucleation’ has been carefully chosen, as often the point of detection is not the rapid crystal proliferation by primary nucleation, but it is secondary nucleation following growth of a crystal initially formed by primary nucleation, which turns the solution turbid, this is otherwise known as the single nucleus mechanism[26] (1.4.4). Therefore, when nucleation is assessed, it is also important to consider what is being measured. This is something which seems to cause some confusion. For example, one study compared primary nucleation rates estimated at 1 mL from probability distributions of induction times with those estimated at 100 mL from crystal number densities obtained by using optical reflectance measurements[27]. It was concluded that the small-scale experiments cannot be used for scale-up for primary nucleation kinetics,

because these nucleation rates differed by many orders of magnitude. However, nucleation rates estimated at 100 mL scale were most likely corresponding to secondary nucleation rather than primary nucleation, and therefore their conclusion is not valid. In fact, it can be expected that secondary nucleation is much faster than primary nucleation under typical crystallisation conditions[28]. Therefore, more work should focus on identifying the appropriate way to measure both primary and secondary nucleation kinetics independently.

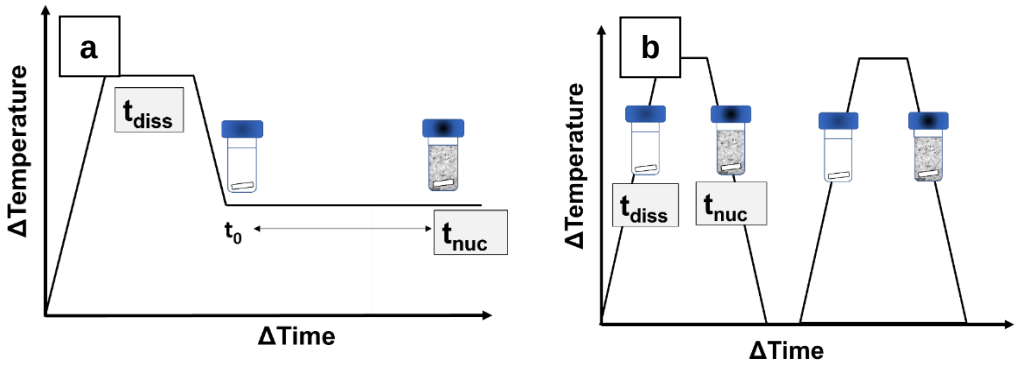

Figure. 1.4. (a) diagram representing the method used to detect nucleation using the isothermal approach, the clouded vial and t_{nuc} represent the point of detection. (b) represents the polythermal approach, t_{nuc} and the clouded vial indicate the point of detection on cooling.

It is true that primary nucleation kinetics, often assessed following induction time measurements are known to be scale dependent[29] and therefore the challenge remains of how best to gain useful information which can aid the crystallisation process design. Other techniques which provide real mechanistic insight, such as microfluidics enable rapid screening and may provide more controllable parameters for understanding the mechanism of

primary nucleation in a particular system, but this may not scale-up when agitation, surface to volume ratio and other factors are taken into consideration.

1.3.5 Seeded Crystallisation

It is well understood that the intrinsic stochasticity of primary nucleation[30] makes prediction and control of crystallisation challenging. Typically, in unseeded batch crystallisation, an initial high supersaturation is necessary to 'self-seed' before navigation through the metastable zone width to control nucleation and growth. This requires knowledge of the boundaries within each region of the MSZW to prevent loss of control. As suggested, there are many challenges with achieving control in unseeded batch crystallisation and this has resulted in the move towards seeded batch and continuous crystallisation. Seeding enables control over nucleation, helping to regulate the initiation of the process, control the generation rate of further nuclei and achieve desired product properties such as size distribution, shape, and form. The increasing attention to secondary nucleation has been reflected in the literature with the recent publication of high quality review papers[31,32].

As mentioned, to achieve a more controlled start-up, operation and final crystal size distribution, a known quantity of crystals which have been previously well-characterised are added to the crystallisation vessel at a known supersaturation. These crystals are known as seeds. Seed crystals are the same compound and form as the product being crystallised. The addition of

seeds removes the requirement for high initial supersaturations to instigate ‘self-seeding’ by primary nucleation and can therefore be more efficient for the process. Typically, they are prepared by sieving or milling of the product crystal and washing under suspension to remove any fine particles from the surface. Once ready for addition, it is essential that the kinetics, seed load and size of seeds have been considered to achieve a controlled crystallisation.

1.4 Secondary Nucleation

Secondary nucleation is often defined as the birth of new crystals resulting from the presence of a seed (parent) crystal of the same compound as the one being crystallised. This is induced by fluid shear or mechanical impact on a seed crystal and is thought to be a dominant mode of nucleation in many industrial crystallisation processes[33]. The term secondary nucleation in often used when new crystals are formed by mechanical division of an existing seed[34] where there is no phase transformation, such as in crystal breakage or attrition. This mechanism has been extensively studied in the literature[35], but it can be argued that this mechanism should not be seen as nucleation, although it is a source term for new particles in an overall population balance. Instead, secondary nucleation should refer to those conditions where the existing seed retains its mechanical integrity and fluid shear or mechanical impact remove clusters or nuclei from the solution layer next to the seed surface[31]. Although secondary nucleation is a mechanism which has been investigated for decades, it seems that little progress has been made in

understanding solute layer removal mechanisms and quantifying their kinetics while the mechanical integrity of seed crystals is retained. Figure 1.5. outlines two mechanisms which are discussed frequently in literature, fluid shear and mechanical impact.

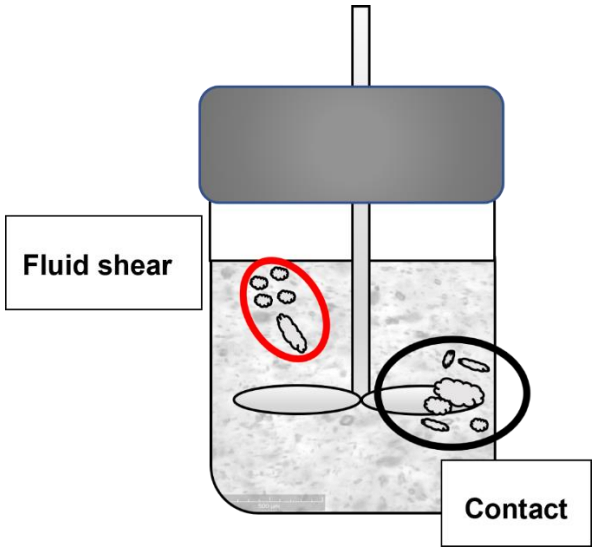

Figure. 1.5. A diagram showing the secondary nucleation mechanisms, the black circled region highlights a seed crystal colliding with the impeller and the red circles region shows fluid shear taking place. Both aim to show how one crystal seed produces multiple further nuclei.

1.4.2 Secondary Nucleation Threshold

The secondary nucleation threshold (SNT) has been introduced in literature to describe a specific region within the metastable zone which must be reached for crystal proliferation from a seed. Below this point, it is assumed that only crystal growth takes place. As secondary nucleation is a mechanical process it is also worth mentioning that this is a kinetically driven mechanism meaning that processing conditions, seed load and seed size[3] may all manipulate the location of this boundary. Knowledge of this region is often exploited in

continuous operation to achieve steady state where consistent generation of crystals may be required. It has been suggested that fluid shear, one of the secondary nucleation mechanisms discussed later (1.4.3.2) is not activated below the secondary nucleation threshold and only contact induced attrition can take place[31]. Interestingly, this highlights one of the challenges identified and discussed throughout this thesis, which is the measurement of secondary nucleation kinetics. To be able to accurately predict and control a crystallisation process, the mechanisms must be well understood and kinetics quantified across a range of conditions.

1.4.3 Secondary Nucleation Mechanisms

Researchers have spent decades[36] attempting to understand the fundamental mechanisms of secondary nucleation but there seems to still be some disagreement, especially in relation to the significance of fluid shear. The lack of progress could be due to the complexity of replicating conditions experimentally and isolating individual mechanisms to assess them using 'offline' techniques.

In theory, anything that exerts 'enough' stress onto the surface of the seed crystal may lead to detachment of viable crystal nuclei. With that said, it seems that there is a hierarchical structure with shear and contact acting to initiate secondary nucleation, providing the force to remove nuclei from the surface of the seed, with other mechanisms contributing to the significance of each. Other mechanisms include polycrystalline or dendritic breeding[1], surface nuclei breeding[4] and the embryo coagulation secondary nucleation theory[37]. In any

case, it is likely that the prevailing mechanism will depend on the level of supersaturation.

1.4.3.1 Contact - Attrition and Breakage

Contact induced nucleation may be defined as a separation of crystal fragments from parent, larger crystals due to collisions which could be a result of the impeller, vessel walls or other crystals[38,39]. Often, crystal breakage due to impeller and crystal-crystal collisions are reported to be the dominant secondary nucleation mechanism, seeming to be the simplest mechanism to comprehend. Offline approaches have been developed which have attempted to prove this, but these set-ups are not always completely representative of the complex interactions which may occur in a crystalliser. Some researchers have attached a seed to the bottom of a metal rod and contacted it at a known force on a solid surface[40], others have ground a ‘seed’ in the form of a tablet with a rod to continuously generate nuclei[41]. Admittedly, with many alternative studies attempting to assess secondary nucleation by suspending seeds in a stirred tank, offline techniques may be the best and only option to really separate individual mechanisms and develop an understanding of their behaviour.

1.4.3.2 Fluid Shear

Fluid shear is the second mechanism which is well outlined in literature and can be identified as the removal of nuclei from the surface of a seed crystal

due to the shearing of fluid as the seeds are exposed to fluid flow. Mechanisms such a surface nuclei breeding suggest that molecules and clusters use the surface of the seed as a ‘base’ to grow until they are beyond a critical size before being more easily dislodged and swept away into the bulk of solution.

The challenge lays in the lack of experimental evidence for specific mechanisms. There have been some attempts to develop an understanding, with investigators using various techniques to monitor and observe fluid shear in action. One method previously employed is the ‘seed on a stick’ technique. The idea is to hold a seed in a specific location within a shearing fluid and count the resulting crystals formed. Taylor Couette flow[42,43], fluid jets[44,45] and stirred tanks[46] have been employed. The limitation with many of the experimental techniques was the evaluation and quantification of secondary nucleation. In some cases, secondary nuclei were formed under one set of conditions (i.e., agitation rate, supersaturation etc) for secondary nucleation before being grown under a different set of conditions. Considering the solution will still be in a supersaturated region, and if taken for growth, likely a much more highly supersaturated region, indirect measurements such as these can introduce further effects, e.g., primary nucleation, growth and breeding if transported[47]. The Taylor Couette flow cell experiments with (seed addition) have used inner rotating cylinders. Flow regimes in Couette cell set-ups were investigated[48] using various rotational rates and it was found that if the outer cylinder was rotated rather than the inner, laminar flow could be maintained at higher rotational rates. Therefore, it is possible to use Couette cells to

introduce both laminar and turbulent flow conditions for investigation of fluid shear effects on primary and secondary nucleation.

To analyse this experimental information in a manner which can be applied in the design and optimisation of industrial crystallisation processes, it is important to ensure that the conditions selected are relevant and realistic in an industrial crystallisation vessel. Although this is not the aim in this thesis, it is important to recognise that in a stirred tank crystalliser, the shear rates will be distributed unevenly throughout the vessel. Using computational fluid dynamics (CFD) and particle tracking technology, researchers have quantified these shear rate distributions[49] noticing that near the impeller tip, there were large spikes in the shear rate values before decreasing to lows at the positions furthest away. Success in developing an understanding of secondary nucleation mechanisms will thus require both experimental set-ups using ‘state of the art’ technology, coupled with models and insight into the fluid dynamics in individual crystallisation vessels.

Table 1.1. A brief list of literature sources which have estimated and outlined shear rate distributions in stirred tank reactors across multiple volumes. This will be most relevant in Chapter. 5.

Literature Source	Experimental Set-up	Values (S^{-1})
Achermann et al[50]	Characterised small volume vials using CFD and validated with X-ray CT.	Average ~ 100 s^{-1} Range – 10 (s) - 1100 s^{-1}
Marchisio et al[51,49]	Stirred tank with a volume of 7.68 L.	Vessel averaged 75 - 150 s^{-1} Range - 10 (s) - 600 s^{-1}
Nappo et al[52]	Small volume vials (2 ml)	Average - 150 s^{-1}

1.4.4 Measuring Secondary Nucleation Rates

It seems that there has been a lack of techniques used to measure secondary nucleation kinetics as opposed to primary nucleation kinetics[53], in any case, nucleation kinetics measurements seem to be more challenging than crystal growth measurements which are relatively well established (1.5.1), although assessing the secondary nucleation kinetics is just as important for development of crystallisation processes. It was mentioned earlier that in order to observe primary nucleation, crystal nuclei must grow to be large and/or numerous enough to be detected and/or to induce secondary nucleation which rapidly generates further crystals that can then be detected (single nucleus mechanism). Although it seems to be particularly challenging to decouple primary and secondary nucleation effects in industrial crystallisation, as mentioned, it is broadly accepted that secondary nucleation is the dominant

mechanism. As the nucleation rate dictates the generation of new crystals in industrial crystallisation processes, it is essential that the kinetics are accurately predicted and monitored to know the expected final crystal size distribution i.e., a higher rate of secondary nucleation will result in smaller crystals.

There are several different approaches to determine secondary nucleation kinetics, based on particle counting[3] or particle sizing[54]. Each of these approaches relies on certain assumptions about the process and underlying models used to estimate primary or secondary nucleation rates. Table 1.2. gives an overview of the factors which must be considered for the underlying models. Experimental techniques developed to measure the secondary nucleation kinetics will be outlined in Chapters 4 and 5.

Table 1.2. A list of just some of the factors typically considered in secondary nucleation models is shown[34].

Secondary Nucleation Rate - Influences	
Supersaturation	Impeller rotational rate
Crystal concentration or mass	Impeller tip velocity
Crystal mechanical properties	Impeller geometry
Individual crystal size	Vessel geometry

1.4.5 Secondary Nucleation Summary

Properties of crystallisation solution and slurries, as well as the geometry and hydrodynamics of crystallisation vessels, all result in vastly different nucleation behaviour. With that said, new tools and technology are creating a real opportunity to develop better understanding of secondary nucleation in the course of industrial crystallisation processes, while there seems to be a real lack of experimental evidence for testing various secondary nucleation hypothesises. Therefore, developing tools to directly measure secondary nucleation in a representative, controlled and quantifiable manner is a priority for facilitating development, design and optimisation of crystallisation processes.

Some pioneering experiments were completed decades ago when technology such as high-resolution cameras and probes which enable observation of the bulk crystallisation system were not available. This meant detection was made by eye or under a microscope at the end of the experiment. New technologies can enable more accurate, quantitative approaches to detection of nucleation in real time providing insight into the secondary nucleation mechanisms taking place. Due to its importance in industrial crystallisation processes, secondary nucleation is of great interest, which is reflected in reviews on this topic recently published[55,32].

1.5 Crystal Growth

Once nucleation has been achieved and a cluster is formed that is larger than a critical size by either primary or secondary nucleation, the following step is crystal growth. As with nucleation, the thermodynamic driving force for crystal growth is supersaturation. The first step involves the movement and deposition of growth units to the face of the crystal followed by integration to the crystal[56] where the number of growth units joining (deposition) the surface under supersaturated conditions will be higher than those leaving, disrupting the equilibrium flux. The following step will require integration of the growth units into the surface.

Knowledge of crystal growth is not only important for the prediction of size distributions, but it will also affect the level of impurity and shape of the crystals.

1.5.1 Measuring Crystal Growth

Crystal growth rate measurements are relatively well established, although often time consuming. Typically, measurements are carried out based on single crystal growth observations for fundamental analysis of growth mechanisms or de-supersaturation measurements in seeded crystallisation[57] are completed, carefully controlled to minimise nucleation. The well-studied glycine in water system is one example, although there is a significant variability in the kinetics using different methods and from different research groups (Figure 4.7.). It has also been seen that damaged crystals grow faster than non-damaged[58] and therefore this may lead to disagreements between

de-supersaturation in seeded crystallisation and face specific growth rates. Another consideration is also the limitation in detection and image analysis processing methodology which may produce a variety of size distributions.

1.6 Nucleation and Crystal Growth Relationship

Crystal nucleation and growth are inevitably linked when thought of in typical observations of crystallisation behaviour, conspiring together to determine the final particle size and shape distribution. With this, often, nucleation and growth kinetics are presented independently from one another with only a few attempts to develop a relationship between the two in the form of a classification system. Classifications of crystallisation behaviour in terms of fast/slow nucleation/growth thus strongly depend on supersaturation as well as on agitation and solute/solvent properties (Table 1.2.).

In literature one method was proposed[59] suggesting that the induction time be plotted vs the crystal growth rate. With the induction time also known to be a function of nucleation (primary and secondary) and growth time (t_g) it seems that there is almost certainly likely to be a relationship between the two. A concern with this classification is that the induction time on its own does not provide information which could be used to estimate final crystalline properties such as the crystal size distribution. A second classification methodology[60] showed nucleation rate against the growth rates to predict the crystal morphology. From this study, it was concluded that the nucleation and growth relationship could be related to the final crystal shape and size variation. The

diagram below in Figure 1.6., outlines how a classification system may be presented.

In the work presented in this thesis, a classification workflow was developed and outlined in Chapter 4.

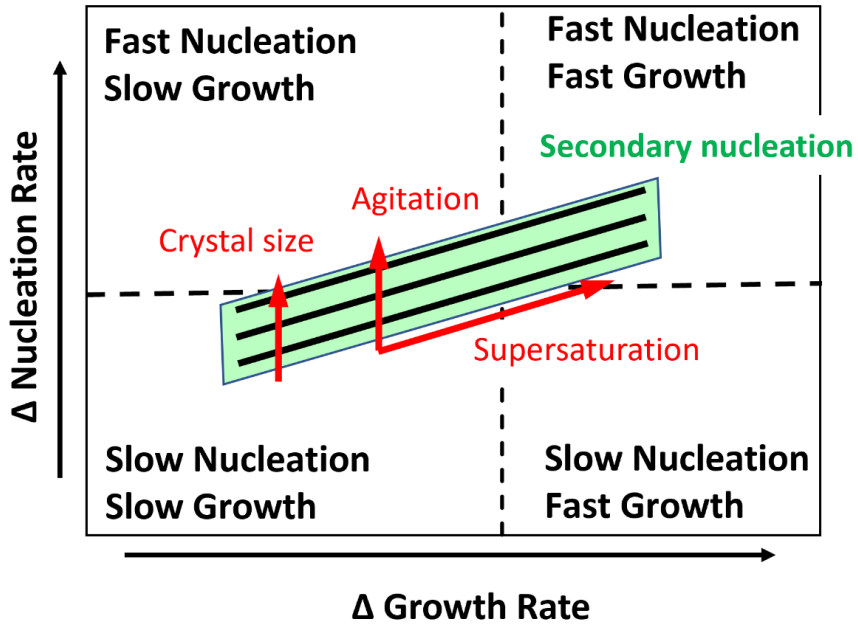

Figure 1.6. An example of how the relationship between secondary nucleation rates and crystal growth rates might look in the form of a classification diagram. With an increase in the crystal size, agitation, and the other parameters from Table 1.2. the nucleation rate can be increased. With an increase in supersaturation the crystal growth rates can also be increased.

1.7 Process Analytical Technology

With the pharmaceutical industry now accelerating the switch from traditional batch crystallisation towards continuous operation, process monitoring, and process control take an increased responsibility. With this, there is a requirement for the product to be analysed in a direct approach.

In recent times process analytical technology (PAT) has certainly gone through a remarkable period of advancement and as the researcher reaches PAT selection, there are a series of questions which ought to be answered. One crucial decision may be of which parameter must be measured and controlled, this could include nucleation and growth kinetics, concentration, or solid form. As mentioned in section 1.6, nucleation and crystal growth have an intricate relationship which is complicated by the dynamic nature of crystallisation. Direct monitoring allows the researcher to gain some real insight into this universe of interactions. Only with access to this information can we attempt to gain control of the process and begin to manipulate the parameters to gain favourable crystal quality attributes. There is a significant amount of technology now available but choosing the right tool can still be challenging. Prior to selection, consideration must be given to both the sensitivity of the probe and the ability to generate real, quantitative information, quickly and accurately. Tools typically used in crystallisation process monitoring and the applications will be outlined in Chapter. 2.

1.8 Significance of this Thesis

Although it is widely accepted that secondary nucleation is one of the most important mechanisms in industrial crystallisation processes there is still a limited understanding of how this occurs[4]. This lack of knowledge is limiting the ability to design, optimise and scale-up crystallisation processes. Continuous manufacturing with increased efficiency, sustainability, and

reduced costs, is now seen as the future of manufacturing in the pharmaceutical industry. In continuous processes seeding is almost always employed to achieve a desired crystal size distribution and reduce start-up times. With seeding, at low supersaturations it may then be assumed that secondary nucleation is the single generator of nuclei at low supersaturations. To develop a robust crystallisation process it is therefore essential that secondary nucleation must be understood, measured, and controlled across multiple scales.

This thesis proposes a methodology which can be used to rapidly assess nucleation and growth kinetics of a compound in development at small-scale which aims to reduce both the time and cost of process development, design, and optimisation. A novel experimental technique has been developed which enables *in-line* monitoring of secondary nucleation and quantification of kinetics by well controlled laminar fluid shear. This should provide a better understanding of secondary nucleation mechanisms and generate new insights into how secondary nucleation is affected by process conditions in industrial crystallisation processes.

1.9. Challenges Identified

- Understand the challenges associated with solubility measurements using a range of experimental techniques under challenging conditions. Which technique should be used, where and why? **(Chapter. 3)**
- How should nucleation kinetics be quantified? Can primary and secondary nucleation be identified and distinguished clearly from each other? **(Chapter. 4).**
- Can a classification system be developed which enables the relationship between between nucleation and crystal growth to be rapidly evaulated? **(Chapter. 4)**
- How can fluid shear be isolated and controlled in a way which enables the screening of a relevant range of experimental conditions. Can the secondary nucleation kinetics be directly assessed under controlled fluid shear which is representative of the level of shear typically experienced in a crystallisation vessel? **(Chapter. 5)**

References

(1) Lewis, A.; Seckler, M.; Kramer, H.; Van Rosmalen, G. M. *Industrial Crystallisation. Fundamentals and Applications*; Cambridge University Press, 2015.

(2) Chen, J.; Sarma, B.; Evans, J. M. B.; Myerson, A. S. Pharmaceutical Crystallization. *Cryst. Growth Des.* **2011**, 887. https://doi.org/10.1021/cg101556s.

(3) Briuglia, M.; Sefcik, J.; ter. Horst, J. Measuring Secondary Nucleation through Single Crystal Seeding. *Cryst. growth Des.* **2019**, *19*, 421–429. https://doi.org/http://dx.doi.org/10.1021/acs.cgd.8b01515.

(4) Anwar, J.; Khan, S.; Lindfors, L. Secondary Crystal Nucleation: Nuclei Breeding Factory Uncovered. *Angew. Chemie - Int. Ed.* **2015**, No. 54, 14681–14684. https://doi.org/10.1002/anie.201501216.

(5) Plumb, K. Continuous Processig in the Pharmaceutical Industry: Changing the Mind Set. *Chem. Eng. Res. Des.* **2005**, No. 83, 730–738. https://doi.org/10.1205/cherd.04359.

(6) Black, S.; Dang, L.; Liu, C.; Wei, H. On the Measurement of Solubility. *Organic Process Research and Development*. 2013, pp 486–492. https://doi.org/10.1021/op300336n.

(7) Dalton, J.; Schmidt, C. The Solubilities of Certain Amino Acids in Water, the Densities of Their Solutions at Twenty-Five Degrees, and the Calculated Heats of Solution and Partial Molal Volumes. *J. Biol. Chem. 103* (2), 549–578. https://doi.org/10.1016/S0021-9258(18)75835-3.

(8) Dunn, M.; Ross, F.; Read, L. The Solubility of Amino Acids in Water. *J. Biol. Chem.* **1933**, *103* (2), 579–595. https://doi.org/10.1016/S0021-9258(18)75836-5.

(9) Jelinska-Kazimierczuk, M.; Szydlowski, J. Isotope Effect on the Solubility of Amino Acids in Water. **1996**, *25* (12).

(10) Yi, Y.; Hatziavramidis, D.; Myerson, A. S.; Waldo, M.; Beylin, V. G. Development of a Small-Scale Automated Solubility Measurement Apparatus. **2005**, No. 44, 5427–5433.

(11) Yang. Solubility of Form α and Form γ of Glycine in Aqueous Solutions. *J. Chem. Eng. Data* **2008**, No. 53, 1133–1137.

(12) Park, K.; Evans, J. M. B.; Myerson, A. S. Determination of Solubility of Polymorphs Using Differential Scanning Calorimetry. *Cryst. Growth Des.* **2003**, No. 6, 991–995. https://doi.org/10.1021/cg0340502.

(13) Sun, H.; Wang, L.; Liu, B. Solubility of a -Glycine in Water with Additives at a Temperature Range Thermodynamic Modeling. *Fluid Phase Equilib.* **2017**, *434*, 167–175. https://doi.org/10.1016/j.fluid.2016.12.003.

(14) Igarashi, B. K.; Sasaki, Y.; Azuma, M.; Noda, H.; Ooshima, H. Control of Polymorphs on the Crystallization of Glycine Using a WWDJ Batch Crystallizer. **2003**, *3*, 159–163.

(15) Devi, K. R.; Gnanakamatchi, V.; Srinivasan, K. Attainment of Unstable β Nucleation of Glycine through Novel Swift Cooling Crystallization Process. *J. Cryst. Growth* **2014**, *400*, 34–42. https://doi.org/10.1016/j.jcrysgro.2014.04.029.

(16) Rowland, D. Thermodynamic Properties of the Glycine + H2O System. *J. Phys. Chem. Ref. Data* **2018**, No. 47, 023104-1-023104–023115. https://doi.org/10.1063/1.5016677.

(17) Liu, Y.; Black, J. F. B.; Boon, K. F.; Cruz-Cabeza, A. J.; Davey, R. J.; Dowling, R. J.; George, N.; Hutchinson, A.; Montis, R. When Crystals Do Not Grow: The Growth Dead Zone. *Cryst. Growth Des.* **2019**, 4579–4587. https://doi.org/10.1021/acs.cgd.9b00478.

(18) Threlfall, T. L.; Coles, S. J. A Perspective on the Growth-Only Zone, the Secondary Nucleation Threshold and Crystal Size Distribution in Solution Crystallisation. *CrystEngComm*. 2016, pp 369–378.

https://doi.org/10.1039/c5ce01608h.

(19) Srisa-Nga, S.; Flood, A. E.; White, E. T. The Secondary Nucleation Threshold and Crystal Growth of α-Glucose Monohydrate in Aqueous Solution. *Cryst. Growth Des.* **2006**, No. 6, 795–801. https://doi.org/10.1021/cg050432r.

(20) Davey, R. J.; Schroeder, S. L. M.; Ter Horst, J. H. Nucleation of Organic Crystals - A Molecular Perspective. *Angew. Chemie - Int. Ed.* **2013**, No. 52, 2166 – 2179. https://doi.org/10.1002/anie.201204824.

(21) B. Szilagyi, A. Majumber, Z. N. CHAPTER 2. Fundamentals of Population Balance Based Crystallization Process Modelling. In *The Handbook of Continuous Crystallization*; 2020; pp 51–101.

(22) Vekilov, P. G. Nucleation. *Cryst. Growth Des.* **2010**, *10* (12), 5007–5019. https://doi.org/10.1021/cg1011633.

(23) Karthika, S.; Radhakrishnan, T. K.; Kalaichelvi, P. A Review of Classical and Nonclassical Nucleation Theories. *Cryst. Growth Des.* **2016**, *16*, 6663–6681. https://doi.org/10.1021/acs.cgd.6b00794.

(24) Nyvlt, J. Kinetics of Nucleation in Solutions. *J. Cryst. Growth* **1968**, *3–4*, 377–383.

(25) Kubota, N. A New Interpretation of Metastable Zone Widths Measured for Unseeded Solutions. *J. Cryst. Growth* **2008**, No. 310, 629–634. https://doi.org/10.1016/j.jcrysgro.2007.11.123.

(26) Brandel, C.; ter Horst, J. H. Measuring Induction Times and Crystal Nucleation Rates. *Faraday Discuss.* **2015**, No. 179, 199–214. https://doi.org/10.1039/c4fd00230j.

(27) Cedeno, R.; Maosoongnern, S.; Flood, A. Direct Measurements of Primary Nucleation Rates of P-Aminobenzoic Acid and Glutamic Acid and Comparison with Predictions from Induction Time Distributions. *Ind. Eng. Chem. Res.* **2018**, *57* (51), 17504–17515.

https://doi.org/10.1021/acs.iecr.8b03625.

(28) Ho, J.; Flannigan, J.; Cashmore, A.; Gerard, C. J. J.; Steendam, R. E.; Haw, M. D.; Sefcik, J.; Joop, H. The Unexpected Dominance of Secondary over Primary Nucleation. **2022**, 109–131. https://doi.org/10.1039/d1fd00098e.

(29) Steendam, R. R. E.; Keshavarz, L.; Blijlevens, M. A. R.; De Souza, B.; Croker, D. M.; Frawley, P. J. Effects of Scale-Up on the Mechanism and Kinetics of Crystal Nucleation. *Cryst. Growth Des.* **2018**, No. 18, 5547–5555. https://doi.org/10.1021/acs.cgd.8b00857.

(30) Maggioni, G. M.; Mazzotti, M. Modelling the Stochastic Behaviour of Primary Nucleation. *Faraday Discuss.* **2015**, No. 179, 359–382. https://doi.org/10.1039/c4fd00255e.

(31) Agrawal, S. G.; Paterson, A. H. J. Secondary Nucleation : Mechanisms and Models Secondary Nucleation : Mechanisms and Models. *Chem. Eng. Commun.* **2015**, *202* (5), 698–706. https://doi.org/10.1080/00986445.2014.969369.

(32) Xu, S.; Hou, Z.; Chuai, X.; Wang, Y. Overview of Secondary Nucleation: From Fundamentals to Application. *Ind. Eng. Chem. Res.* **2020**, No. 59, 18335–18356. https://doi.org/10.1021/acs.iecr.0c03304.

(33) Frawley, P. J.; Mitchell, N. A.; Ó'Ciardhá, C. T.; Hutton, K. W. The Effects of Supersaturation, Temperature, Agitation and Seed Surface Area on the Secondary Nucleation of Paracetamol in Ethanol Solutions. *Chem. Eng. Sci.* **2012**, No. 75, 183–197. https://doi.org/10.1016/j.ces.2012.03.041.

(34) McGinty, J.; Yazdanpanah, N.; Price, C.; ter Horst, J. H.; Sefcik, J. CHAPTER 1. Nucleation and Crystal Growth in Continuous Crystallization. In *The Handbook of Continuous Crystallization*; 2020; pp 1–50. https://doi.org/10.1039/9781788013581-00001.

(35) Mersmann, A. Attrition and Attrition Controlled Secondary Nucleation. In *Crystallization Technology Handbook*; Marcel Dekker: New York, 2001.

(36) Denk, E. G.; Botsaris, G. D. Fundamental Studies in Secondary Nucleation from Solution. *J. Cryst. Growth* **1972**, No. 13–14, 493–499. https://doi.org/10.1016/0022-0248(72)90287-4.

(37) Qian, R. Y.; Botsaris, G. D. A New Mechanism for Nuclei Formation in Suspension Crystallizers: The Role of Interparticle Forces. *Chem. Eng. Sci.* **1997**, No. 20, 3429 3440,. https://doi.org/10.1016/S0009-2509(97)89691-1.

(38) Mason, R. E. A.; Strickland-Constable, R. F. Breeding of Crystal Nuclei. *Trans. Faraday Soc.* **1965**, *62*, 455–461.

(39) Virone, C.; Ter Horst, J. H.; Kramer, H. J. M.; Jansens, P. J. Growth Rate Dispersion of Ammonium Sulphate Attrition Fragments. In *Journal of Crystal Growth*; 2005; pp 1397–1401. https://doi.org/10.1016/j.jcrysgro.2004.11.167.

(40) Cui, Y.; Myerson, A. S. Experimental Evaluation of Contact Secondary Nucleation Mechanisms. *Cryst. Growth Des.* **2014**, 5152–5157. https://doi.org/10.1021/cg500861f.

(41) Wong, S. Y.; Cui, Y.; Myerson, A. S. Contact Secondary Nucleation as a Means of Creating Seeds for Continuous Tubular Crystallizers. *Cryst. Growth Des.* **2013**, No. 13, 2514–2521. https://doi.org/10.1021/cg4002303.

(42) Sung, C. Y.; Estrin, J.; Youngquist, G. R. Secondary Nucleation of Magnesium Sulfate by Fluid Shear. *AIChE J.* **1973**, *19* (5), 957–962. https://doi.org/10.1002/aic.690190511.

(43) Wang, M. -L; Huang, H. -T; Estrin, J. Secondary Nucleation of Citric Acid Due to Fluid Forces in a Couette Flow Crystallizer. *AIChE J.* **1981**, *27* (2), 312–315. https://doi.org/10.1002/aic.690270222.

(44) Tai, C. Y.; Tai, C. Der; Chang, M. H. Effect of Interfacial Supersaturation on Secondary Nucleation. *J. Taiwan Inst. Chem. Eng.* **2009**, No. 40, 439–442. https://doi.org/10.1016/j.jtice.2009.01.006.

(45) Steendam, R. R. E.; Frawley, P. J. Secondary Nucleation of Sodium Chlorate: The Role of Initial Breeding. *Cryst. Growth Des.* **2019**, *21*, E.

(46) Yousuf, M.; Frawley, P. J. Experimental Evaluation of Fluid Shear Stress Impact on Secondary Nucleation in a Solution Crystallization of Paracetamol. *Cryst. Growth Des.* **2018**, No. 18, 6843–6852. https://doi.org/10.1021/acs.cgd.8b01074.

(47) Wang, M. -L; Huang, H. -T; Estrin, J. Secondary Nucleation of Citric Acid Due to Fluid Forces in a Couette Flow Crystallizer. *AIChE J.* **1981**, *27* (2), 312–315. https://doi.org/10.1002/aic.690270222.

(48) Swinney, H. L. Flow Regimes in a Circular Couette System with Independently Rotating Cylinders. *J. Fluid Mech.* **1986**, *164*, 155–183. https://doi.org/10.1017/S0022112086002513.

(49) Marchisio, D. L.; Soos, M.; Sefcik, J.; Morbidelli, M. Role of Turbulent Shear Rate Distribution in Aggregation and Breakage Processes. *AIChE J.* **2006**, *52* (1), 158–173. https://doi.org/10.1002/aic.10614.

(50) Achermann, R.; Adams, R.; Prasser, H.; Mazzotti, M. Characterization of a Small-Scale Crystallizer Using CFD Simulations and X-Ray CT Measurements. *Chem. Eng. Sci.* **2022**, No. 256, 1–12. https://doi.org/10.1016/j.ces.2022.117697.

(51) Marchisio, B. D. L.; Soos, M.; Sefcik, J.; Morbidelli, M.; Barresi, A. A.; Baldi, G. Effect of Fluid Dynamics on Particle Size Distribution in Particulate Processes. **2006**, No. 2, 191–199. https://doi.org/10.1002/ceat.200500358.

(52) Nappo, V.; Sullivan, R.; Davey, R.; Kuhn, S.; Gavriilidis, A.; Mazzei, L. Effect of Shear Rate on Primary Nucleation of Para-Amino Benzoic Acid

in Solution under Different Fluid Dynamic Conditions. *Chem. Eng. Res. Des.* **2018**, *136*, 48–56. https://doi.org/10.1016/j.cherd.2018.04.039.

(53) Devos, C.; Gerven, T. Van; Kuhn, S. A Review of Experimental Methods for Nucleation Rate Determination in Large-Volume Batch and Micro Fl Uidic Crystallization. **2021**, No. 21, 2541–2565. https://doi.org/10.1021/acs.cgd.0c01606.

(54) Garside, J.; Shah, M. Crystallization Kinetics from MSMPR Crystallizers. *Ind. Eng. Chem. Process Des, Dev.* **1980**, *19*, 509–514.

(55) Zhang, D.; Wang, X.; Ulrich, J.; Tang, W.; Xu, S.; Li, Z.; Rohani, S.; Gong, J. Control of Crystal Properties in a Mixed-Suspension Mixed-Product Removal Crystallizer: General Methods and the Effects of Secondary Nucleation. *Cryst. Growth Des.* **2019**, No. 19, 3070–3084. https://doi.org/10.1021/acs.cgd.8b01530.

(56) Davey, R.; Garside, J. *From Molecules to Crystallizers. An Introduction to Crystallization.*; 2000.

(57) Crystallisation, 4th Edition. *Org. Process Res. Dev.* **2002**. https://doi.org/10.1021/op0101005.

(58) Schiele, S. A.; Hupfer, R.; Luxenburger, F.; Briesen, H. Growth of Abraded Crystals Tracked in Three Dimensions. **2021**, No. 21, 6373–6384.

(59) Rathi, S.; Chavan, R. B.; Shastri, N. R. Classification of the Crystallization Tendency of Active Pharmaceutical Ingredients (APIs) and Nutraceuticals Based on Their Nucleation and Crystal Growth Behaviour in Solution State. **2020**, 70–82.

(60) Acevedo, D.; Nagy, Z. K. Systematic Classification of Unseeded Batch Crystallization Systems for Achievable Shape and Size Analysis. *J. Cryst. Growth* **2014**, *394*, 97–105. https://doi.org/10.1016/j.jcrysgro.2014.02.024.

Chapter. 2. Materials and Methods

2.1. Materials

2.1.1 Glycine

The model compound selected for this piece of work was glycine which was purchased from Sigma Aldrich (≥99% electrophoresis). De-ionised water was used as the solvent and sourced on-site (Milli-Q, 18.2 MΩ cm).

Glycine is an amino acid often studied due to its molecular simplicity. Under ambient conditions there are three known crystalline forms, two metastable forms, alpha (α) and beta (β) and the most thermodynamically stable form, gamma (γ). Following most paths to crystal formation (i.e., cooling crystallisation), α-glycine will typically crystallise from aqueous solution[1]. As the purpose of this study was not to necessarily select and control the polymorphic form which is crystallised (which is an ongoing challenge), it was decided that α-glycine would be the form of interest.

The different glycine morphologies are shown below (Figure. 2.1.), γ-glycine takes a more needle like shape and α-glycine takes a more plate like shape.

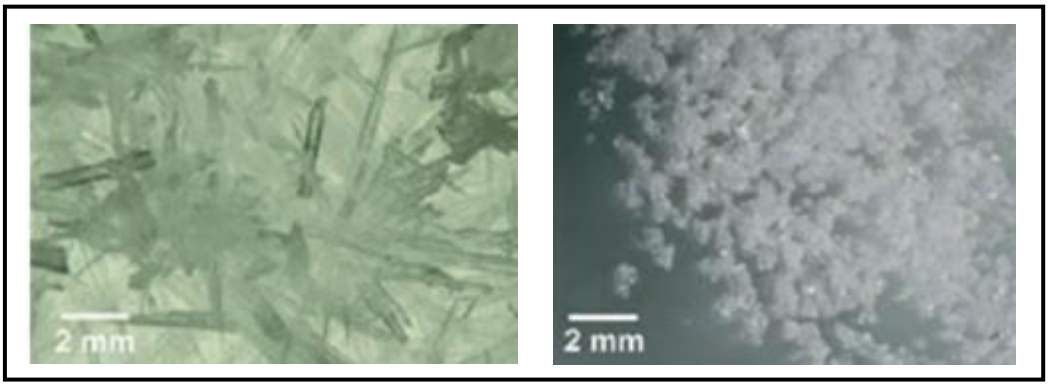

Figure. 2.1. Two glycine polymorphic forms analysed using Optical Microscopy. (a) Represents multiple needle-like γ glycine crystals. (b) Shows precipitated α glycine crystals which are more plate like in shape (taken from Ref. 1[1]).

2.2. Methods overview

To achieve a reliable and robust crystallisation process in which desired properties are achieved, precise knowledge and control over the processing conditions, solid form, size, and shape are required.

In industrial crystallisation, fluid shear is one of the two dominant mechanisms inducing secondary nucleation and the rate of shear is expected to have a significant effect on the rate of crystal removal from the seed. At present time, although it is accepted that fluid shear does induce secondary nucleation, the significance of this mechanism is subject to debate. To gain an insight to the fundamental role of shear, observation of the mechanism must be carried out under well controlled experimental conditions. Using a Couette flow cell in which the inner cylinder is fixed, and the outer cylinder rotated, provides a continuous, stable laminar shear flow such that the applied shear rate can be calculated and controlled.

Crystallisation was carried out using experimental crystallisation set-ups which have precise control over the temperature with a mixture of integrated capabilities of process analytical tools, such as in-situ visual monitoring for detecting phase changes, counting, and sizing crystal populations or the ability to rapidly screen multiple conditions at once. This included the Crystal 16, Crystalline, EasyMax and OptiMax. The different scales of these devices produced a useful ‘ladder’ of scale-up and a range of flow conditions to enable exploration of the role of flow and scale.

Process analytical tools were selected based on previous experimental studies and characterisation was completed using in-line and off-line techniques. The off-line techniques included X-Ray Powder Diffraction (XRPD), Attenuated Total Reflectance Fourier Transform Infrared Spectroscopy (ATR FTIR) and Raman Spectroscopy for crystal form analysis. Optical Microscopy was used to observe the morphological features and size the seed crystals. To maintain consistency across scale, Particle Vision Measurement (PVM) imaging was selected as the only in-line technique to calculate nucleation rates although, Focused Beam Reflectance Measurements were used to validate what was being recorded. An overview of the applications of specific process analytical technology is provided in Table. 2.1.

Table. 2.1. An overview of process analytical technology (PAT) typically used in crystallisation process control and the potential applications.

Process Analytical Technology (PAT)	Application
Raman Spectroscopy	Monitoring and control over the solid form.
Turbidity	Measuring induction time, point of nucleation detected by change in transmission.
Infra-Red	Detect any major change in system, monitor concentration of solution throughout experiment (continuous operation).
Imaging	Imaging enables detection of any major nucleation events and can be used to estimate kinetics of nucleation and crystal growth.
FBRM	Detect nucleation and crystal growth kinetics by recording and tracking the crystal number and size.

2.3 Crystallisation set-ups

2.3.1 Polar Bear (Cambridge reactor designs)

The Polar Bear Plus Crystal is a device manufactured by Cambridge Reactor Designs employed to achieve precise control over temperature to ±0.1°C. Interchangeable aluminium plates enable simple switching of volume and vessel type for different applications. The precise temperature control provided by the Polar Bear indicates that it is the perfect tool to measure solubility using the gravimetric equilibration technique (Chapter. 3.). As a note, the Polar Bear can also be used to set heating and cooling profiles at specific rates.

2.3.2 Crystal 16 and Crystalline

The Crystal 16 and Crystalline from Technobis are multi-reactor tools which are often used to rapidly screen crystallisation processing conditions and generate large sets of data.

The Crystal 16 contains 16 independent chambers with a sample capacity of 1.5 mL and enables precise and specific temperature control. Within each chamber there is a light transmission probe to detect a change in turbidity of the system which indicates formation/ dissolution of crystals. In this work, the Crystal 16 was used to measure the metastable zone width (Chapter. 4). To achieve this, temperature cycles are set, enabling the point of dissolution to be determined (solubility) on heating, and the point of recrystallisation (nucleation) on cooling (Figure 2.2.). To determine primary nucleation rates, the Crystal 16 can be used to rapidly generate large numbers of induction time

measurements (Chapter. 3.)[2]. The induction time is recorded under isothermal conditions and a solution is brought to a selected temperature generating a known supersaturation. Once the supersaturation is generated, the temperature is maintained until nucleation spontaneously occurs and the time taken for this to take place is recorded.

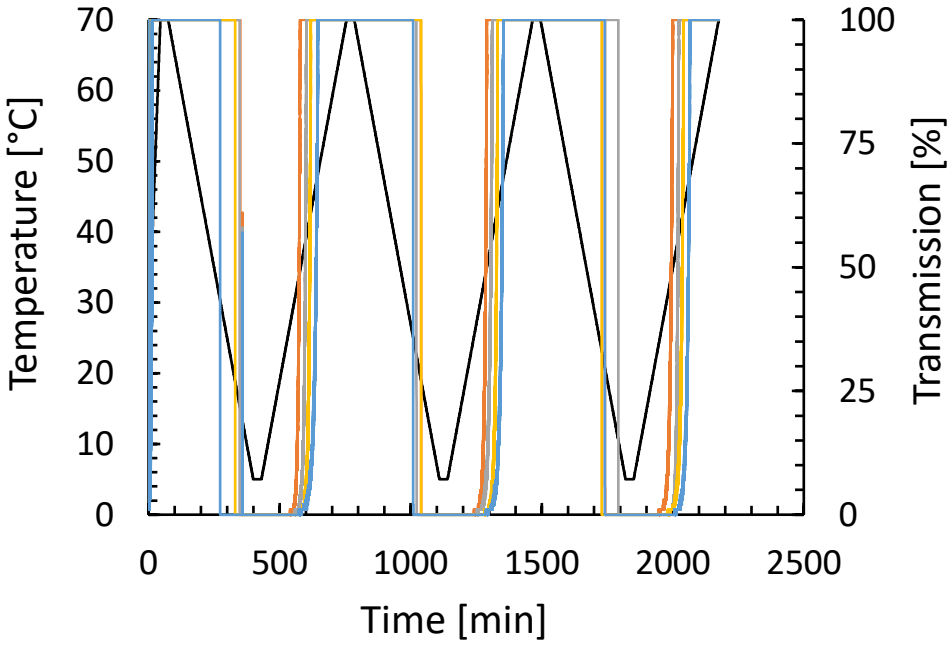

Figure. 2.2. Transmission trace for 4 different concentration solutions. The temperature is increased (black line) to 70°C to ensure complete dissolution and held for a period of 30 minutes. It is then decreased at a known cooling rate to 5°C and held for 30 minutes. It is then subsequently heated up again for dissolution and a new repeat cycle of crystallisation/ dissolution is commenced. The figure thus shows three repeat cycles each providing measurements of light transmission through each sample over the temperature cycle. The point during the temperature decrease at which transmission reduces from 100% to 0 indicates formation of crystals i.e., the temperature limit of the metastable zone for the given sample's concentration; the point during the subsequent temperature increase where transmission increases again to 100% indicates dissolution of the crystal, i.e., the temperature which the given sample's concentration equals the solubility.

One limitation of the Crystal 16 is the lack of imaging to observe and validate what is seen on the traces.

The Crystalline by Technobis is a precision heating and cooling device with in-situ imaging combined with transmission. The vials are 8 mL which means larger volumes can be analysed but unfortunately the productivity is reduced due to the number of reactors halved from that of the Crystal 16. The incorporation of a camera imaging each sample makes this a much more powerful tool than the Crystal 16 as the transmission traces can be validated, crystal numbers can be recorded, and the crystal size evaluated. Images are typically taken at various intervals depending on the length of experiment and individual requirements (5,10, 15 seconds etc). By obtaining crystal numbers and sizes from the images, the secondary nucleation rate (Chapter. 4.) can be determined as can the crystal growth rate. Figure. 2.3. displays the change in crystal number at a particular time for an example experiment. This can be used to confirm the point of detection of secondary nucleation.

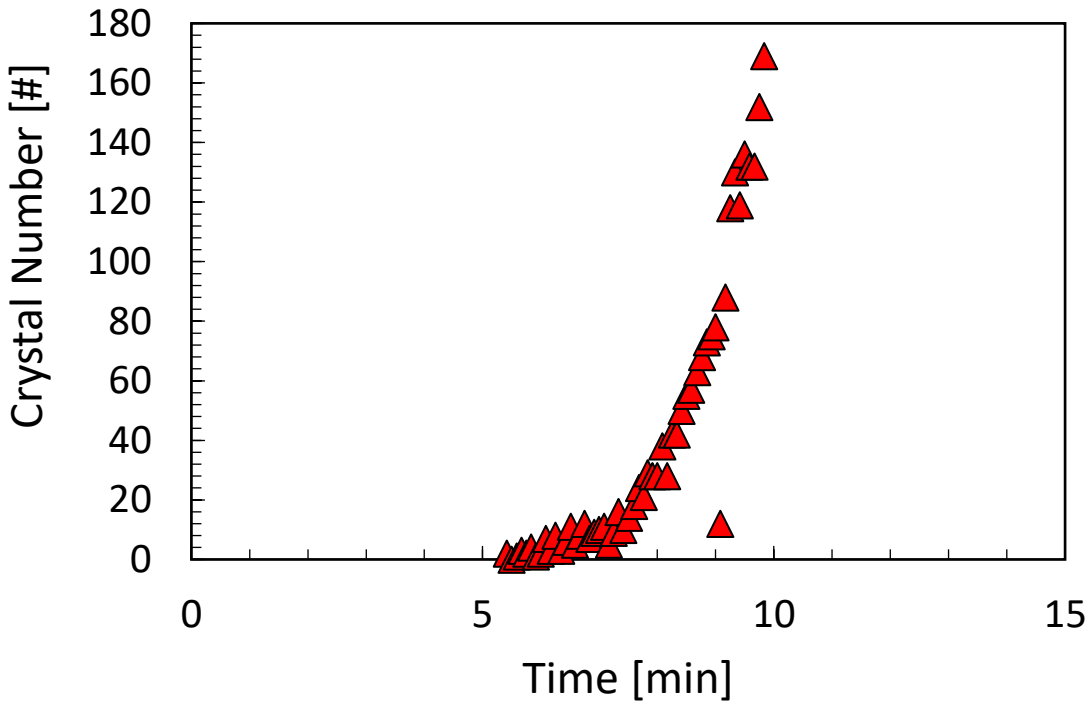

Figure. 2.3. The crystal number is shown against the corresponding time giving some information regarding the point at which nucleation is taking place. As shown in the figure, nucleation is initiated at a time between 5 and 8 minutes. The interpretation of such data is outlined in Chapter 4.

An example of a number weighted particle size distribution trace at a given time, following secondary nucleation detection is shown in Figure. 2.4. The Crystalline automatically outputs the particle size against time to a series of 99 bins ranging from 3 – 300 µm. This number weighted crystal size distribution can be converted to a volume weighted crystal size distribution to estimate the crystal growth rate (Chapter. 4.). Traces can be displayed at different points throughout the nucleation process to observe the evolution of the distribution. The details of how one goes from this 'raw' data to actual nucleation rates, crystal growth rates etc (i.e., calibration, noise levels, fitting etc) will be described in detail in Chapter. 4.

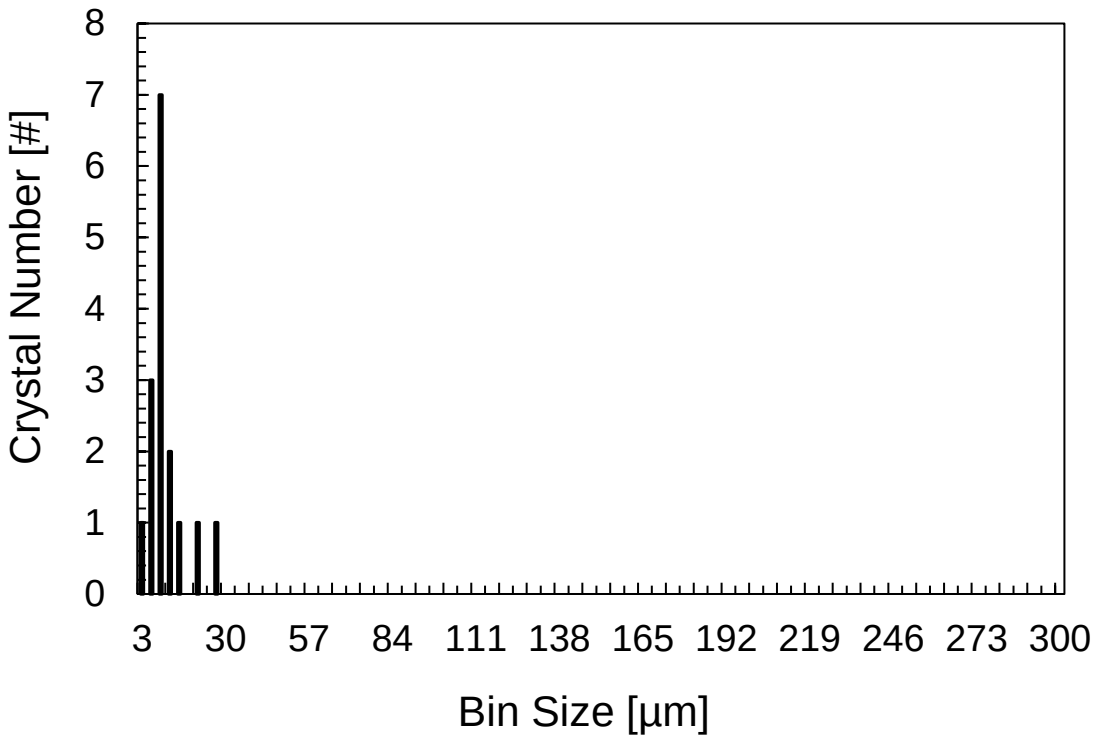

Figure. 2.4. A bar chart showing the crystal size distribution at the point of detection of secondary nucleation (Chapter 4.). This number weighted crystal size distribution is automatically generated from the Crystalline precision heating and cooling instrument.

2.3.3 Larger scale stirred tank reactors

The EasyMax (100 mL) and OptiMax (1 L) stirred tanks by Mettler Toledo are commercially available reactors which have a robust user interface enabling simple design of precisely maintained temperature profiles. If data is logged using Mettler Toledo process analytical technology (PAT) tools (FBRM, PVM or IR see section 2.4), the traces can be easily integrated using the IControl software. This enables simple interpretation of data, how shifts (dissolution, nucleation, or particle counts) relate to changes in the system and comparisons between different tools. Real time and post experimentation analysis of the process then becomes much simpler. Precise temperature

control is available, as well as a range of agitation conditions by using different impellers. Adjustment of temperature and agitation speed are easily achieved using the interactive touchscreen. A 45° pitched blade impeller was used in both reactors and the two experimental set-ups are utilised in Chapter. 5.

2.4 Analytical Tools

A brief overview of the theory and application of each analytical tool used in this thesis has been given below. A range of tools was required to determine polymorphic forms, detect changes in the system and count crystal numbers.

2.4.1 Powder X-ray Diffraction

X-ray power diffraction is a widely used, rapid technique for structural characterisation of materials and determining polymorphic forms. Quantitative information can be achieved regarding (potentially) multiple forms in each sample or impurities. This technique was used in Chapter. 3. to determine the polymorphic form of glycine for solubility analysis. The crystalline sample was firstly ground to a fine powder for analysis before measurements.

This information is detected when x-rays directed onto a powder sample are diffracted by the crystalline atomic structure, creating an intensity pattern which is essentially a fingerprint of the crystal form present in the sample. This technique was used in Chapter. 3. to confirm the polymorphic form of the crystallised solid that was taken forwards for equilibration concentration.

2.4.2 Attenuated Total Reflectance Fourier Transform Infrared Spectroscopy (ATR FTIR)

The ATR FTIR (Bruker Tensor II) can be used to generate structural information regarding the solid phase of a material following observation of the absorbance profiles of a sample. The somewhat limited sample preparation, requirement of only small quantities and rapid generation of an IR spectrum make this a powerful tool. Absorption is recorded as a function of wavelength and specific absorption bands represent functional groups in a sample. The resulting spectrum produced is then essentially a fingerprint of the compound. This technique was used to analyse finely ground sample used in the solubility experiments in Chapter.3. and employed to compliment the information gathered using Powder X-ray Diffraction.

2.4.3 Raman Spectroscopy

In Chapter. 4 seed crystals were prepared for secondary nucleation and crystal growth analysis. As previous analysis techniques were destructive (required ground powder), it was important to also analyse samples of the seed crystals which would be directly used in the experiments. The RXN1 Raman Spectrometer with PhAT probe from Kaiser was used for this application.

Raman spectroscopy is a simple tool used to assess the solid-form, solvent composition, and solute concentration. Monochromatic light is shone onto the

sample and a resulting change in the polarisation of the molecules makes them Raman active.

2.4.4 Optical Microscopy

Optical microscopy is a relatively simple technique which is widely used to visually characterise a sample. In this work, the Leica DM6000M 1Optical microscope was used to evaluate the size of the seed crystals (Chapter. 4. and Chapter. 5.) as well as the surface properties and shape. The differences in shape may indicate a different polymorphic form as mentioned in section 2.1.

This non-destructive technique enabled the same seeds analysed to be used in the experiments. The seeds were placed onto a slide which was moved onto a microscope stage. The microscope was focused, and images could be captured.

2.4.4 Particle Vision and Measurement (PVM)

Enhancements in quality and the relatively low cost of cameras make in-line analysis with probes such as the PVM (Mettler Toledo) an ideal choice for process monitoring. A 2-dimensional image of a crystal is produced as it passes through its field of view. Combined with image analysis software, the number, size, and shape of the particles in view may then be either processed in real time or post-processed to generate a nucleation or crystal growth rate. As the images can be seen in real-time, any morphological irregularities

resulting from polymorphic changes can be spotted instantly and the process can be corrected.

2.5. Couette Flow Cell

2.5.1 Summary and Background

Since the goal of the thesis is to explore the role of shear flow on secondary nucleation, a method to generate controlled simple laminar shear flow applied to a crystallising solution is required. The Couette cell with an outer rotating cylinder enables precise control over the flow regime of the solution within the gap. In order to provide a comparison of more complex geometries and a well-controlled simple flow, estimations were made regarding the typical shear rate distributions to be expected in the previously mentioned experimental set-ups (Crystalline, EasyMax and OptiMax), where flow is typically significantly more complex and less controlled involving a range of shear rates depending on location in the crystalliser and impeller design etc. The Couette cell was then designed and constructed with the idea to replicate these typical experimental flow conditions in a precise manner. It was also necessary to ensure that supersaturation could be precisely controlled by regulating temperature. It is however key to acknowledge that as measurements were conducted under isothermal conditions they can be defined as desupersaturation experiments. This indicates that as nucleation and crystal growth take place the supersaturation will not remain constant. Finally, it was essential that nucleation could be observed, and the kinetics estimated.

2.5.3 Flow Regimes in Couette Cell

When fluid is trapped in the gap between two concentric cylinders, and one of the cylinders is rotated, the fluid is sheared. The stability and form of the shear flow depends on which cylinder is rotated and which is held stationary. If the inner cylinder is rotated, at low velocities flow is known as cylindrical Couette flow and is stable, but this stability is swiftly lost as the velocity is increased forming Taylor vortices. Figure. 2.5. illustrates the map of flow regimes which can be explored by adjusting the Reynolds number (rotational rate in relation to time). The vortices are formed by the high-speed rotation of the inner cylinder causing fluid to be carried outwards and low-speed fluid at the outer cylinder carried inwards.

Conversely, when the inner cylinder is fixed and the outer cylinder is rotated, there is no formation of the Taylor vortices and there is a more stable laminar flow at higher velocities. In this study, a fixed inner cylinder was used with a rotating outer cylinder for precisely this reason. The aim was to ensure that for all measures of shear experiments, laminar shear was produced.

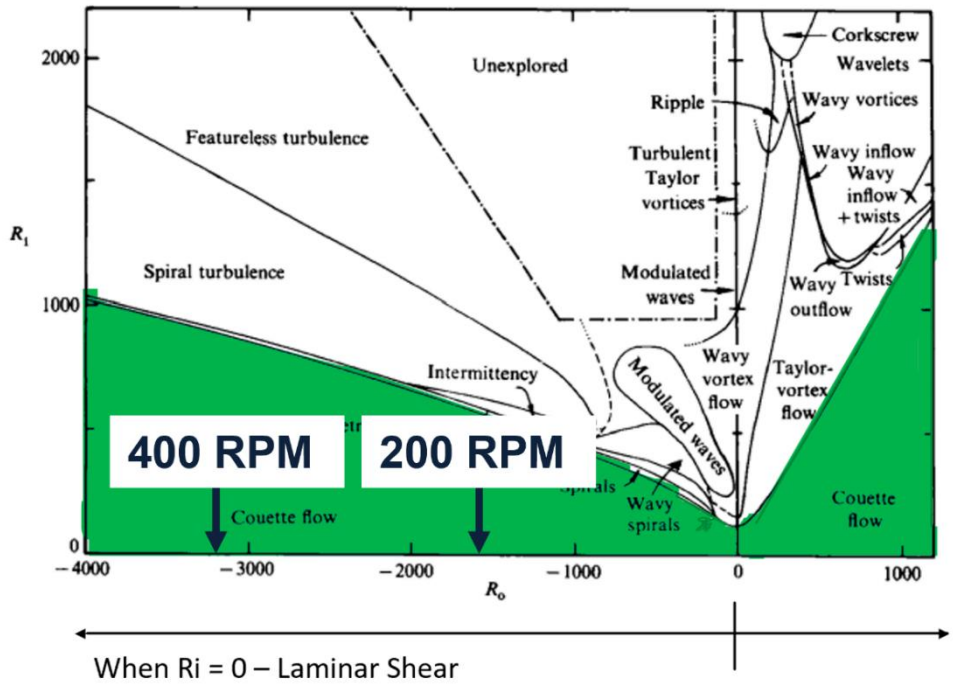

Figure. 2.5. The flow regimes experienced in a Couette flow cell showing the regimes for both inner (Ri on the y-axis which indicates Reynolds number with inner cylinder rotation) and outer (Ro on the x-axis which indicates Reynolds number with outer cylinder rotation) cylinder rotation. It seems that when assuming that the cylinders are correctly aligned, outer cylinder rotation with a stationary inner cylinder should result in laminar Couette flow. Adapted from Ref 3[3]. The two vertical arrows from the rotational rates indicate the approximate corresponding Reynolds numbers under the conditions in this work.

The Reynolds number is here used to determine the probable flow regime. As mentioned, by rotating the outer cylinder, it is expected that a laminar flow should be achieved, whereas inner cylinder rotation results in a range of complex flow behaviour which will not be covered in this work.

A basic definition of the Reynolds number is shown in equation 2.1. Where ρ is the density, v is the characteristic velocity, η is the absolute viscosity and D is the scale.

$$Re = \frac{\rho v D}{\eta} \quad \textbf{(Eq. 2.1)}$$

In this work the Reynolds number in the Couette cell can be calculated from equation 2.2 where *N* is the rotational rate, r_{out} is the radius of the outer cylinder r_{in} is the radius of the inner cylinder, with r_{out}-r_{in} providing the characteristic scale. $2\pi N r_{out}$ then gives the characteristic velocity (the speed of the outer rotating cylinder).

$$Re = \frac{\rho(2\pi N r_{out})(r_{out} - r_{in})}{\eta} \quad \textbf{(Eq. 2.2)}$$

The shear rate was then calculated from the characteristic velocity and the characteristic scale. This is shown in equation 2.3 which assumes a linear velocity profile across the gap where at the inner, stationary cylinder, assuming there is no slip, the velocity will be zero and at the outer, rotating cylinder, the velocity will be at its maximum, given by the rotational speed of the outer cylinder. This linear velocity profile across a gap is depicted in Figure. 2.6. with the arrows used to show velocity gradient. This implies that we are also assuming the shear rate is a constant across the gap, i.e., a simple laminar shear flow.

$$\dot{\gamma}_{avg} = \frac{2\pi N r_{out}}{r_{out} - r_{in}} \quad \textbf{(Eq. 2.3)}$$

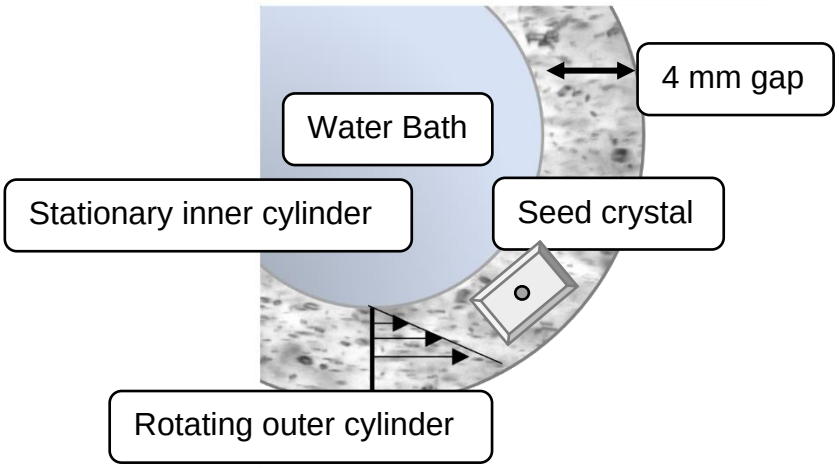

Figure. 2.6. A view from the top. The Couette cell is shown with the flow field displayed. The gap between the two cylinders is 4 mm allowing a 2 mm seed to be held in place, the outer cylinder is rotated, and the inner cylinder is kept stationary. The water bath system controls the temperature and therefore the supersaturation at a given sample concentration.

2.5.2 Design of the Couette Flow Cell

A Couette flow cell was designed and constructed with an aim to achieve laminar flow with an outer rotating cylinder. Two concentric, glass cylinders were manufactured with exact specifications regarding the dimensions (outer cylinder, 64 mm diameter and inner cylinder with a diameter of 56 mm), ensuring that there was a 4 mm gap between the two holding a volume of 50 mL of glycine solution throughout each experiment. A gap size of 4 mm was selected as the seed (2 mm ± 0.5) required space to be held to prevent any contact with the vessel wall. The gap at the base of the inner cylinder was 4 mm throughout each experiment with the aim to keep it as small as possible to prevent complications with the flow regime. The experimental set-up is depicted in Figure. 2.8.

The inner cylinder was hollow and used as a water-bath to maintain a constant temperature in the gap throughout the experiment. The water-bath temperature was maintained using a pump system connected to a heater/ chiller. In order to maintain similarities to previous experiments, temperature profiles were then set with the heater/ chiller system which enabled precise control from the dissolution temperature of 40°C to the working temperature of 25°C. Previous Couette cell experiments didn't have this level of temperature control[4] and so, confirming an accurate supersaturation with precise control may have been difficult. The temperature profile was then validated using two thermocouples, one in the central cylinder (water bath) and the other in the gap between the two cylinders. The temperature profiles were recorded using the PicoLog TC-08 and corresponding software. This is shown in Figure 2.7.

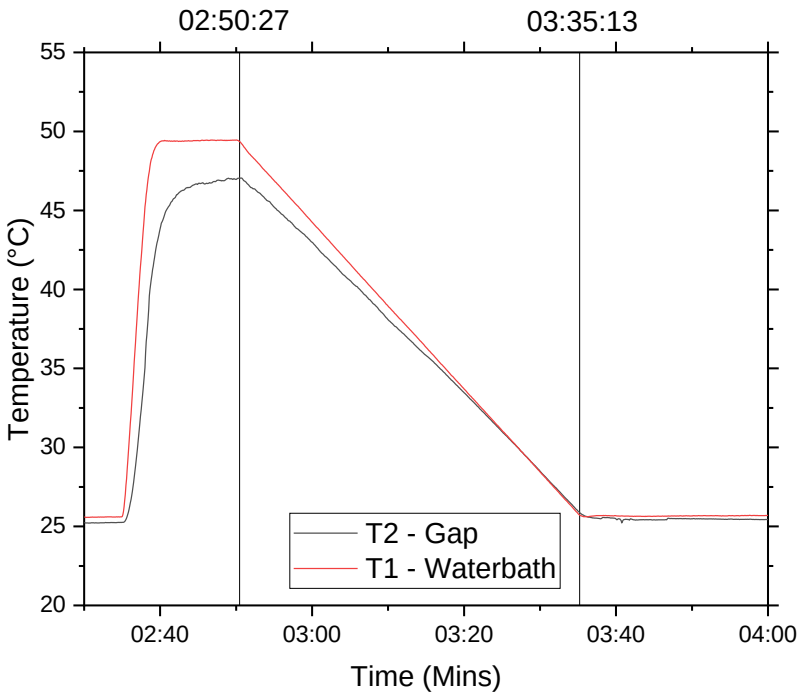

Figure. 2.7. The temperature profile with a thermocouple located within the centre of the water bath (red line) and one thermocouple located in the gap (black line) where the seed crystal would be located, showing that the gap temperature responds quickly to a change in bath temperature, validating the method used to control the supersaturation.

The outer cylinder was then connected at the base to a motor (Radleys RS50) and fixed in place, the rotational rate could be controlled using the analogue display on the front of the motor. The inner cylinder was attached to a stand and could move only directly upwards or downwards guaranteeing that the position of entry was unchanged each time. As an extra precaution, a guide was printed and fitted between the two cylinders which the inner cylinder must pass through upon entry. Within the guide (Figure 2.8) there was a hole with a diameter of 1.5 mm, used to hold the seed-holder (Hirschmann glass capillary tube, 100 mm L, 1.5 mm OD) in place. The seed was then glued to the base of the holder (Loctite Precision Max) and slotted between the two concentric cylinders.

The experimental set-up was then monitored using a high-speed camera, where the seed was observed throughout the experiment and images were taken every 5 seconds. Stability of the flow regime was confirmed using the video function of the high-speed camera. The Photron FASTCAM SA1.1. high-speed camera was used in this study with a capability to record short sequences of images at a framerate of 5400 fps at a resolution of 1024 x 1024 pixels. A suspension was created, and the direction and path of the particles was tracked. Other, more accurate techniques are available, but this provided a quick and easy confirmation. Details outlining solution and seed preparation

are outlined in Chapter.5. with the experimental results from the Couette cell work.

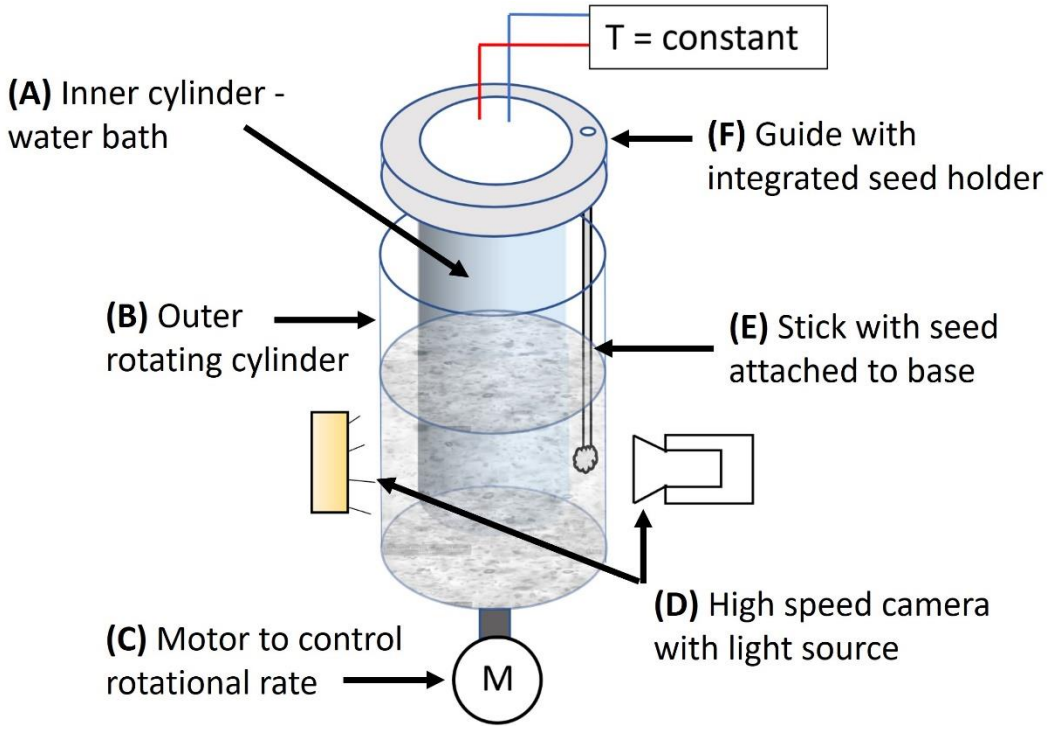

Figure. 2.8. The experimental set-up for the Couette cell experiments. The outer cylinder was rotated at a selected rotational rate using a motor attached to the base. A seed was held in place and subject to controlled shear at a selected shear rate for a period of time. The temperature and thus, supersaturation, was controlled with constant cycling through a heater/ chiller system. The experiment was monitored using a high-speed camera throughout.

2.5.3 Measuring Nucleation in Couette flow cell

A simple approach to gain quantitative insight from the Couette flow cell was to use imaging. High quality imaging combined with image processing tools, enables not only the point of nucleation to be detected but depending on the camera, real information regarding the number and size of the crystals to be analysed. In this work snapshots were taken every 5 seconds throughout an

experiment and images were post processed. The images were processed using an algorithm previously developed at CMAC Future Manufacturing Research Hub. Crystals were automatically detected and the number of crystals in focus were recorded at a corresponding time (Figure 2.10.). The large, seed crystal held in place was then simultaneously imaged in order to record a change in size over time. This was then taken as the rate of growth (Figure. 2.9.).

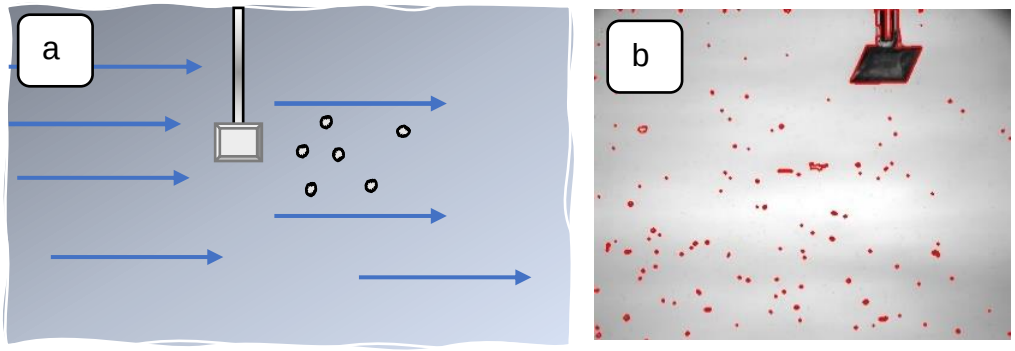

Figure. 2.9. (a) A schematic of the seed held in place and flow past the seed removing crystallites from the surface. (b) an actual image taken using the high-speed camera and processed using the image analysis algorithm. As shown, the size of the seed crystal is tracked, and the number of crystals is recorded.

The induction time was recorded at the point of inflection following a period of stabilised number counts. The inflection point, shown in Figure. 2.10. by the arrow labelled T_{ind} is in this case a clear and obvious rise in number count beyond 20 crystals. As this set-up was designed, constructed, and built 'in-house', the position of the background lighting in relation to the camera was not fixed in place. Therefore, there is a significant baseline noise level of objects that the image processing detects in any image, and the exact level of

this noise depends on the lighting condition. Therefore, it was not possible to set clear boundaries (as done with the Crystalline) and say that beyond 20 crystals, nucleation was initiated each time. One way to circumvent this issue would be to use background reduction algorithms or build a fixed bracket ensuring that the camera set-up was in the precise, same location for each experimental run. As the onset of nucleation (T_{ind}) could still be clearly identified (Figure 2.10) as the point at which the number of identified objects begins to rise consistently and rapidly above the noise, the elevated background was not interpreted as a significant concern for this work.

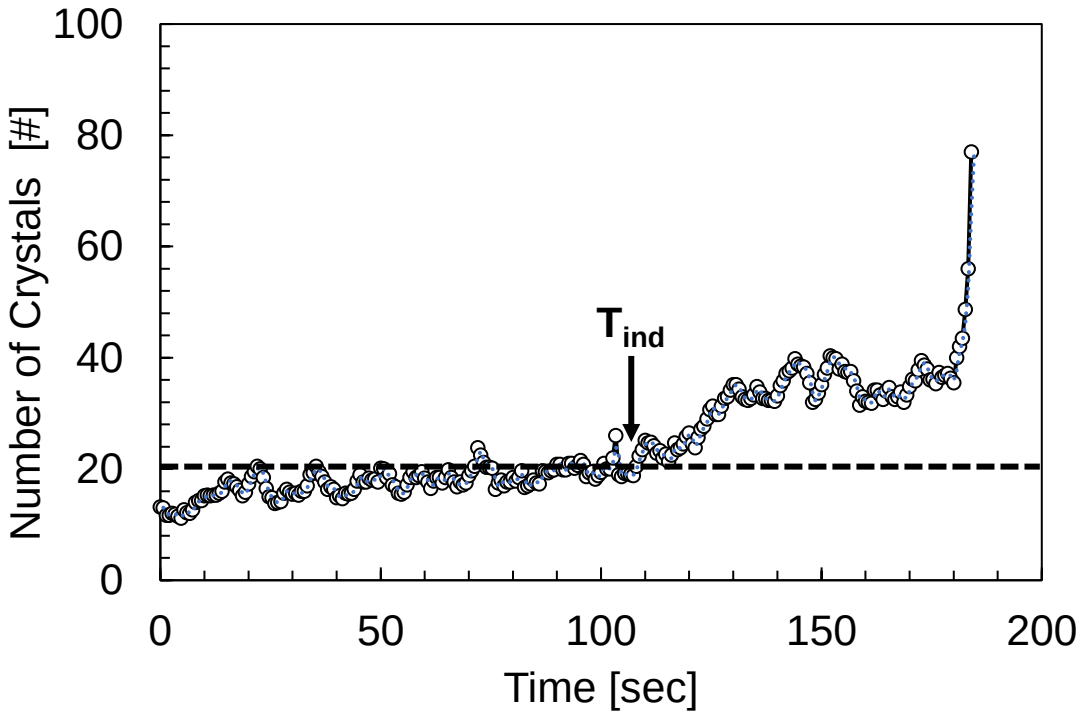

Figure. 2.10. The induction time is recorded from the number of particles tracked against time. As a clear and consistent increase in the number of crystals is detected, the induction time is recorded.

2.6. Key Points

- Model compound identified and information provided regarding solid form and morphology.
- Overview of the reactors used in the small- and large-scale stirred tank experiments and methodology of measuring solubility and metastable zone via in-situ visual techniques.
- Description of the theoretical and application of typical process analytical technology used and advanced characterisation techniques.
- An overview of the design and development of a Couette flow cell with in-line particle counting technology enabling application of a laminar shear flow to the nucleating solution, with or without a suspended seed, at shear rates comparable with the typical rates of the more complex uncontrolled flows in the stirred tank reactors.

2.7. References

(1) Vesga, M. J.; McKechnie, D.; Mulheran, P. A.; Johnston, K.; Sefcik, J. Conundrum of γ Glycine Nucleation Revisited: To Stir or Not to Stir? *CrystEngComm* **2019**, No. 21, 2234–2243. https://doi.org/10.1039/c8ce01829d.

(2) Brandel, C.; ter Horst, J. H. Measuring Induction Times and Crystal Nucleation Rates. *Faraday Discuss.* **2015**, No. 179, 199–214. https://doi.org/10.1039/c4fd00230j.

(3) Swinney, H. L. Flow Regimes in a Circular Couette System with Independently Rotating Cylinders. *J. Fluid Mech.* **1986**, *164*, 155–183. https://doi.org/10.1017/S0022112086002513.

(4) Forsyth, C.; Mulheran, P. A.; Forsyth, C.; Haw, M. D.; Burns, I. S.; Sefcik, J. Influence of Controlled Fluid Shear on Nucleation Rates in Glycine Aqueous Solutions. *Cryst. Growth Des.* **2015**, No. 15, 94–102. https://doi.org/10.1021/cg5008878.

Chapter. 3. An Experimental Evaluation of α-glycine Solubility Using Multiple Experimental Techniques

3.1 Introduction

Crystallisation is a purification technique, in which the success depends on accurate and precise knowledge of the thermodynamic properties of a system including the solubility of a compound in a selected solvent.

Solubility can be defined as the maximum mass of solute per mass of solvent, i.e., solute mass concentration C*(T), that will dissolve in the solvent and be at equilibrium in the solution phase; any increase in solute will take the solution out of equilibrium and the excess solute will form a crystal phase to re-establish equilibrium. Measurements of C*(T) at a range of temperatures – where C* is the solute concentration at which crystal forms at the temperature T – lead to the concentration vs temperature phase diagram to be depicted and the solubility line obtained, i.e., how the solubility or saturation concentration C*(T) depends on temperature. If the concentration is increased or decreased beyond or below the saturation concentration, the solution becomes either supersaturated or undersaturated disrupting the balanced state of equilibrium and results in crystallisation, or dissolution, respectively to regain stability. Therefore, the driving force for nucleation and crystal growth is supersaturation.

Supersaturation may be defined in a variety of ways such as, C(T)/C*(T) where C(T) is the working concentration and C*(T) is the solubility. The degree to which a solution is supersaturated will have a significant effect on the crystal nucleation and growth kinetics in a crystallisation process, and thus supersaturation is a key control parameter in process design. For example in a seeded crystal manufacture process based on secondary nucleation, if the

supersaturation is too high then primary nucleation may occur resulting in metastable forms or oiling out[1] and if it is too low (and the solubility is not precise) then dissolution of seeds may take place. Thus, calculating the correct supersaturation depends on accurate knowledge of the true solubility C*(T), and inaccurate solubility measurements will be detrimental to the design of a robust industrial crystallisation process.

An accurate measure of the solubility of a compound in a particular solvent across a wide range of temperatures is thus necessary for optimal design of a crystallisation process. Ideally, the solute to be crystallised should be readily soluble in the solvent[2]. Typically, a route to crystallisation would then be selected based on the thermodynamic properties of the compound i.e., the solubility curve. In most situations, an increase in the temperature typically leads to an increase in the saturation concentration. Preferably there would be a rapid change in C* for small change in T (steep solubility curve) enabling nucleation to take place and temperature be used to navigate the metastable zone (Chapter 1.). Unfortunately, this is not always the case e.g., the solubility of NaCl in water[3]. In these instances, alternative crystallisation methods must be selected to increase the yield. Some of these alternatives include, melt crystallisation[3], evaporative, precipitation and anti-solvent. In this work we focus on supersaturation-driven crystallisation from solution so these other methods will not be considered further.

Over the years many techniques have been proposed for the measurement of solubility, and currently there is a lot of time spent in the solvent screening and selection stages for optimal drug solubility[4]. Therefore, two key questions are

generated. What is the most accurate way to measure solubility and what is the most time and resource efficient technique? Although this property is known to be critical in the design and control of a process, a quick scan through the published literature clarifies that not all techniques are equal[5]. Reported experimental results for systems such as glycine[6,7] (Chapter 1., Figure 1.1.) show inordinate spreads in values under the same, given set of process conditions. One method previously developed, showing promising results is the application of pressure to measure solubility at high temperature. This technique raises the boiling point and controls evaporation making measurement easier[8]. Unfortunately, the specialised equipment required for this technique results in it being overlooked.

In this chapter, three simple methods frequently used to measure solubility will be critically evaluated across a range of conditions and the results compared with thermodynamic models taken from literature. The aim will be to then provide an informative, practical guide to researchers when choosing to select the appropriate method for solubility analysis.

3.2 Experimental

3.2.1 Preparation of Stock Solution and Crystallisation of α and γ-Glycine

The first challenge is to ensure that the solubility measurements are carried out involving a given polymorphic crystal form. Glycine as purchased is supplied as a solid powder with an unknown crystal polymorph and hence,

recrystallisation is essential in a controlled way to obtain a known polymorph. Glycine was re-crystallised using a simple cooling crystallisation method[9]. To acquire crystalline α-glycine, a solution was prepared with a concentration of ~300 g glycine per kg water. Solid commercial glycine powder (≥99% electrophoresis, Sigma Aldrich) and de-ionised water (Milli-Q, 18.2 MΩ cm) were used. Using a hot plate (IKA RCT Basic) with magnetic agitation the solution was heated to ~70°C and stirred at 700 rpm ensuring the solution was completely dissolved. The solution was subsequently cooled to room temperature by simply removing the vessel from the hot plate. However, a previously outlined methodology[9] was followed in order to crystallise γ-glycine. This involved a quench cooling technique where the vial was removed from the hot-plate and immediately placed into an ice-bucket to 'crash-cool'.

Following crystallisation, a thorough characterisation was completed to determine whether the correct polymorphic form could be reliably obtained. The crystalline sample was removed from the vial and placed onto a dish for any remaining solvent evaporation. Once dry, a pestle and mortar were used to grind the crystals to a fine powder for analysis.

A combination of Attenuated Total Reflectance Fourier Transform Infrared Spectroscopy (ATR FTIR) and Powder X-ray Diffraction (XRPD) was used to confirm the polymorphic form of the glycine material obtained under the given crystallisation conditions, to ensure that we know to which polymorph the subsequent solubility measurements apply. The ABB MB300 was the FTIR used for this experimental study at a wave number between 600 and 4000 cm^{-1}. The PXRD pattern was obtained using the Brucker D8 Advance II

diffractometer with Cu Kα radiation at 50 mA and 40 kV. All FTIR spectra and XRPD patterns were obtained at 20°C temperature.

3.2.2 Gravimetric Equilibration Method

Equilibrium concentration measurements are widely accepted as an accurate technique for solubility determination. A suspension is firstly created of a known mass of solute, in a known mass of solvent under a given set of conditions (temperature and pressure) and held for a period to allow dissolution. Quantification of the solution composition can then be achieved by gravimetric analysis or high-performance liquid chromatography.

As outlined in Chapter 2 the Polar Bear Crystal Plus from Cambridge Reactor Designs is a precision heating and cooling instrument capable of maintaining temperature for long periods with minimal temperature variation. In the work presented here, this instrument was used to maintain the temperature of solutions assessed using gravimetric analysis by measuring the mass of solute in the saturated solution at equilibrium with the crystal, at a given temperature, this technique provides a measure of the solubility or saturation concentration and its dependence on temperature.

At each temperature, three solutions containing an excess of solid, finely ground α-glycine were prepared by weighing a known mass of glycine directly into vials (VWR; 10mL screw neck vials) followed by the addition of 10 mL de-ionised water. Three new 10 mL solutions were prepared at each temperature. A Teflon coated magnetic stir bar was then added to each of the individual

vials. The vials were placed into the Polar Bear and kept under isothermal conditions at a selected temperature for an equilibration period of 24 hours stirred at 600 rpm.

Measurements were recorded at intervals of 10°C ranging from 5 to 65°C. To record a measurement, a sample was removed directly from the vial using a syringe (3 mL), the sample solution was subsequently passed through a 0.2 μm filter onto an empty plastic dish to remove the excess, suspended solid glycine. The mass of the plastic dish was weighed firstly empty and then weighed again with the filtered glycine solution. The dish was placed into a vacuum oven for a period of three days to ensure that all the solvent was removed. The plastic dish containing solid, crystalline glycine was then weighed again. By subtracting the known mass of the plastic dish from each sample, the complete mass of solution and mass of glycine in solution is known. Once the total mass of filtered solution and mass of glycine in solution is known, a simple calculation enables the determination of the solution concentration representative of the saturation concentration (solubility) at that temperature. This is shown in equation. 3.1.

$$\text{Solution concentration} = \left(\frac{\text{Final Mass Glycine}}{\text{Mass Water}}\right) \quad \textbf{(Eq. 3.1)}$$

Challenges with measuring solubility at high temperature have been previously outlined in literature[6]. Physically taking a sample in a ‘direct sampling’ procedure such as gravimetric analysis becomes difficult as temperature is increased. Not only from a safety perspective, but other unforeseen events

obscure the result. In this work, as the temperature of the solution was increased, immediate recrystallisation was spotted within the syringe on sampling which was thought to be due to a rapid drop in temperature. Therefore, only with the implementation of an extra step could solubility measurements be recorded at high temperatures, beyond 65°C. The syringe was partially filled with a known quantity of de-ionised water creating an instant dilution or reduction in glycine concentration on sampling. This provided a chance to filter, avoiding spontaneous crystallisation and ultimately enabled measurements to be taken at 100°C.

3.2.3 Solute Addition for High Temperature Solubility and Triple Point

Next, the solute addition technique was carried out using the Polar Bear Crystal Plus but here, a different fixture was mounted to the top which allowed a larger volume to be used. The vessel was sealed, and glycine was added directly using a funnel ensuring that there was no loss of solvent throughout.

250 g of de-ionised water was firstly added to the Polar Bear at 50°C followed by the addition of 125 g of glycine. The glycine was dispersed using an overhead stirrer (SciQuip Basic 20 using a Teflon coated blade pitched impellor) at 500 rpm. The temperature was continuously and gradually increased, monitored visually until dissolution occurred and at this point, the sample concentration is effectively equal to the saturation concentration at the current temperature, i.e., C*(T) = C = current mass of added glycine /mass of water, giving a measure of C*(T). Subsequently, with the temperature still

increasing, known further quantities of glycine are added, increasing again until dissolution is observed, giving the next value of C*(T), and so on. Known quantities of glycine were then added in series and the point of dissolution (temperature) was noted up until the moment when the temperature no longer increased with an increase in glycine concentration i.e., the triple point.

3.2.4 Polythermal Approach

The metastable zone width is a region between the solubility curve and the metastable limit: in this region, nucleation of crystal phase from the supersaturated solution takes some finite time which reduces to zero at the metastable limit (Chapter 4.). This region provides the working parameters for secondary nucleation studies where we require primary nucleation to be suppressed for long enough such that secondary nucleation becomes the dominant process. The polythermal approach was completed using the Crystal 16 by Technobis Crystallisation Systems. This is a reactor enabling precise control over the temperature cycling programmes of individual vials with built in laser technology to measure clear (solubility) and cloud (metastable limit) points (Chapter 2.).

Individual vials were firstly prepared by weighing a known mass of finely ground glycine directly into the vials (VWR; screw vial, ID = 1156587 411.6 mm x 32 mm height, neck diameter 8 mm, total volume 1.5 mL). Once de-ionised water (1 mL) was added, the vials were tightly sealed and placed into the reactor system. Four heating rates were selected from 0.1 - 0.5°C/ min with

a temperature range used of 5-95°C with three cycles. At the highest concentrations beyond 700 mg/g the temperature range was set from 5-105°C. As the sample is heated, a change in transmissivity takes place and once dissolved the transmissivity reaches 100%. A series of concentrations were measured ranging from 225 mg/g to 725 mg/g.

To estimate the 'true' equilibrium solubility, the solubility was measured at each heating rate (0.1 - 0.5°C/ min) for a particular concentration and plotted vs heating rate. The theoretical 'zero heating rate' solubility representative of the 'true' equilibrium was then obtained by extrapolating a linear fit to the measured solubility vs heating rate to the 0°C/ min intercept.

3.3 Results and Discussion

3.3.1 Selective Crystallisation of Glycine Polymorphs

Ensuring both alpha and gamma glycine could be selectively crystallised was an essential first step before recording α-glycine solubility. It is often assumed that under stirred conditions, alpha glycine would be consistently obtained. To obtain gamma glycine, a crash cooling methodology would need to be employed.

To characterise the glycine crystals using either Attenuated Total Reflectance Fourier Transform Infrared Spectroscopy (ATR FTIR) or powder X-ray diffraction (PXRD) the crystals needed to firstly be ground into a fine powder. All spectra were recorded under ambient conditions.

Characteristic IR peaks were identified for the α polymorphic form at 907 cm^{-1}, with γ showing a characteristic peak at 927 cm^{-1}. There was a shared peak at 887 cm^{-1} as shown below in the example spectra (Figure 3.1.).

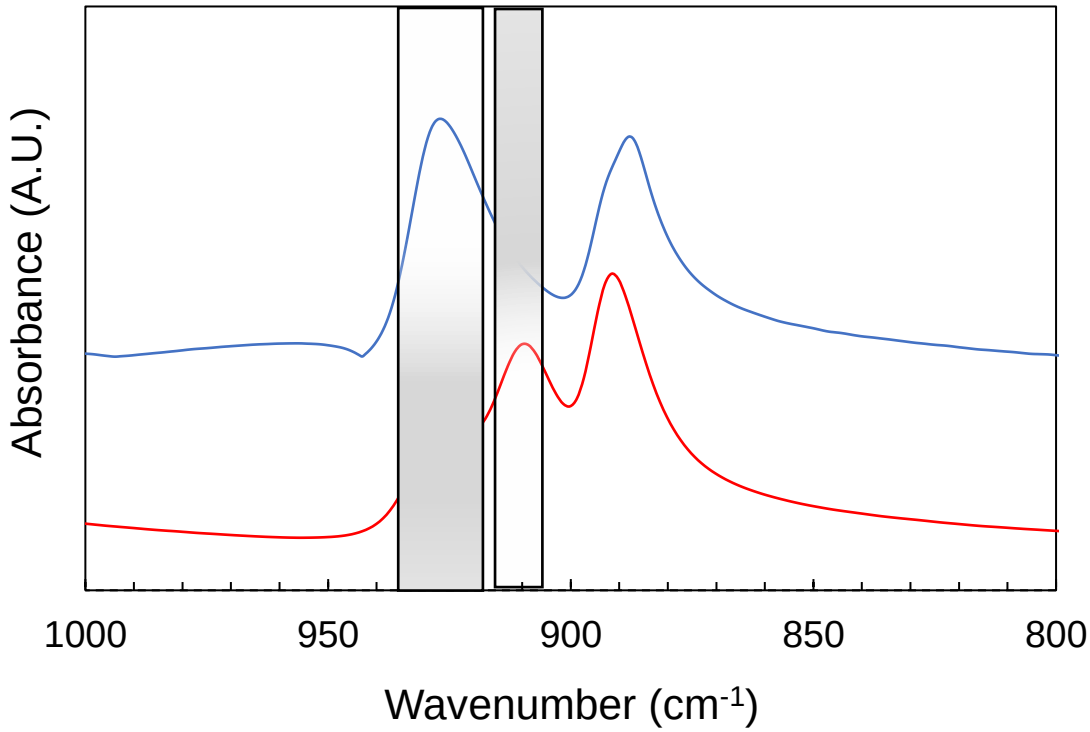

Figure 3.1. Characteristic IR spectra for α (red) and γ-glycine (blue)**.** The grey shaded boxes represent the characteristic peaks. Peaks are visible at 910 cm^{-1} for α-glycine and 928 cm^{-1} γ-glycine.

The PXRD pattern highlighted peaks at 2θ of 19° and 30° in correlation with what has been seen in literature for α-glycine[9] and 22° and 25.5° for γ glycine. The characteristic diffraction is shown in Figure 3.2. confirming that the correct form can be selectively obtained following the crystallisation methods described in this work.

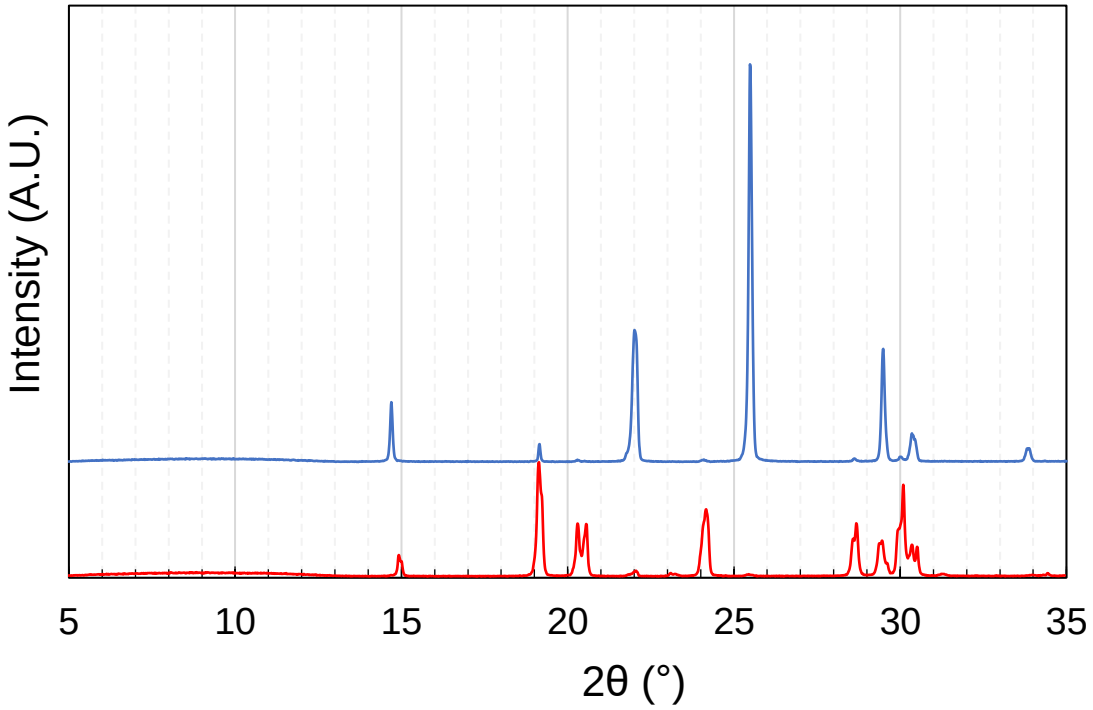

Figure 3.2. *C*haracteristic powder X-ray diffraction pattern for (a) for α-glycine and (b) γ-glycine. Characteristic peaks at 2θ of 19 and 30 α-glycine and 21° and 25.3° for γ glycine.

3.3.2 Equilibrium Concentration

In this study, gravimetric analysis was selected, and an equilibration period was provided of 24 hours to ensure that there was a thermodynamic state of balance within the system before any sampling. When considering the use of this technique, it was essential that excellent control over the temperature of the solution was maintained as this would result in an increase or decrease in the dissolved solute. In this work, α-glycine was selected as the model compound.

3.3.2.1 Gravimetric Equilibration Method

The most significant challenge faced was preventing re-crystallisation within the syringe following withdrawal of hot sample from the vial. Without the application of the ‘dilution’ technique above 65°C it was not possible to sample without the immediate and visible crystallisation of the solution on contact with the surface of the syringe. By partially filling the syringe with a known mass of water, the concentration of the solution was instantly reduced, and crystallisation could be visually prevented. Unfortunately, it is clear that there is still a loss of mass of solute on sampling at temperatures at >80°C. This is likely to be a result of an unaccountable increase in solvent due to the dilution method or crystallisation within either the syringe or filter making gravimetric analysis unsuitable for elevated temperature solubility measurements.

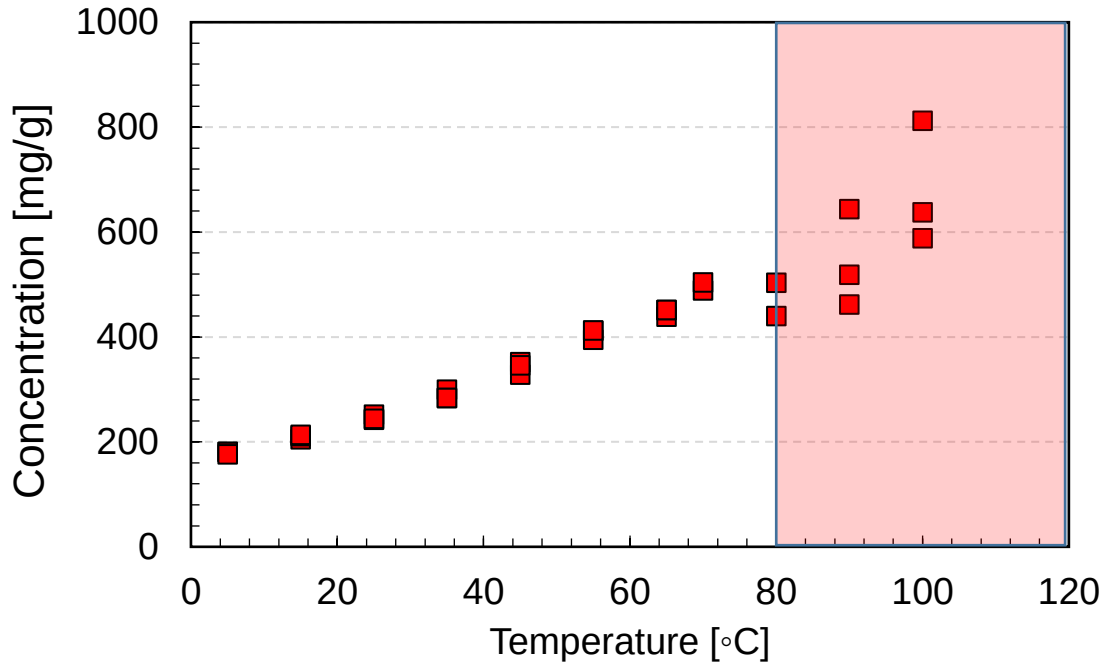

Figure 3.3. The solubility diagram of glycine in water recorded using the gravimetric equilibration method at temperatures ranging from 5 - 100°C. The red shaded region indicates the temperature at which recording a

measurement for the solubility of glycine becomes challenging due to recrystallisation within the syringe.

3.3.3.2 Solute Addition for High Temperature Solubility Measurements

There are a series of challenges encountered when recording a solubility measurement at elevated temperatures. This region is indicated by the red shaded region above 500 mg/g in Figure 3.3. where it was concluded that gravimetric analysis may not be suitable under these conditions. Under challenging conditions, such as the high temperature region in Figure 3.3., to record accurate and precise measurements the contact between operator and sample should be minimised to prevent loss of mass due to evaporation and recrystallisation on other colder parts of the apparatus used. The term contact here refers to physically having to remove a sample to record a solubility measurement.

The solute addition method is compared with results from the equilibration technique in Figure 3.4. displaying solubility values ranging from 70°C to the triple point at 108.3°C with a concentration of 918.8 (±10) mg/g. Glycine was added in known quantities as temperature was continuously, gradually increased and the point of dissolution noted following each addition, removing any requirement of manual sampling. All weights were recorded, including those of the funnel and transportation vessel, ensuring that it was only the exact mass of glycine added to the beaker that was documented in the solubility calculation.

The values recorded using the solute addition method are in the projected region, in line with those solubility values measured under standard and unchallenging conditions below 500 mg/g. This indicates that there is no solute loss, which is likely a result of the lack of sampling, and there is no significant increase in concentration which would result from loss of solvent by evaporation, possible when working at elevated temperatures.

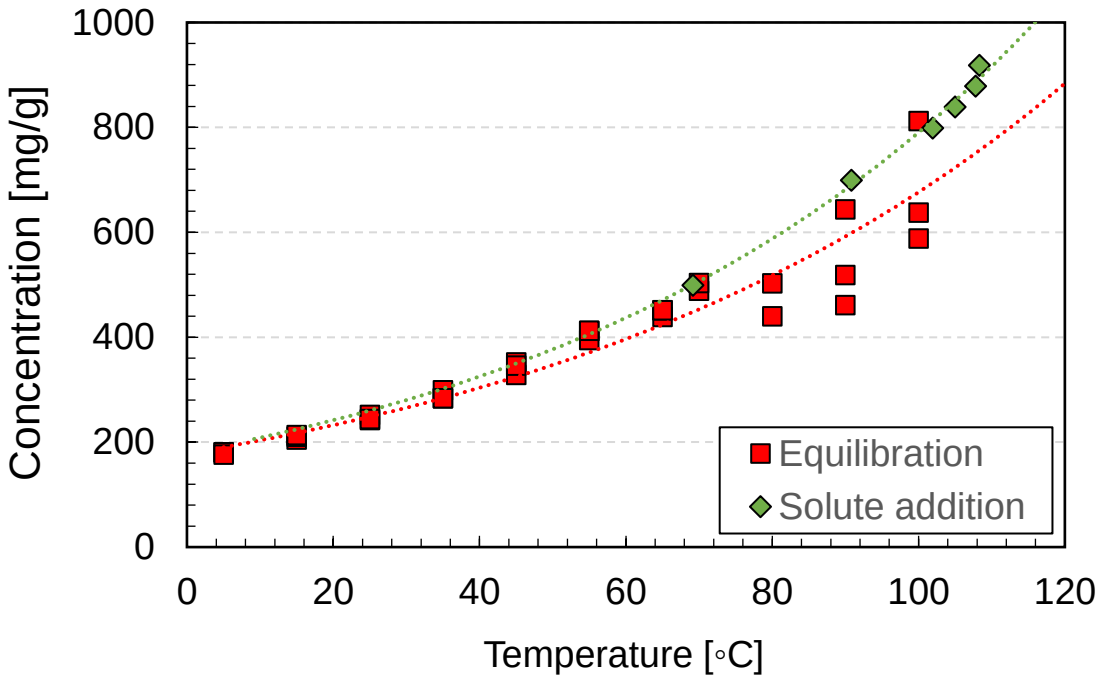

Figure 3.4. The glycine in water solubility diagram and the high temperature solubility measurement recorded using the solute addition approach (green diamonds). As the temperature was increased, glycine was added at known quantities until the point at which no further glycine was dissolving and the temperature of solution was not increasing any further.

3.3.3 Polythermal Temperature Cycling

As mentioned, the equilibrium concentration method can be both laborious and time consuming. Even if this technique was accurate and precise, this may not be the only aspect an operator is looking for.

The polythermal approach is one in which solubility values can be rapidly generated. An example of an approach used in industry to select a suitable solvent may typically begin with an initial broad computational solubility screen, followed by a two-point (~8 solvents) solubility measurement with a final complete assessment of the thermodynamic properties of two or three solvents using small-scale set-ups such as the Crystal 16 and Crystalline (Technobis Crystalline Systems). A selection may then be made in relation to the ability to achieve a high yield under efficient (temperature, pressure) processing conditions.

Although the polythermal method enables rapid solubility generation, often the dependence of ‘recorded’ solubility on the heating rate is overlooked. Therefore, operators may select a ‘fast’ heating rate but inadvertently generate incorrect values for solubility affecting the downstream processability and reproducibility.

In many of the polythermal techniques, a change in the system is detected by monitoring the ‘cloud point’ or ‘clear point’ using a transmission probe. The sensitivity of this method means that it is not always the point of solubility or recrystallisation which initiates an increase or decrease in transmission (e.g., impurity or region of low crystal density).

3.3.3.1 Assessing Solubility using the Crystal 16

The solubility of α-glycine in water was estimated from clear point temperatures measured at several different heating rates between 0.1 and 0.5°C/min over a wide range of glycine concentrations. Below, in Figure 3.5., the complete spread of solubility values of α-glycine recorded using the polythermal approach are displayed.

As solubility is a thermodynamic property, the solubility should not change in relation to the selected processing conditions, but the rate of detection can limit the ability to record a precise measurement. As mentioned, the Crystal 16 was used in this study which relies on transmission to determine the presence or absence of crystals.

It is apparent from Figure 3.5. that at each concentration, the subsequent dissolution (solubility) temperature is increased across all concentrations with an increase in heating rate suggesting that the heating rate should be considered when assessing solubility using the polythermal approach.

With a heating rate of 0.1°C/min, there seems to be some variation in the recorded values at concentrations between 425 – 600 mg/g, and it is consistent throughout all three cycles. Although it wasn't possible to observe images, one explanation is that, given the increased time spent at each temperature, the stir bar was immobilised upon recrystallisation and the glycine was not mixed efficiently, this inefficient mixing was shown recently using CFD simulations and x-ray CT imaging[10] and may hinder the ability to of solid crystalline glycine to dissolve.

The relationship between heating rate on solubility must then be a result of the limitations of the technique selected. It can be hypothesised that as the temperature changes more quickly through the cycle, the heat transfer may be rate limiting, hindering the ability of the solution to reach a thermodynamic equilibrium. Thus, it is likely that at a rate of 0.5°C /min there is a discrepancy between the temperature of the reactor (which we record) and the temperature of solution. The slower the heating rate, the more time available for the solution to equilibrate.

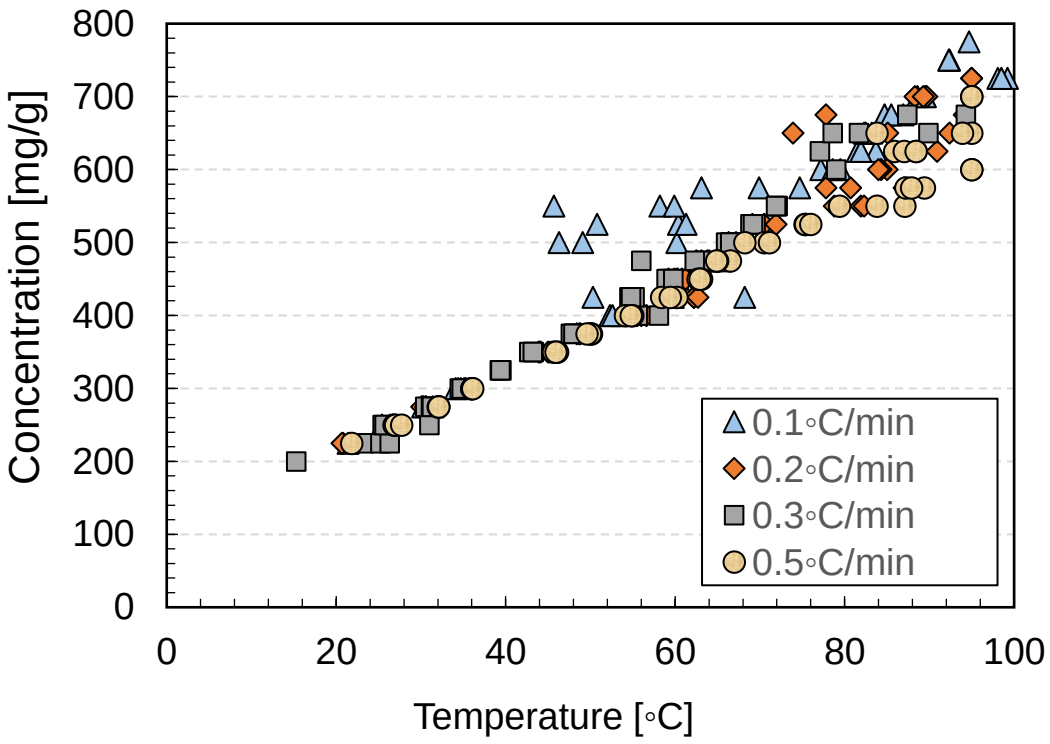

Figure 3.5. The solubility recorded using Crystal 16 at 4 different heating rates. The graph indicates that at the same concentration with a faster heating rate, the solubility temperature recorded is higher signalling a dependence of solubility temperature on heating rate.

However, it must be noted that a continuous decrease in the rate of temperature change does not always produce an increase in the precision of the results gained. This would only in effect increase the experimental time to above that necessary with no corresponding increase in the reliability of the gained results.

In an attempt to understand the system better and validate what is happening within the vials, it may be appropriate to suggest that alternative instruments such as the Crystalline with in-situ cameras should provide more robust analysis. It would be favourable to validate any detection using transmission with an in-situ camera.

3.3.3.2 Polythermal Solubility Extrapolations

Figure 3.5. suggests that there is a dependence of the clear point on the heating rate indicating that dissolution of suspended crystals during heating is kinetically limited. Hence, it is necessary to check the dependence of clear point temperatures on the heating rate and extrapolate to the zero-heating rate in order to estimate the solubility temperature corresponding to the ‘true’ thermodynamic equilibrium. Below a concentration of 400 mg/g data recorded shows reasonable reproducibility of clear point temperatures over repeated experiments at all four heating rates as shown in Figure 3.6. At each concentration, clear point temperatures are plotted for each heating rate (with three temperature cycles per concentration per heating rate) and a linear fit

calculated. The intercept of the fit (heating rate effectively zero) was then taken as the thermodynamic ‘true’ equilibrium solubility.

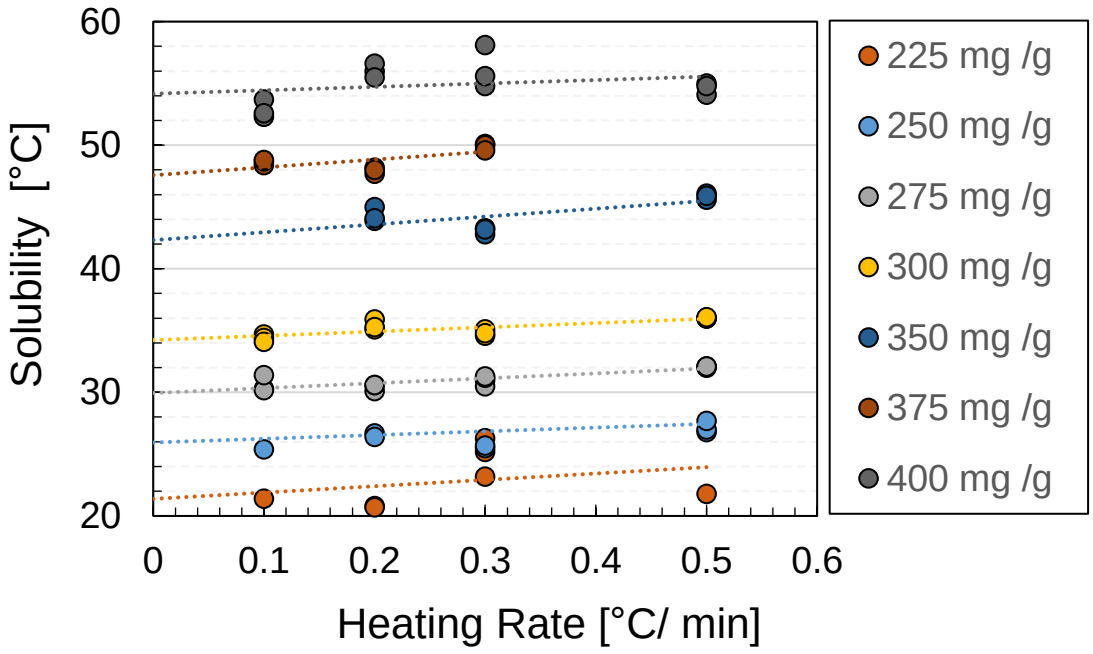

Figure 3.6. Solubility temperature extrapolations from a concentration of 225 mg/g to 400 mg/g. Four heating rates were selected ranging from 0.1 to 0.5°C /min, the intercept was taken as the ‘true’ solubility value.

The ‘true’ equilibrium solubility values from Figure 3.6. are then displayed in Table 3.1. with the corresponding concentration and the confidence interval on the intercept. It is clear that it is necessary to take the heating rate into account in conducting polythermal measurements of solubility. Here, the extrapolation of a linear fit was selected as the method in the absence of any more detailed theoretical basis. This is a technique which has been previously outlined in literature[11].

Table 3.1. The extrapolated solubility values recorded from the Crystal 16. The solubility column here is taken from the intercept and the confidence interval is shown in relation to this value.

Concentration (mg/g)	Solubility Temperature (°C)	Standard Error (±)
225	21.38	2.24
250	25.94	1.48
275	29.94	0.28
300	34.23	0.28
350	42.31	0.94
375	47.17	0.58
400	54.16	1.01

Figure 3.7. shows the same, extrapolation technique used for high concentration solubility measurements. As mentioned previously (section 3.3.2), sampling (e.g., gravimetric) methods of measuring the solubility at high temperature is challenging and limiting the contact that the operator is having with the solution is key to recording an accurate measurement to prevent losses of both solvent and solute due to evaporation and recrystallisation during sampling procedure. Furthermore, in methods such as the polythermal measurements discussed here, clear point measurements are also much less reproducible at higher concentrations which must be for other reasons, as

there is no sampling involved. This may be a result of several factors, including poor mixing and possible intermittent encrustation of glycine at the surface during temperature cycling in highly concentrated solutions.

Figure 3.7. reveals the true extent to the challenges discussed. There is evidently still a dependence of the solubility on the heating rate, but the reproducibility at a given concentration over the three repeat temperature cycles at each heating rate is now much more doubtful. Concentrations are displayed from 425 – 725 mg/g.

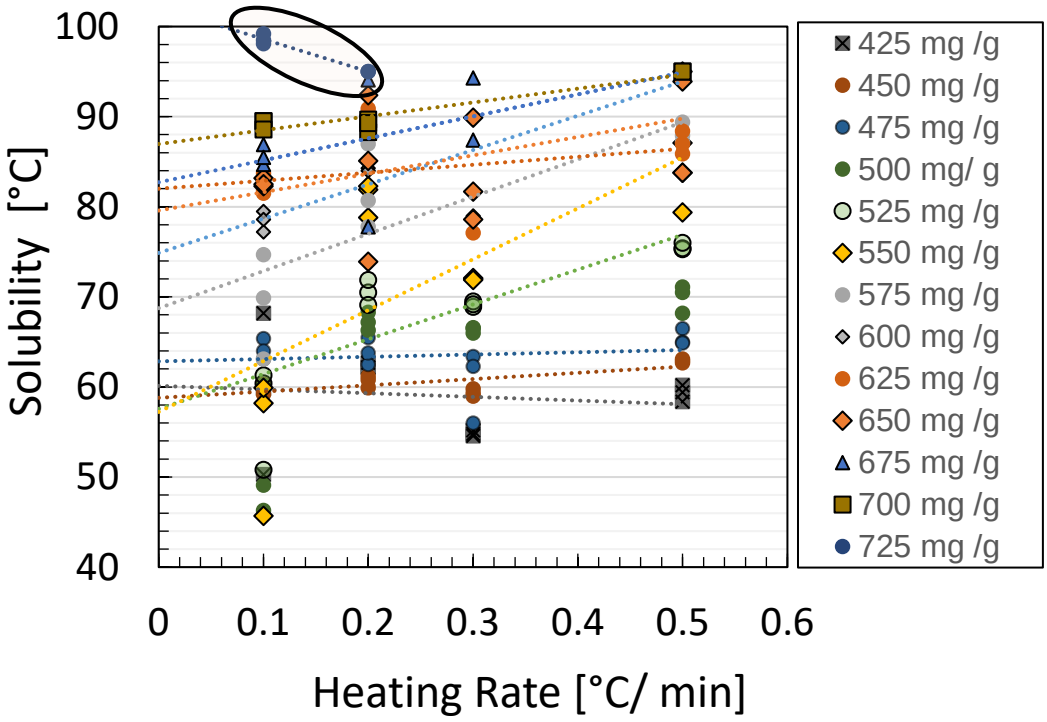

Figure 3.7. Solubility extrapolations from measurements at concentrations of 425 mg/g to 725 mg/g. Four heating rates were selected ranging from 0.1 to 0.5°C /min, the intercept was taken as the 'true' solubility value. The circled points represent an incomplete dataset at the maximum concentration of 725 mg/g and indicates a potential reason for the low standard error in Table 3.2.

Table 3.2. then shows the equilibrium solubility estimated from the linear fit in Figure 3.7. As mentioned, the solubility represents the intercept, and confidence interval on the intercept is then presented.

Table 3.2. The extrapolated solubility values recorded from the crystal 16. The solubility column here is taken from the intercept and the confidence interval is shown in relation to this value.

Concentration (mg/g)	Solubility Temperature (°C)	Standard Error (±)
425	60.12	3.01
450	58.79	0.66
475	62.84	1.71
500	53.57	3.57
525	57.56	2.76
550	57.23	5.64
575	68.7	3.55
600	74.87	2.02
625	79.58	3.56
650	82.00	2.97
675	82.71	5.33

700	86.96	0.64
725	102.2	0.62

The complete set of estimated, ‘equilibrium solubility as estimated from the heating rate extrapolation’ is plotted in Figure 3.8. As realised, using the polythermal technique to measure solubility provides a two-tier data set between ‘high’ and ‘low’ concentrations with intermittent encrustation and poor mixing of highly concentrated solutions thought to be the underlying issue. This seems to be displayed in Figure 3.8. where the dissolution (solubility) temperature is significantly lower at a particular concentration beyond 500 mg/g which suggests that the concentration in solution is much lower.

Within a typical working range of 20-50°C, the method can rapidly and accurately generate solubility data. As a threshold in concentration is reached (>500 mg/g) there are sudden, large deviations in the recorded values.

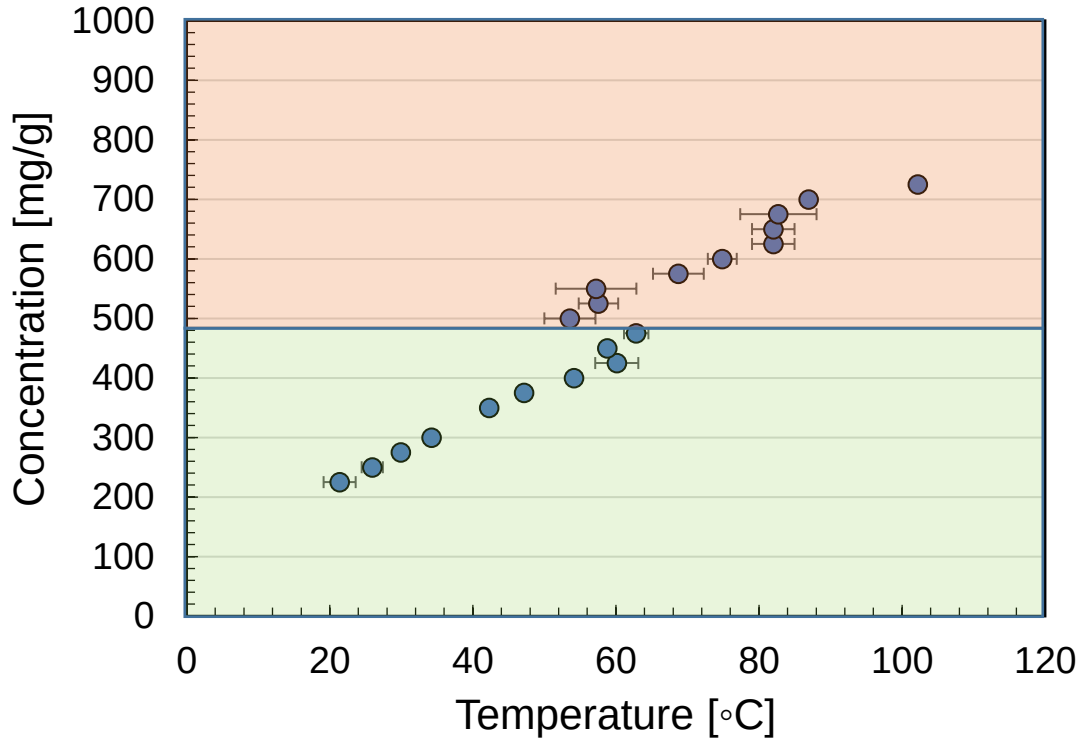

Figure 3.8. The glycine in water solubility diagram across the range of concentrations measured using the extrapolation, polythermal technique. This represents the value from the extrapolations of the heating rate vs temperature diagrams previously outlined (Figures 3.6 and 3.7.).

3.3.4 Comparing Techniques

The solubility of α-glycine measured using the three previously summarised techniques, polythermal temperature cycling, equilibrium concentration with gravimetric analysis and solute addition have been plotted together in Figure 3.9.

Below 400 mg/g, depending on individual requirements, any technique will enable the simple recording of accurate solubility data with values very nearly overlapping. However, as the concentration is increased beyond 400 mg/g, gravimetric analysis and polythermal temperature cycles present vastly

different challenges which must be overcome. Equilibrium concentration begins to show a loss of solute, most evidently at 80°C and beyond. From a health and safety perspective, it may not be practical to remove samples above this temperature range, even if a suitable method is found to enable representative sampling and prevent loss of mass. On the other hand, the polythermal method with heating rate extrapolation begins to show an increased distribution of solubility values at 500 mg/g. Ultimately, it seems that to achieve the recording of accurate solubility measurements at high temperatures, the only sufficient technique is solute addition, but this requires a significant amount of compound to be used and more operator time available for regular sampling and observation.

It can be concluded that selection of an appropriate technique depends on many aspects including time available, compound availability and regions of interest. The polythermal technique enables rapid data generation of solubility values but the heating rate needs to be considered and if possible, multiple heating rates should be utilised to enable the extrapolation backwards to the true equilibrium solubility. The ability of the magnetic stirrer to disperse the highly concentrated solution should also be studied as this may affect the dissolution process. Equilibration techniques enable precise measurements to be recorded at lower temperatures, but sampling becomes challenging as temperature is increased. This is also labour and time intensive as we wait for equilibration to be achieved. The solute addition method appears to be the most accurate technique and is the only feasible option at high temperatures due to the lack of sampling and ability of large overhead stirrers to be used for

dispersion. Once again, this technique is labour intensive and requires a significant amount of compound especially if it is highly soluble.

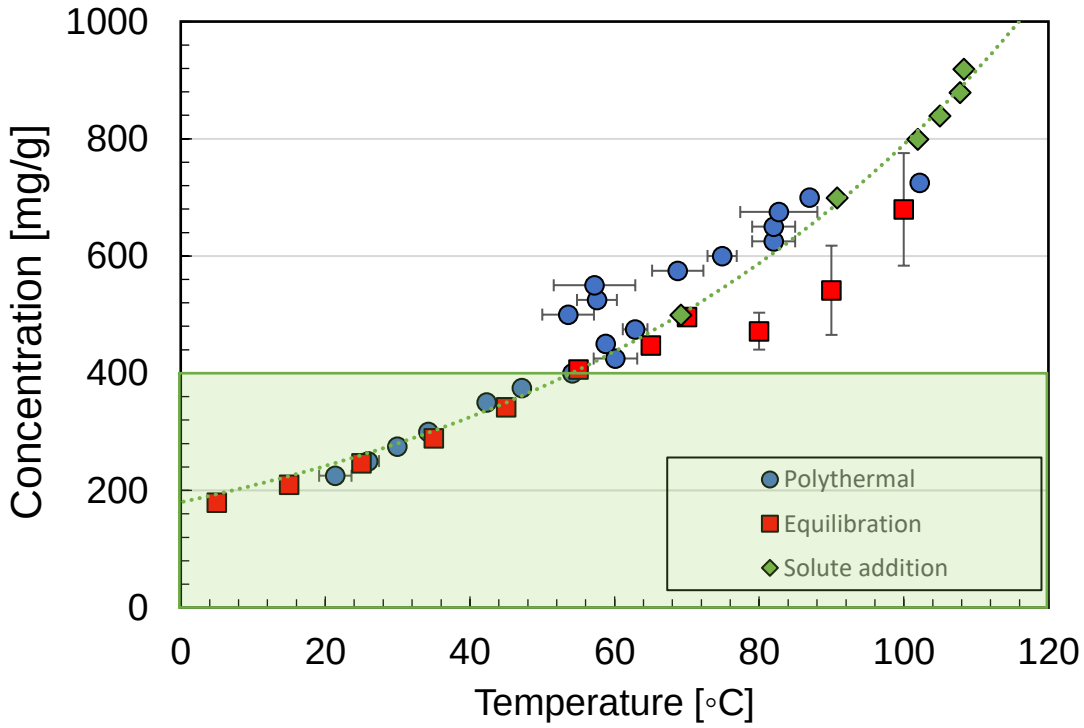

Figure 3.9. The glycine in water solubility diagram across the range of concentrations measured, using all three techniques. The blue circles represent the measurements recorded using the polythermal technique and the red squares represent the values recorded using the equilibrium concentration method with gravimetric analysis. The green shaded area represents the area below 400 mg/g and 50°C. This is the region where any of the three techniques showed no sign of problems. Beyond this, sampling should be avoided and only the solute addition technique (green diamonds) is proven to be accurate and reliable. The line is an exponential fit to the solute addition method of determining the solubility.

The solubility measurements recorded in this study were then finally compared with values taken from literature and thermodynamic models. This is shown in Figure 3.10. From Figure 3.10., our measured values disagree with other data reported in literature, where high temperature glycine solubility was measured

using a novel application of differential scanning calorimetry (DSC)[12]. Interestingly, both sets of solubility measurements (i.e., solute addition and DSC) are supported by extrapolations[13], derived from thermodynamic data reported at 25°C.

Differences in extrapolated solubility at elevated temperature derive from chosen excess Gibbs free energy models (i.e., Scatchard-Hildebrand and Scatchard-Hildebrand-Flory-Huggins) used to fit experimental data reported at 25°C. Assuming both the extrapolation framework and solute addition measurements are accurate, this may suggest glycine-water solutions are accurately described by the Scatchard-Hildebrand functional form at 25°C. However, extrapolations at temperatures beyond 60°C are sensitive to several factors (i.e., glycine-water solution model choice, measurement uncertainty and approximate nature of predictive framework), as such it is challenging to conclude this with much certainty, particularly in the absence of additional independent thermodynamic data.

In theory, more accurate model-based estimates of high temperature solubility, and subsequent assessment of the accuracy of different solubility approaches, is possible with more comprehensive thermodynamic studies on the glycine-water system.

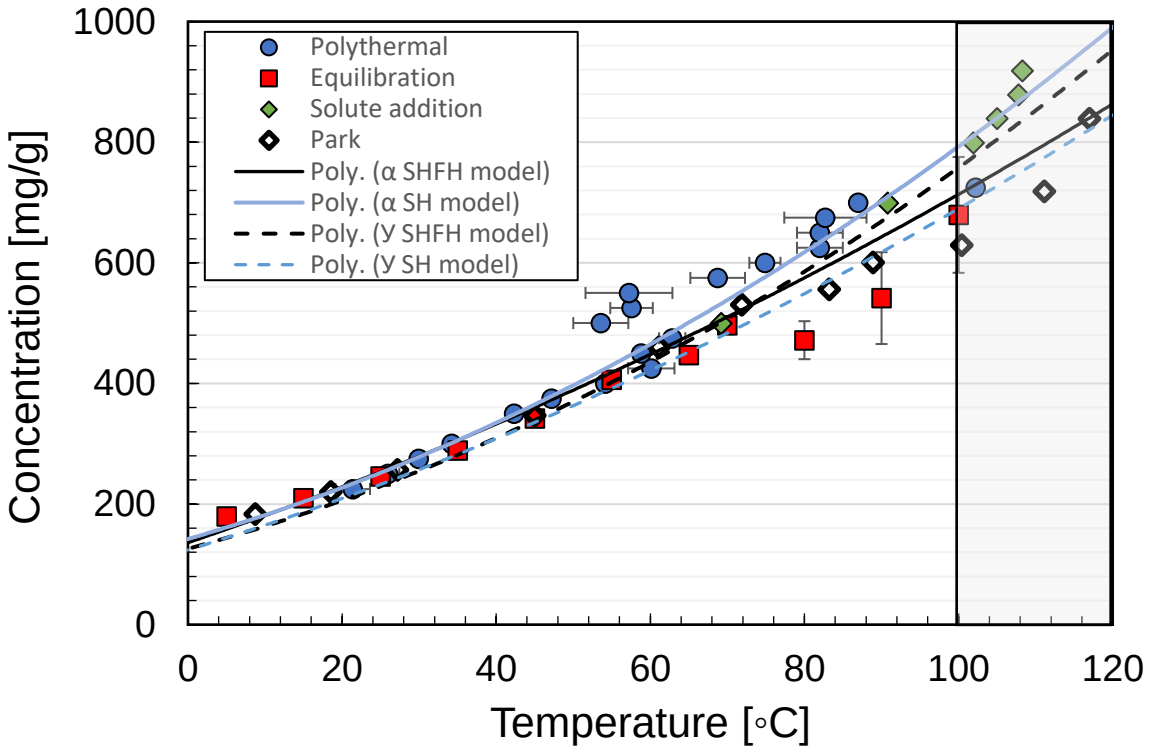

Figure 3.10. The solubility of α-glycine, recorded in this study, using three experimental techniques, compared with experimental data taken from literature[12] and two thermodynamic models[13]. Data recorded using gravimetric analysis is shown by red squares, polythermal (zero heating rate limit) is shown with blue circles and solute addition with green diamonds.

3.4 Conclusions

Three techniques were assessed in this study to record solubility measurements across a range of experimental conditions from 5 – 108.3°C. The equilibrium method using gravimetric analysis has long been known for its accurate solubility analysis. The polythermal technique, with modern equipment such as the Crystal 16 and Crystalline, enables the rapid screening of systems and generation of huge sets of data and the solute addition

technique is something which can be used at a larger scale with better mixing and no sampling required.

All techniques utilised in this study highlighted specific challenges and therefore it might be more useful to discuss the selection of a technique based on individual requirements and regions of interest. The equilibrium method seemed to show sensitivity at higher temperatures which resulted in recrystallisation of solute and evaporation of solvent. This resulted in values which were significantly lower than what would typically be expected. To overcome this major challenge, a dilution method was proposed, in which the syringe was partially filled with solvent but recording the weight of each piece of equipment and the mass of solvent added was laborious. Otherwise, it isn't practical to sample in a safe manner beyond 80°C. To circumvent this, future experiments may consider the application of probes to determine the solution concentration and remove the requirement for sampling. The polythermal technique showed challenges of its own. Although data could be rapidly generated, it seemed that encrustation on the surface and insufficient mixing led to the appearance of higher solubility measurements recorded in a specific region (450 – 550 mg/g). So, the polythermal technique showed, rather, a sensitivity to concentration than temperature. The practicalities of sampling are obviously, greatly improved in this technique as there is no interaction between the operator and the solution requiring sampling and the technique is much less labour intensive. The solute addition technique also totally removed the requirement to manually take a sample, but the volume and mass of glycine required was significantly larger than the previous measurements to ensure

that there was sufficient mixing of the highly concentrated solutions. Further experiments are now needed, especially triple point measurements to determine accurate and reliable solubilities.

It can be concluded that the operator's individual requirements should dictate the method employed to record solubility. If the aim is to generate data rapidly, then the Crystal 16 with the 16 individual reactors provides the tool to achieve this. If there are doubts related to detection, then the Crystalline is another alternative which allows in-situ visual monitoring with a camera, but the number of reactors is halved, reducing the productivity. If accuracy at elevated temperatures is required then the solute addition is the best technique, but this will require access to a significant increase in compound, time, and operator effort. This study should therefore aid the decision of researchers when selecting the most suitable method for analysing the solubility of a particular system.

3.5 Key Points

- The solubility of glycine in water was recorded using multiple techniques (equilibrium concentration, polythermal, solute addition) and critically evaluated.
- An extrapolation technique was used to predict ‘true equilibrium solubility’ at heating rate of 0°C/ min.
- All three methods were compared with thermodynamic predictions from literature.
- Further experiments including triple point measurements needed to determine accurate and reliable glycine solubility values.

3.6 References

(1) Muller, F. L.; Fielding, M.; Black, S. A Practical Approach for Using Solubility to Design Cooling Crystallisations. *Org. Process Res. Dev.* **2009**, No. 13, 1315–1321. https://doi.org/10.1021/op9001438.

(2) Mullin, J. W. *Crystallisation, 4th Edition*; 2001. https://doi.org/10.1021/op0101005.

(3) Davey, R.; Garside, J. *From Molecules to Crystallizers: An Introduction to Crystallization*; 2000.

(4) Brown, C. J.; Mcglone, T.; Yerdelen, S.; Srirambhatla, V.; Mabbott, F.; Gurung, R.; Briuglia, M. L.; Ahmed, B.; Polyzois, H.; Mcginty, J.; Perciballi, F.; Fysikopoulos, D.; Macfhionnghaile, P.; Siddique, H.; Raval, V.; Harrington, T. S.; Vassileiou, A. D.; Robertson, M.; Prasad, E.; Johnston, A.; Johnston, B.; Nordon, A.; Srai, J. S.; Halbert, G.; Ter Horst, J. H.; Price, C. J.; Rielly, C. D.; Sefcik, J.; Florence, A. J. Enabling Precision Manufacturing of Active Pharmaceutical Ingredients: Workflow for Seeded Cooling Continuous Crystallisations. *Mol. Syst. Des. Eng.* **2018**, No. 3, 421–592. https://doi.org/10.1039/c7me00096k.

(5) Black, S.; Dang, L.; Liu, C.; Wei, H. On the Measurement of Solubility. *Organic Process Research and Development*. 2013, pp 486–492. https://doi.org/10.1021/op300336n.

(6) Rowland, D. Thermodynamic Properties of the Glycine + H2O System. *J. Phys. Chem. Ref. Data* **2018**, No. 47, 023104-1-023104–023115. https://doi.org/10.1063/1.5016677.

(7) Datta, A.; Hossain, A.; Guin, P. S.; Roy, S. Solubility Data of Glycine in Water and Justification of Literature Results: A Review. *Asian J. Chem.* **2020**, *7*, 1525–1533.

(8) De Souza, B.; Keshavarz, L.; Cogoni, G.; Frawley, P. J. Pressurized-Synthetic Methodology for Solubility Determination at Elevated Temperatures with Application to Paracetamol in Pure Solvents. *J.*

Chem. Eng. Data **2017**, *62* (5), 1689–1700. https://doi.org/10.1021/acs.jced.7b00118.

(9) Vesga, M. J.; McKechnie, D.; Mulheran, P. A.; Johnston, K.; Sefcik, J. Conundrum of γ Glycine Nucleation Revisited: To Stir or Not to Stir? *CrystEngComm* **2019**, No. 21, 2234–2243. https://doi.org/10.1039/c8ce01829d.

(10) Achermann, R.; Adams, R.; Prasser, H.; Mazzotti, M. Characterization of a Small-Scale Crystallizer Using CFD Simulations and X-Ray CT Measurements. *Chem. Eng. Sci.* **2022**, No. 256, 1–12. https://doi.org/10.1016/j.ces.2022.117697.

(11) Kaskiewicz, P. L.; Rosbottom, I.; Corzo, M. C.; Hammond, R. B.; Downie, R.; Dowding, P. J.; George, N.; Roberts, K. J. Influence of Solution Chemistry on the Solubility, Crystallisability and Nucleation Behaviour of Eicosane in Toluene : Acetone Mixed-Solvents. **2021**, No. 23, 3109–3125. https://doi.org/10.1039/d1ce00322d.

(12) Park, K.; Evans, J. M. B.; Myerson, A. S. Determination of Solubility of Polymorphs Using Differential Scanning Calorimetry. *Cryst. Growth Des.* **2003**, No. 6, 991–995. https://doi.org/10.1021/cg0340502.

(13) Manson, A.; Sefcik, J.; Lue, L. Temperature Dependence of Solubility Predicted from Thermodynamic Data Measured at a Single Temperature: Application to α, β, and γ-Glycine. *Cryst. Growth Des.* **2022**, *22* (3), 1691–1706. https://doi.org/10.1021/acs.cgd.1c01217.

Chapter. 4. Nucleation and Crystal Growth of α-Glycine: Classification of Crystallisation Behaviour

4.1 Introduction

To assess the best conditions for secondary nucleation of a given compound (and, where relevant, crystal polymorph), a comprehensive analysis of the primary nucleation behaviour must first be undertaken. This provides the range of conditions for which primary nucleation is delayed long enough for secondary nucleation to dominate the crystallisation process. Precise solubility and metastable limit measurements are required to obtain the metastable zone width. Within the metastable zone, the solution is in a state of supersaturation, where supersaturation may be defined as $S=C/C^*$ where C^* is the solubility concentration and C is the working concentration at a particular temperature. In the metastable zone, the crystal phase is thermodynamically favoured, and primary nucleation will therefore take place spontaneously. However, the degree of supersaturation (S) determines the nucleation probability: the rate at which primary nuclei appear, or alternatively how likely nucleation is to be observed in a given time. Unlike solubility, the metastable limit and metastable zone width are not thermodynamic properties but indicate beyond which the chance of primary nucleation occurring in the experimental time window approaches zero. The metastable zone width therefore is dependent on detection limitations and is also affected by heating and cooling rates which bring in time window dependence, meaning that at quicker cooling rates, nucleation will have less time at each temperature point to become detectable leading to larger metastable zone widths. Having defined the metastable zone, induction time measurements are required, i.e., the time taken to observe the onset of primary nucleation at a given supersaturation within the metastable

zone, under isothermal conditions. Induction time at a given supersaturation and temperature then provides the time available for seed addition and completion of the secondary nucleation process without competition from primary nucleation.

Once the primary nucleation behaviour has been thus comprehensively assessed, seeding studies can be conducted under controlled and well-defined supersaturation and temperature as well as agitation conditions. Following seed addition, seed crystal growth takes place and secondary nucleation is presumed to involve sections of the growing crystal or the interfacial layer adjacent to the crystal surface being detached by collisions or fluid shear. Because this removal process will depend on the seed growth, it is essential to be able to assess the rate at which the crystal grows. Finally, in practice, a secondary nucleation threshold[1,2] is often defined describing the minimum supersaturation required for secondary nucleation and crystal proliferation (although this, as discussed below, may be better thought of as a 'threshold' of growth rate below which significant secondary nucleation will not take place in the experimental or manufacturing time window).

There have been few attempts to develop a robust classification system[3,4] which enable enhanced understanding of the relationship between nucleation and crystal growth. This chapter proposes a classification workflow based on a rapid experimental screening within the crystalline platform. *In-situ* imaging enables the most direct observation of the system with results in days rather than weeks or months. Nucleation and growth kinetics are determined from the same experimental vials so results can be directly compared and plotted

onto the same graph. Understanding the nucleation and growth tendencies would then allow the researcher to rapidly screen the suitability for specific operations such as continuous manufacturing with long residence times or unseeded batch operation where new crystals are required to be readily supplied.

In this work we build on recently introduced crystallisation workflows[5,6] based on small scale experiments in agitated vials to estimate primary and secondary nucleation kinetics as well as crystal growth kinetics under isothermal conditions. In particular, we show that all these estimates can be in principle obtained from the same kind of crystallisation experiment. We demonstrate our approach using cooling crystallisation of glycine in water, where α-glycine is known to form under agitation conditions[7]. We then discuss differences between primary and secondary nucleation kinetics and corresponding crystallisation behaviour classification for this system.

4.2 Experimental

4.2.1 Solubility and Metastable Zone Width

In this study the solubility and metastable zone width were determined using the Crystal 16 (Technobis Crystallization Systems) instrument and the solubility presented in this chapter was taken from the polythermal extrapolations outlined in Chapter 3. The Crystal 16 enables precise control over the temperature cycling programmes of individual vials with built in optical

technology to measure a change in transmissivity identifying the temperature where clear points or cloud points are reached, related to complete dissolution or initial crystal formation, respectively.

Individual vials at a given glycine concentration were prepared by weighing a known mass of finely ground glycine crystal directly into the vials (VWR, total volume 1.5 mL). Once de-ionized water (1 mL) was added, the vials were tightly sealed and placed into the reactor system. The solution was first heated from room temperature to 70°C to dissolve the solid glycine and solutions were agitated using a magnetic stirrer bar at 700 RPM. Complete dissolution is indicated by a transmissivity value of 100%. The temperature was then decreased from 70 to 5°C at a fixed cooling rate (cooling rates were from 0.1 to 0.5°C/min). As crystallisation begins, transmissivity decreases. Once transmissivity decreases below 50% the temperature is recorded signifying the metastable limit under given conditions. Following a hold period at 5°C for 15 minutes, the sample was heated back to 70°C at a fixed heating rate (heating rates were from 0.1 to 0.5°C/min), and a change in transmissivity from 0 to 100% is observed on dissolution of suspended crystals. The temperature at which the transmissivity reaches 100% is taken as the solubility temperature at the given concentration. Each cycle was completed three times in order to determine an average and standard deviation. As concentration increases, dissolution and recrystallisation temperatures increase, meaning that a higher maximum temperature (>70°C) must be used to obtain dissolution.

4.2.2 Primary Nucleation Induction Times

Following determination of the metastable zone width, 7 supersaturations (*S*) were selected to determine the dependence of the induction time on *S* under isothermal conditions. All experiments were carried out at a temperature of 25°C. The corresponding solubility of α-glycine used to calculate supersaturation, $S=C/C^*$, was taken as C^*=249.52 mg/g of water, as this was thought to be the most accurate value available in the literature for this system[8]. Induction time measurements were performed using the Crystalline (Technobis Crystallization Systems) instrument at a 3 mL volume. Between 18 and 25 induction time experiments were performed at each supersaturation. A series of stock solutions of glycine in de-ionised water were prepared directly in Crystalline vials at glycine concentrations, calculated in order to reach the desired values of supersaturation at 25°C. The vials were then placed into the instrument, the solid material was dispersed by a magnetic stirrer at 700 rpm and dissolved at 55°C for a period of 30 min. Complete dissolution was confirmed by the transmissivity value reaching 100%. The temperature was then reduced to 25°C at a cooling rate of 5°C/min and vials were then held under isothermal conditions for a period of four hours with stirring continued throughout. Induction time was recorded when the transmissivity value decreased below 50%. The Crystalline instrument's built-in camera was checked to ensure that the measured transmissivity was representative of the state of recrystallisation in the vials. This procedure was cycled numerous times due to the stochasticity of primary nucleation.

4.2.3 Estimation of Primary Nucleation Rates

Due to the stochastic nature of primary nucleation events, a distribution is expected in the measured induction times for a given set of conditions. The observed variation in measurements can be explained through considering the single nucleus mechanism[9,10]. This assumes that there is a constant primary nucleation rate *J*, which is the same in each non-nucleated vial, that there is a single primary nucleation event in each nucleated vial, and that there is a constant delay between the primary nucleation event and the induction time detection. This delay has been designated as growth time t_g, which corresponds to time required for the nucleus to grow to the size where the resulting crystal becomes observable. Under typical agitation conditions, the nucleated crystal become observable indirectly, when it grows sufficiently large to induce sufficiently fast secondary nucleation, resulting in the formation of many small crystals, which is recorded as the induction time. The probability distribution of induction times *P*(*t*) can then be described through equation 4.1[11]:

$$P(t) = 1 - \exp\left(-JV(t - tg)\right) \quad \textbf{(Eq. 4.1)}$$

where *J* is the primary nucleation rate, *V* is the solution volume and t_g is the growth time. The probability distribution *P*(*t*) can be calculated from repeated induction time experiments under same conditions, as expressed through equation 4.2:

$$P(t) = \frac{M^{+}(t)}{M} \quad \textbf{(Eq. 4.2)}$$

where M is the total number of experiments, whilst M^+ is the number of experiments in which nucleation was detected at the time less of equal t. Equation 1 was fitted through least squares regression using the induction times measured in this work. The sample volume was 3 mL, whilst both the primary nucleation rate and growth time were taken as fitting parameters.

4.2.4 Seed Crystal Growth and Characterisation

Following completion of the induction time and metastable zone width measurements the vials were removed from the Crystal 16 instrument and placed directly onto the bench top for crystal growth to occur. Typical seed crystal size produced was 2.5 mm with variations seed to seed of ±1.0 mm. Single crystals were then selected and placed onto a plastic dish to dry before analysis with a Leica DM6000M 1 optical microscope, to confirm and to characterise its morphological features, size and a single crystal rather than an agglomerate is present. This was followed by Raman analysis using a RXN1 Raman Spectrometer and PhAT probe (Kaiser Optical Systems) on randomly selected seed crystals. Comparison with literature Raman spectra[12-13] showed that all seed crystals were the α-glycine polymorph.

4.2.5 Single Crystal Seeding

For each seeded sample, a single crystal seed was added to a vial containing 3 mL of solution at the glycine concentration required to obtain the desired supersaturation at the experimental temperature of T=25°C. The vials were agitated at 700 RPM throughout and so the seed was added immediately to an agitated solution once T reached 25°C. From a single experiment, it is possible to rapidly determine both crystal growth and secondary nucleation kinetics (see below). The in-situ camera allows real time monitoring of the progress of the experiment.

The crystalline instrument's image analysis algorithm enables data to be saved as both a number weighted particle size distribution and a particle count against time. From these two data sets, it is possible to process the data in order to estimate both crystal growth and secondary nucleation rates.

4.2.6 Secondary Nucleation Kinetics

The secondary nucleation rate, defined by the rate of increase in the number of crystals in a given volume was measured over a range of supersaturations by preparing a minimum of 3 individual samples at each experimental supersaturation, adding a single seed crystal to each sample and measuring the increase in the number of visible crystals over time. From the primary nucleation induction times measured under the same conditions (see above), we can select conditions to ensure that no primary nucleation takes place

during the secondary nucleation measurements. Experiments were conducted in 3 mL volumes under agitation by magnetic stirrer using the Crystalline instrument, obtaining the number of crystals in the observed volume from analysis of images taken with instrument's built-in camera. All measurements were obtained under isothermal conditions at T=25°C, i.e., matching the conditions of the induction time measurements.

The solution, at a given concentration to provide the required supersaturation at T=25°C, was first heated to 55°C and held for a period of 30 minutes to ensure full dissolution. The temperature was then reduced to 25°C at a rate of 5°C/min to reach the desired supersaturation. At this point, a single crystal seed of a known size (length of 2.5 ± 1 mm) was added to each vial, this procedure is shown in Figure 4.1. The solution was constantly agitated. The Crystalline instrument's image analysis software provides a particle count as a function of time. Particle counts below 10 were subject to background effects, while the maximum number of particles in focus to obtain an accurate particle count using the Crystalline imaging software was found to be about 160. A calibration curve was previously determined for estimation of the particle number density in the vial from particle count data[6]. The time window to be used was selected by consideration of the limits of the image analysis and the secondary nucleation rate was determined over a period of time where the particle count increased from 10 to 160. The secondary nucleation rate (B) can be calculated from the rate of change of the particle number density in time[6].

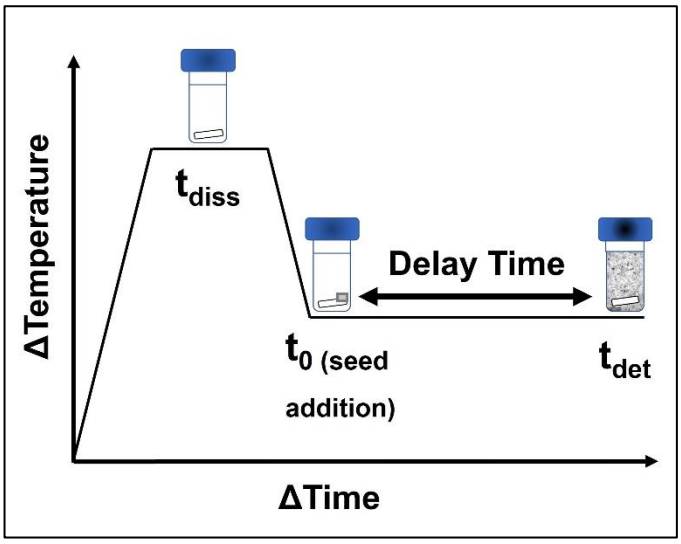

Figure 4.1. A schematic of a typical temperature seeding profile. The temperature is firstly increased to ensure complete dissolution of the solid glycine. This is followed with cooling to the working temperature (and supersaturation) T=25°C. At this point, the seed is added, and the delay time is recorded once secondary nucleation is activated (crystal number >10). The secondary nucleation rate can then be recorded by tracking the change in number over time.

4.2.7 Crystal Growth Rates

The growth rates of α-glycine crystals as a function of supersaturation were also determined from image analysis of the camera output of the Crystalline instrument[5]. The image analysis software measures visible particle size and produces for each time-stamped image a size distribution histogram in 99 bins, linearly spanning the size range from 3 to 300 µm. Seeded experiments were completed at a range of experimental supersaturations. A MATLAB script was used to convert the number weighted particle size distribution data into volume weighted d_{90} values. The d_{90} value gives the size where 90% (by volume) of the particles are smaller than this value. Following the onset of nucleation and above 10 crystals the change in d_{90} was then plotted against time until the

maximum number of 160 particles. The growth rate was recorded from the change in size over time given by the slope. By following the seeding procedure previously outlined, it is possible to estimate both secondary nucleation and growth kinetics from the same experiment in a seeded vial. Significantly, the approach used in this study enables measurement of both crystal growth and secondary nucleation rates from the same experiment even in unseeded vials.

4.3 Results and Discussion

4.3.1 Metastable zone width

In order to estimate the ‘true equilibrium solubility’, the polythermal technique was performed at multiple heating rates and an extrapolation performed to a theoretical ‘0°C/ min’ heating rate. This technique was outlined in detail in Chapter 3. The polythermal technique enables both a dissolution value (solubility) and re-crystallisation (metastable limit) to be recorded and the metastable limit distributions are shown below in Figure 4.2. against the extrapolated, best estimated solubility values.

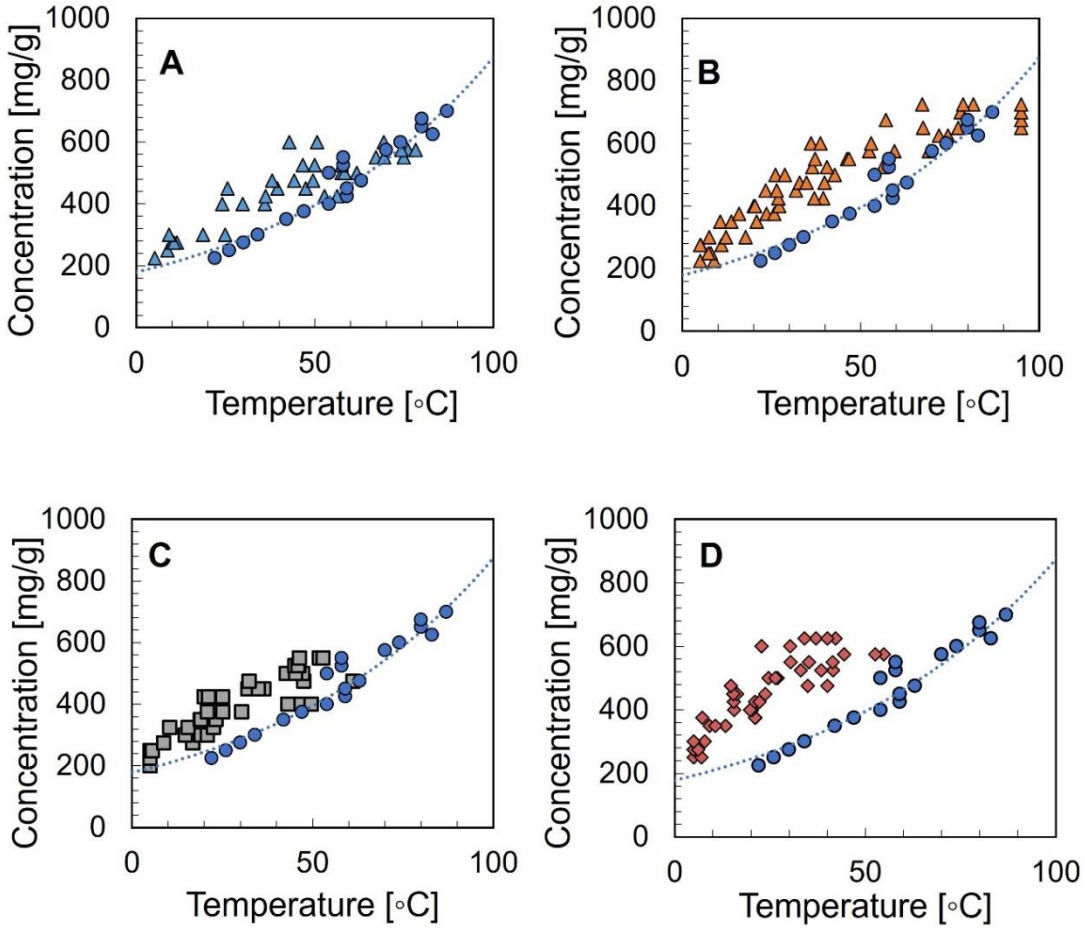

Figure 4.2. The metastable zone width is shown at 4 different cooling rates ranging from 0.1 – 0.5°C/ min. The solubility displayed is the extrapolated solubility value from Chapter 3. A cooling rate of 0.1°C/ min is shown in A with blue triangles, 0.2°C/ min (B) (orange triangles), 0.3°C/ min (C) (grey squares) and 0.5°C/ min (D) (orange diamonds). As shown, the metastable zone width gets broader with an increased rate of cooling.

As the rate of cooling is increased, the system has less time available to reach a thermodynamic equilibrium, for a nucleus to form, and grow to a detectable size. This is shown when comparing the cooling rates at 0.1 and 0.5°C/ min. With a cooling rate of 0.5°C/ min, there is an onset of primary nucleation much later which results in a broad metastable zone width. Alternatively, a cooling rate of 0.1°C/ min suggests that there is a narrow metastable zone. The

significant reduction is therefore expected to be simply representative of the system having enough time to adjust before detection of nucleation which in this case requires multiple successive events (4.3.2). The significant distribution of ‘cloud point’ measurements shown in Figure 4.2. indicates therefore that there is significant stochastic element in these unseeded measurements.

Each of the previous measurements was cycled a minimum of three times and the average metastable limit (point of nucleation) calculated. Table 4.1. shows the average MSL along with the corresponding concentration, heating rate, solubility, and metastable zone width. The metastable zone width describes the difference in temperature between the solubility and the MSL at a specific concentration. As the cooling rate was increased, it is shown that the metastable zone width gets broader over the four heating rates although this dependence is less clear at rates between 0.2 – 0.3°C/ min.

Table 4.1. Shows how the metastable zone width changes in relation to cooling rate across a range of experimental concentrations. The solubility displayed was recorded using the extrapolation technique outlined in Chapter 3. It seems that an increase in the cooling rate results in a broader metastable zone width.

Concentration (mg/g)	Heating Rate (°C/min)	Solubility (°C)	Averaged MSL (°C)	MSZW (°C)
250	0.1	25.9	8.7	17.2
	0.2		7.7	18.2
	0.3		5.2	20.7
	0.5		5.7	20.2
300	0.1	34.2	17.6	16.6
	0.2		15.0	19.2
	0.3		18.2	15.2
	0.5		6.0	28.3
350	0.1	42.3	-	-
	0.2		15.0	27.3
	0.3		20.4	21.9
	0.5		11.0	31.3
450	0.1	58.8	51.6	7.2
	0.2		27.3	31.5
	0.3		34.5	24.3
	0.5		18.5	40.3

Estimated solubilities (Chapter 3.) of α-glycine in water for concentrations up to 400 mg/g are shown in Figure 4.3. Also shown is a temperature dependence of α-glycine solubility based on a thermodynamic model from Rowland, which

is thought to be the most accurate value available in the literature for this system[8], albeit only applicable for temperatures up to 40°C. It can be seen that the solubilities estimated from clear point measurements in this work tend to be slightly higher than those from Rowland, which may be caused by the limitations of detection and limited sensitivity of the transmission-based method to very small amounts of suspended solids shortly before the equilibrium solubility temperature is reached[14]. As mentioned in Chapter 3, validation of the clear point method with in-situ imaging, using tools such as the Crystalline instrument may enable more accurate measurement of the point of dissolution where final suspended solids could still be detected visually.

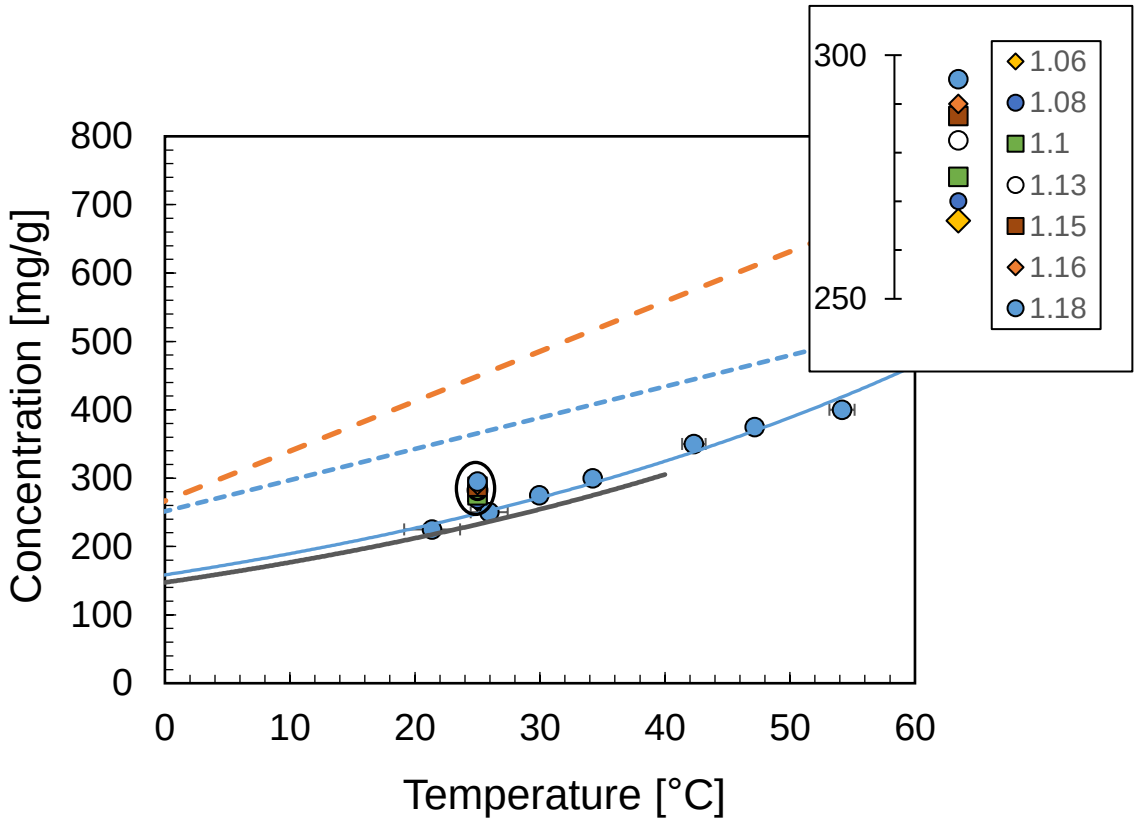

Figure 4.3. Estimated solubilities of a-glycine in water. Temperature dependence of a-glycine solubility in water based on a thermodynamic model from Rowland is shown as a solid line. Approximate metastable zone boundaries in agitated 1 mL vials at cooling rates of 0.5 and 0.1°C/min are shown as orange and blue lines, respectively. Error bars on the solubility values are displayed in terms of confidence intervals from the solubility estimations. The metastable zone is the region between the point of solubility and spontaneous primary nucleation. The supersaturations selected for unseeded induction time measurements are shown with the insert.

As mentioned, the difference between the solubility temperature and the cloud point temperature can be taken as an indication of the metastable zone width. It can be seen in Figure 4.2. and Figure 4.3. that the metastable zone is relatively wide. The metastable zone is expected to be wider still for the much higher cooling rate of 5°C/min which was used for primary and secondary nucleation studies in this work, although all concentrations investigated are well within the metastable zone for the slowest cooling rate of 0.1°C/min, as shown by the insert in Figure 4.3.

4.3.2 Induction Time and Primary Nucleation Kinetics

Induction time measurements provide information on the likelihood of primary nucleation in the metastable zone under isothermal conditions. Figure 4.4. shows induction times recorded at each supersaturation (*S*) together with the percentage of vials that have nucleated within a 4-hour timeframe. At the highest *S* of 0.18 all the vials nucleated within 60 minutes. However, at the lowest *S* of 0.06 the earliest vial nucleated after about 100 minutes and only 15% of the vials nucleated within 4 hours.

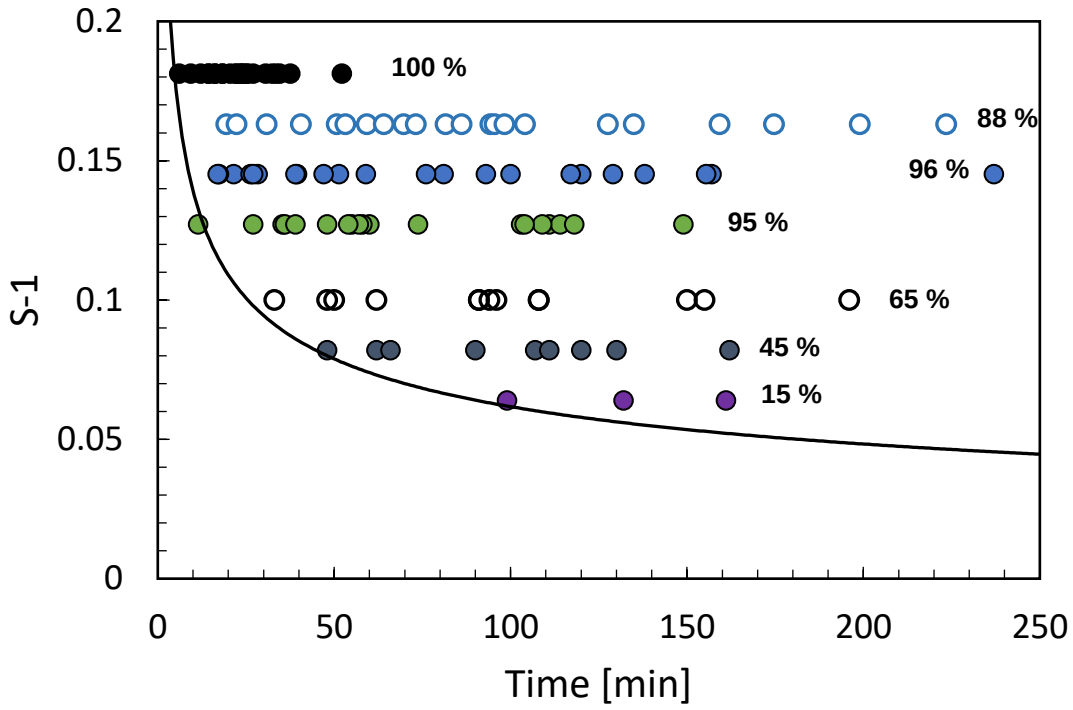

Figure 4.4. Induction times recorded at 7 different supersaturations for α-glycine in water at 25°C. A number of between 18-25 samples were measured per each supersaturation in 3 mL vials with continuous agitation. Points represent time when the first crystals were detected in a given vial. *S*-1=0.18 (black circles), *S*-1=0.16 (hollow blue circles), *S*-1=0.15 (blue circles), *S*-1=0.13 (green circles), *S*-1=0.10 (hollow black circles), *S*-1=0.08 (dark blue circles) and *S*-1=0.06 (purple circles). Percentages show the proportion of the vials that showed nucleation within 4 hours. Line is a theoretical guide based on the time calculated to reach the estimated *L*min (Figure 4.8.) and the growth rate as a function of the supersaturation using the fit from Figure 4.7.

The induction times shown in Figure 4.4. demonstrate a typical stochastic nature of primary nucleation. It can be seen that there is a significant delay between reaching the isothermal conditions (corresponding to time of zero in Figure 4.4.) and the earliest induction time. This delay is indicated by a solid line as a guide to eye and it reflects the growth time t_g, which corresponds to the time required for a nucleus to grow to a size where it triggers secondary nucleation (which is much faster than primary nucleation, as will be discussed

below). Taking the growth time offset into account we can see that the induction times are distributed over 10s to 100s of minutes which gives us an order of magnitude insight into the primary nucleation rate, as the *JV* term in equation (1) should then be on the order of 0.01-0.1 per minute. In other words, the likelihood of a primary nucleation event in a given vial is on the order 0.01 to 0.1 in any given minute across the range of supersaturations considered here.

The induction time data were plotted as probability distributions *P*(*t*) and these were fitted with the functional form from equation 4.1. The raw traces are then shown in Figure 4.5. Table 4.2. shows the estimated values for primary nucleation and growth time.

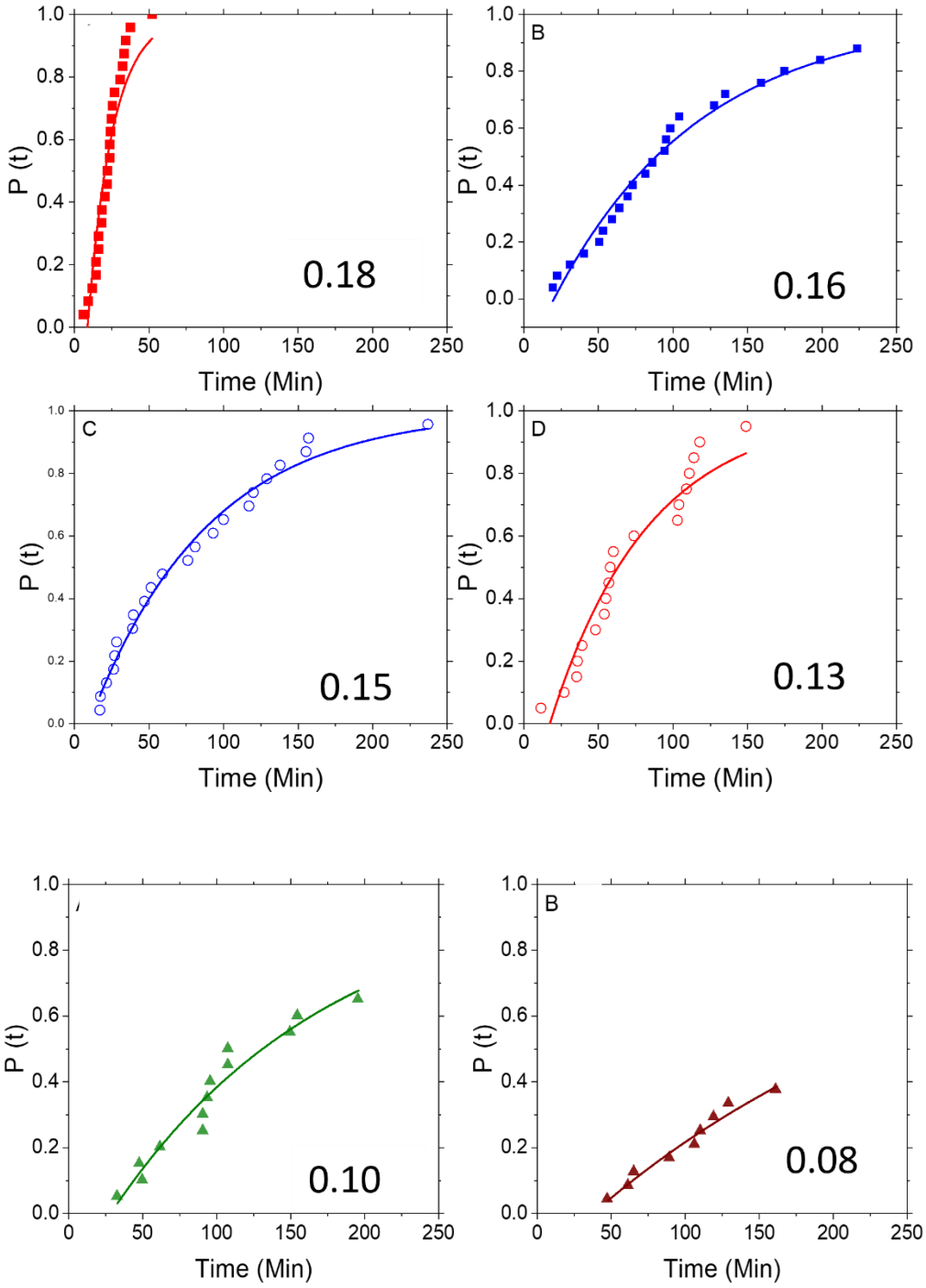

Figure 4.5. Cumulative probability distributions of the stochastic induction time data for the glycine in water system across multiple supersaturations. There is an increase in primary nucleation rate (*J*) indicated by the steepness of the slope, with an increase in the supersaturation. The supersaturation is displayed in the bottom right region of each graph.

Table 4.2. Estimated primary nucleation rates (J) and growth times (t_g) from the unseeded induction time experiments shown vs supersaturation.

S – 1	Primary nucleation rate *J* (# /mL/ min)	Growth time t_g (min)
0.08	1.3×10^{-3} ($\pm 8.5 \times 10^{-5}$)	37 (± 4.09)
0.10	2.2×10^{-3} ($\pm 1.77 \times 10^{-4}$)	29 (± 4.71)
0.13	5.0×10^{-3} ($\pm 3.96 \times 10^{-4}$)	17 (± 2.73)
0.15	4.2×10^{-3} ($\pm 1.53 \times 10^{-4}$)	10 (± 1.43)
0.16	3.3×10^{-3} ($\pm 1.35 \times 10^{-4}$)	20 (± 1.94)
0.18	2.0×10^{-2} ($\pm 1.66 \times 10^{-3}$)	8.7 (± 0.81)

As expected, the primary nucleation rate *J* increases with increasing supersaturation, varying by an order of magnitude across the range of supersaturations investigated here. It can be seen in both Figure 4.5. and Table 4.2. that estimated primary nucleation rates do not strictly follow a monotonous trend with respect to supersaturation (the values of *J* for *S* of 0.15 and 0.16 are lower than the one for *S* of 0.13. This is most likely due to a modest number of induction time experiments and resulting stochastic fluctuations. However, it is clear that there is a consistent and robust estimate of the order of magnitude of the primary nucleation rate across the range of

supersaturations investigated here. It can be seen that the growth time t_g decreased with increasing supersaturation, which is also expected, as the crystal growth rate (and also the secondary nucleation rate, which contributes to rapid indirect detection of the grown crystal at induction time) increases with supersaturation and thus it takes shorter time to progress from the primary nucleation event to the corresponding induction time. To visualise this decrease of growth time t_g and corresponding increase in primary nucleation rate J with increasing supersaturation, they have been presented together in Figure 4.6.

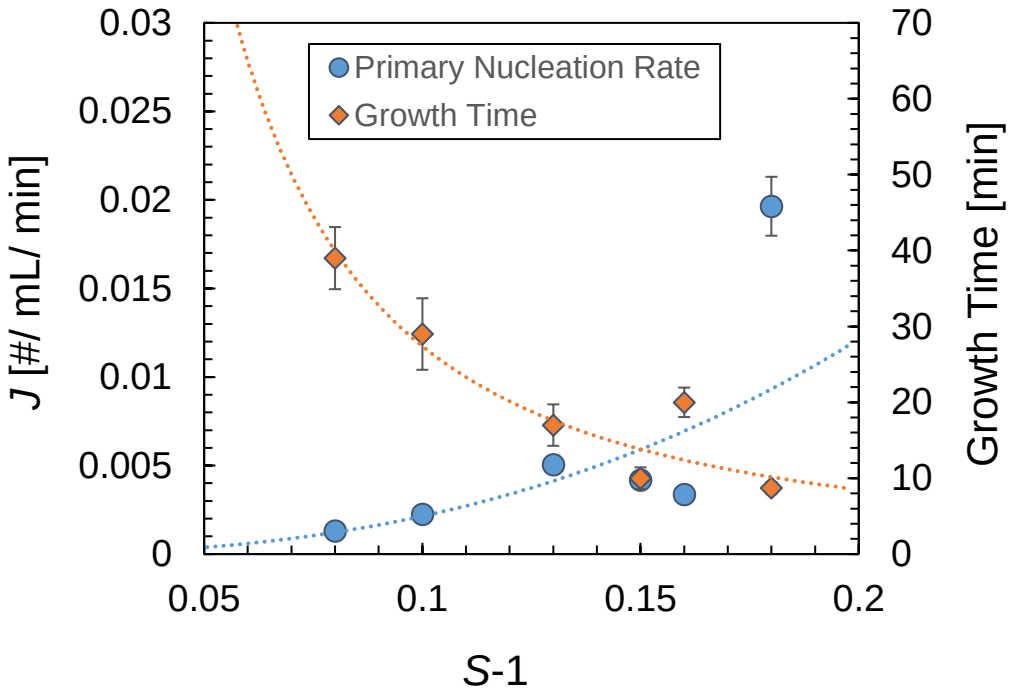

Figure. 4.6. The primary nucleation rate J and growth time t_g estimated from the probability distributions vs the corresponding supersaturation. There is an increase in J with an increase supersaturation whilst t_g decreases. The growth time is shown by the orange diamonds and the primary nucleation rate by the blue circles. A power law fit is shown for both and extrapolated to show theoretical trends.

4.3.3 Crystal Growth Kinetics

The overall crystal growth rates of α-glycine estimated from in situ imaging in agitated vials are presented in Figure 4.7.(a), for both unseeded and seeded experiments. The number of experimental data points varies between different conditions as only those vials which nucleated under unseeded conditions could yield crystal growth information and in situ imaging was not available for all experimental runs.

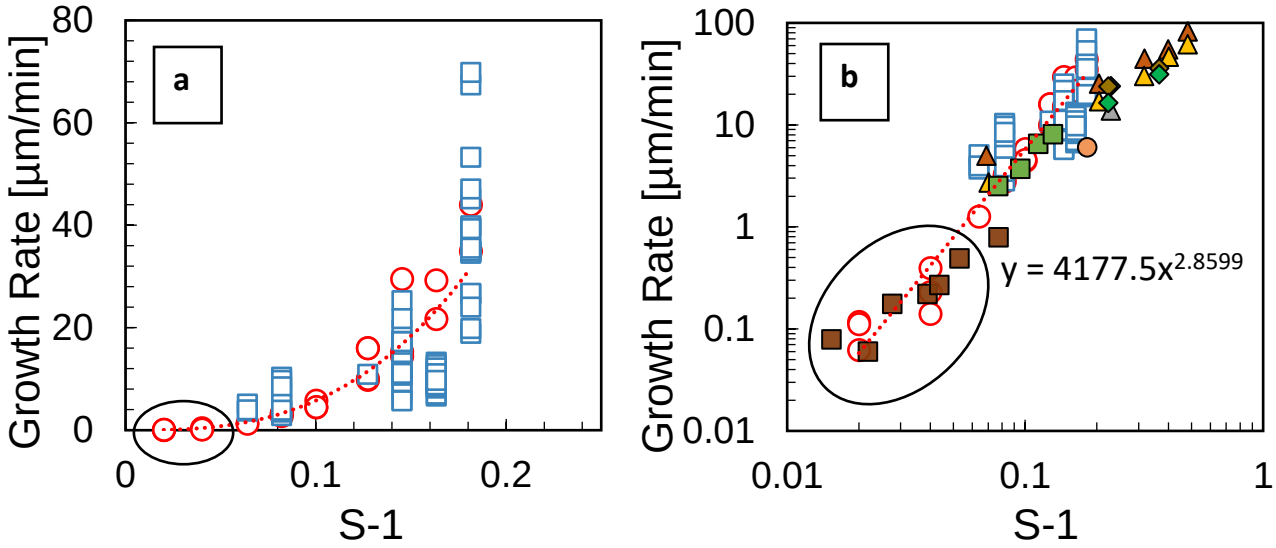

Figure 4.7. Overall crystal growth rates for α-glycine in water vs supersaturation (in term of *S-1*) at 25°C. (a) Measurements from seeded (open red circles) and unseeded (open blue squares) experiments at 9 supersaturations ranging from *S*-1=0.02 to *S*-1=0.18. On a linear scale it appears that there is a dead-zone below around *S*-1=0.05. (b) The same results from seeded (open red circles) and unseeded experiments (open blue diamonds) are compared with values taken from literature using various methods[15,13,16,17,18] with growth rate and supersaturation now plotted on a log scale, demonstrating a power law dependence rather than a dead zone.

Figure 4.7.(a) shows estimated crystal growth rates vs supersaturation (in terms of *S*-1) on a linear scale. It is notable that the range of estimated growth rates from repeated experiments at a given supersaturation can be up to one order of magnitude. This is not surprising in principle, as it is well known that individual crystals (of glycine and very likely other systems) can have a wide range of overall growth rates[19] and there are of course different growth rates for various crystal faces[20,21]. In this work, we used an ensemble based in situ imaging method to estimate overall growth rates from relatively limited data, so an order of magnitude accuracy would be a reasonable expectation for this approach.

Importantly, Figure 4.7. (b) shows there is a good agreement, across three orders of magnitude from 0.1 up to 100 μm/min, between the overall crystal growth rates measured in this study and literature values that have been obtained using far more time consuming techniques, such as *in-situ* microscopic observations of single crystal growth by multiple authors[13,20,15,16,17,18]. It can be seen in Figure 4.7. (b) that single crystal growth rate measurements reported in the literature at the highest supersaturations appear to be somewhat lower than those obtained in this work. This may be due to increasing transport limitations at very high growth rates where agitation in our experiments enhances the mass transport from bulk solution to the surface of rapidly growing crystals compared to other experimental conditions.

There is a power law dependence between the overall crystal growth rate and *S*-1, as can be expected for typical crystal growth rate mechanisms[22], see Figure 4.7. (b), with a power law exponent of 2.86. It can be also seen in Figure

4.7. (b) that some other data subsets from literature may be better described by a power law dependence with power law exponents closer to 2, but further investigation of this is beyond the scope of the present work.

In any case, a power law dependence with exponents between 2 and 3 (or higher) leads to an apparent dead zone for crystal growth, for *S*-1 below about 0.05, when growth rate data are plotted on a linear scale, as can be seen for circled data in Figure 4.7. (a). When the same data (also circled) is viewed on a log scale in Figure 4.7. (b), it is clear that there is no abrupt change, but instead it is just a feature of plotting power law dependencies. Therefore, it should not be argued that there are kinetic dead zones, cut-offs or thresholds for either crystal growth or nucleation kinetics, solely based on linear scale plots.

4.3.4 Crystal Growth and Induction Time Offset

In Figure 4.8., the inverse of the growth rate in unseeded experiments has been assessed against the minimum induction time (a), which is the earliest detected induction time at a particular supersaturation and growth time t_g (b) observed at the corresponding *S*. There is an approximately linear relation between the inverse of the growth rate and both the minimum induction time (MIT) and growth time t_g. This can be explained due to the MIT and t_g being stochastic and variable events dependent on firstly the formation of stable nucleus, followed by growth and then secondary nucleation. The results shown in Figure 4.8. clearly indicate that there is a dependence of on the growth rate

and therefore provide evidence for the single nucleus mechanism. This is something that has been previously mentioned but not visualised[23].

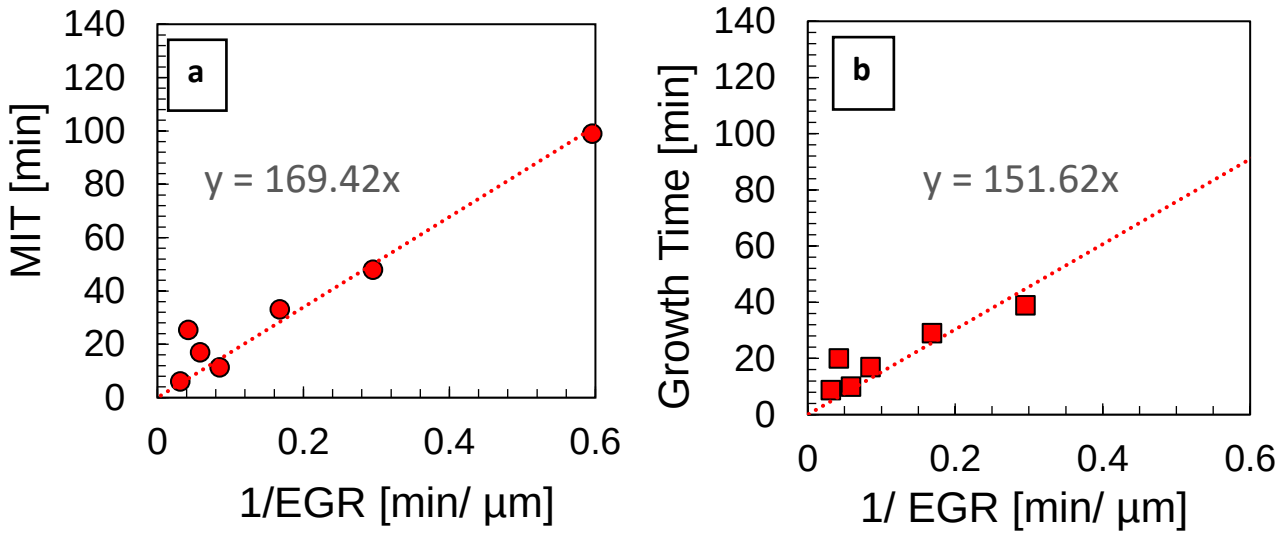

Figure. 4.8. (a) Correlation between minimum induction time (MIT) and the inverse of growth rate estimated (EGR) from the power law fit from Figure 4.7. at the same supersaturation, measured in unseeded experiments. This allows estimation of the minimum size required to activate secondary nucleation (169.4 µM). (b) The correlation between growth time (t_g) and the inverse of growth rate at the same supersaturation in unseeded experiments. The minimum size to initiation secondary nucleation was 151.62 µM.

By fitting a linear function passing through the origin point it is then possible to estimate the minimum size (L_{min}) required for secondary nucleation as it will be equal to the slope of the linear function. The idea that there are inert seeds below a certain size has been identified in literature[24], but this estimation methodology is really valuable.

4.3.5 Seeding

To control the point of nucleation, seeds are added. In this study, seed crystals were firstly prepared following a procedure outlined in section 4.2.5 and analysed. Raman was used on a selected few seed crystals as it is a non-destructive technique and the specific seed crystals could then be added directly to the small-scale crystallisation vessel. The trace is shown in Figure 4.9. Characteristic peaks for α-glycine are seen at 1108, 1326 and 1673 cm^{-1} [12].

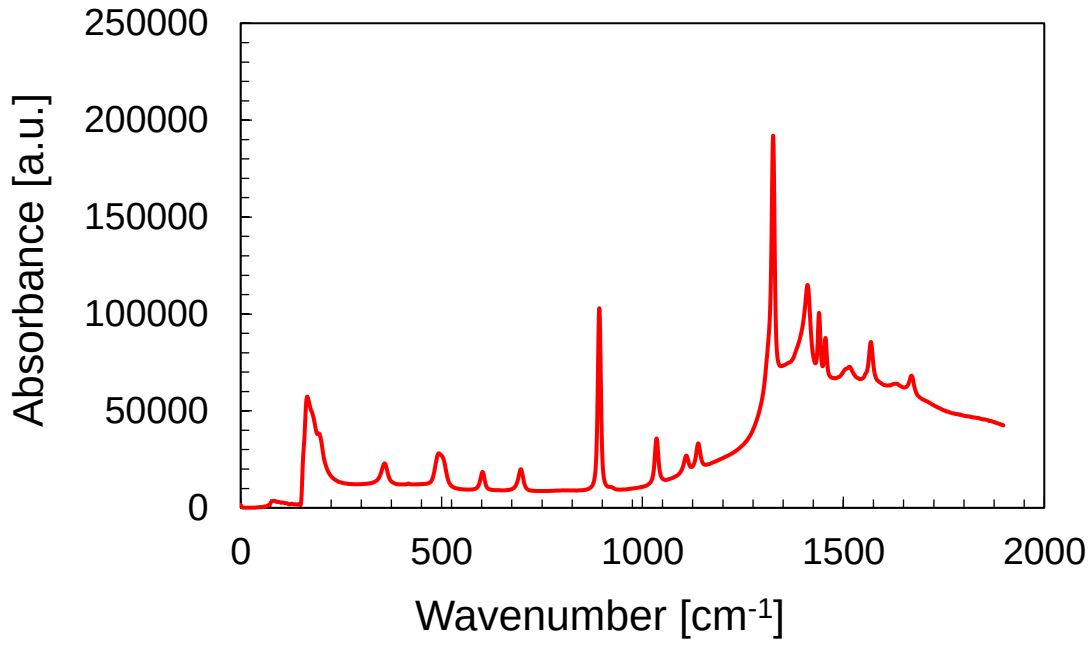

Figure. 4.9. Example Raman spectra for α-glycine with characteristic peaks.

The seeds were also characterised using optical microscopy enabling rapid size analysis on a number of seed crystal candidates and provided the opportunity to visually observe the morphological features. An example is shown in Figure. 4.10.

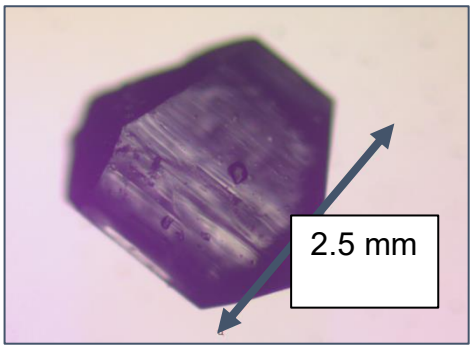

Figure. 4.10. An example seed crystal which was characterised using optical microscopy. This seed may be an example of one which would have been subsequently washed and added directly to a Crystalline vial for analysis of the secondary nucleation and crystal growth kinetics.

4.3.5 Secondary Nucleation Rates

Figure 4.11.(a) shows the crystal count from the Crystalline instrument over time, for seeded secondary nucleation experiments, at two example supersaturations to illustrate the two characteristic effects of changing supersaturation on the rate of secondary crystal nucleation. Firstly, the time taken for the onset of secondary nucleation decreases as S-1 increases, but it does not go to zero at the highest S-1 (see also Figure 4.13.), suggesting a delay time immediately following seeding. Secondly, once secondary nucleation has begun, the slope or rate of appearance of new crystals decreases with decreasing S-1. At lower S-1 the observed particle count features significant fluctuations between measurements at each time point.

While the ‘raw’ particle count in Figure 4.11. (a) indicates the number of identified particles in the Crystalline image at a given time, to obtain a secondary nucleation rate in more useful units we require the number of particles per unit volume. We therefore convert the particle count per image to particles per unit volume using a calibration previously developed[6], as shown in Figure 4.11. (b).

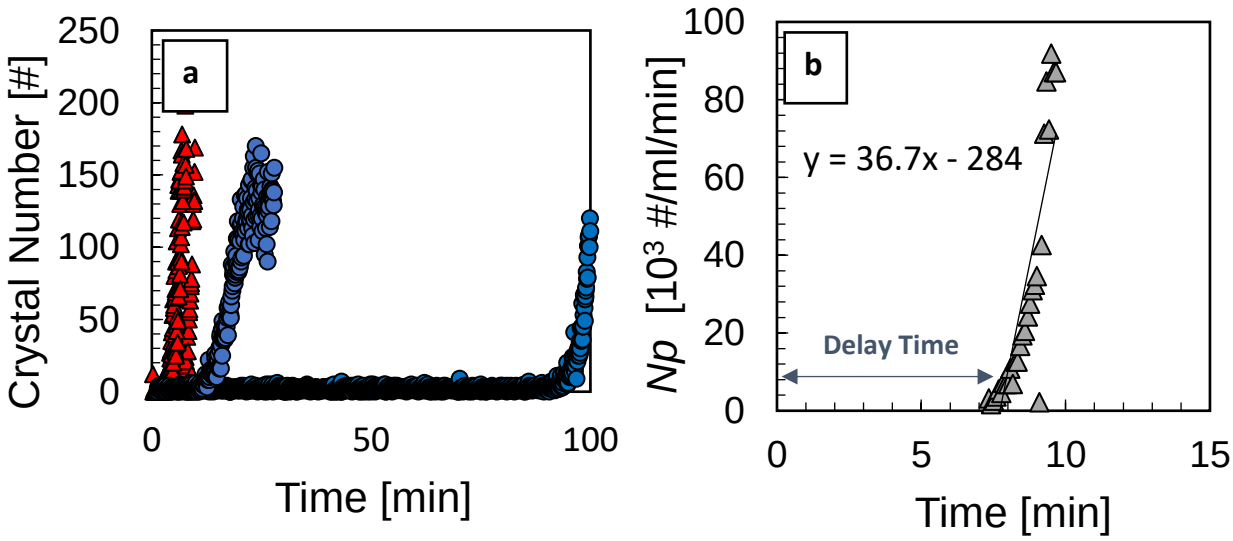

Figure 4.11. (a) The time taken for activation of secondary nucleation with seeding (red triangles) and without seed addition (blue circles) at 25°C. Here we show three repetitions for each, all three seeded vials nucleate within 10 minutes and only 2 of the three unseeded within the given time of 100 minutes. This is the ‘raw’ particle count per image as identified by the Crystalline instrument’s image analysis software. (b) An example of one of the same seeded vials with the calibration applied (see text) to convert the particle count to particles per unit volume.

The secondary nucleation rate (*B*) can be obtained by measuring the slope of the particle count per unit volume *vs* time within a relevant time window which is set by the limits of the particle detection and counting technique, as discussed in the methods section.

Results for secondary nucleation rate *vs* supersaturation are displayed in Figure 4.12. It is useful to note that these secondary nucleation rates were obtained from the same experiments that provided the seeded growth rate measurements in Figure 4.7., highlighting the amount of data that can be extracted rapidly from one single, small scale, seeded experimental run following the approach outlined here.

The secondary nucleation rates were seen to increase with supersaturation to a maximum of 2.8×10^5 particles per mL per minute. The secondary nucleation threshold is usually defined as the minimum supersaturation for secondary nucleation i.e., where the secondary nucleation rate reaches 0. Below the secondary nucleation threshold, it has been proposed that either only growth occurs or there could be nucleation taking place but with zero growth rates. Figure 4.12. (a) indicates that a secondary nucleation threshold can be recorded at $S-1 = 0.08$. Although there will be a value of supersaturation below which the secondary nucleation rate may become insignificant from a practical point of view (i.e., too small to be practically useful in an industrial process) it seems theoretically incorrect to define this as the threshold bordering a 'secondary nucleation dead zone'.

In the successful design of industrial crystallisation processes, it is essential to have an understanding of the growth kinetics at the working supersaturation as this will influence nucleation rates and therefore crystal size distribution[25]. In previous studies, the metastable zone has been divided into distinct regions, including, at minimal supersaturation, the 'dead zone' where there is assumed to be no growth or nucleation (see[26] for a recent review) and, at higher

supersaturation, the ‘growth only region’ where nucleation is negligible but growth of pre-existing crystals can occur. The limit of the growth-only region has been termed the ‘secondary nucleation threshold’, where existing crystals can give rise to new nuclei through secondary nucleation mechanisms.

There are many similarities between the secondary nucleation plot Figure 4.12. and the growth rate plot (Figure 4.7.). On linear plots, as discussed above, both growth rate (Figure 4.7.) and secondary nucleation rate (Figure 4.12.) apparently approach 0 as *S* approaches approximately 0.08 implying the existence of growth and secondary nucleation thresholds at this *S.* However, as with Figure 4.7.(b), plotting secondary nucleation rate respectively on a log scale in Figure 4.12. (b) shows that the hypothesis of a defined secondary nucleation threshold below which secondary nucleation does not take place is flawed.

Figure 4.12.(b) compares unseeded primary nucleation rates with the secondary nucleation rates from seeded experiments at the same supersaturations (all at temperatures of 25°C). Measured primary nucleation rates are similar to secondary nucleation rates, but with much greater variability from vial to vial across a given *S*, especially at the higher *S*. This is unsurprising given the stochasticity involved in primary nucleation and demonstrates that secondary nucleation by seeding provides a better, more controlled process with reduced variability.

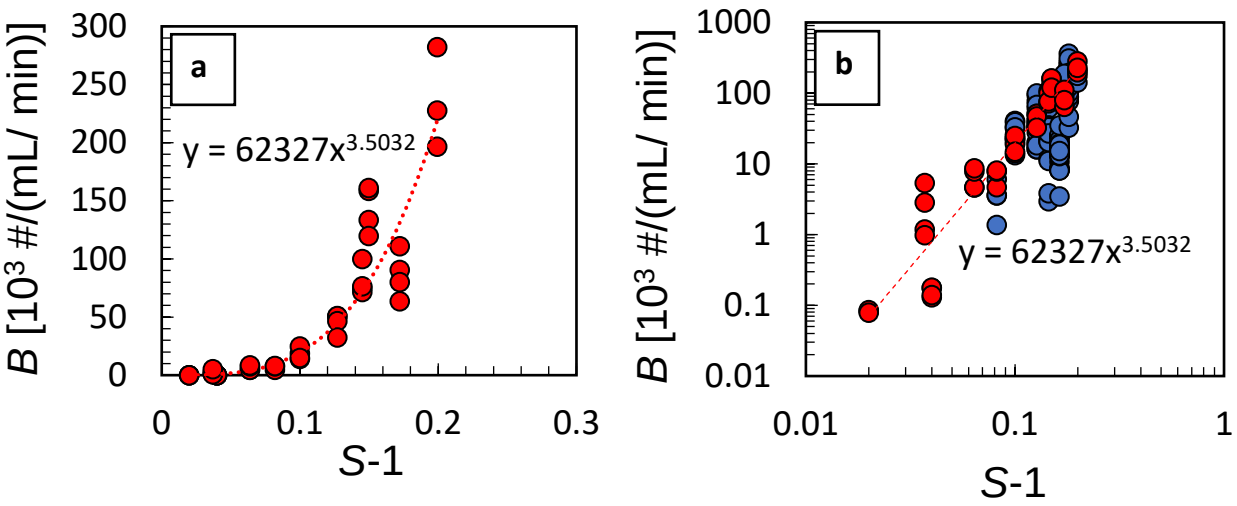

Figure. 4.12. The secondary nucleation rate for α-glycine single crystal seeding. The secondary nucleation rate was estimated at 10 different supersaturations ranging from *S*-1=0.02 to *S*-1=0.20. (a) Secondary nucleation rate plotted on a linear scale, implying the possibility of a 'threshold' below which secondary nucleation does not occur; (b) Secondary nucleation rate plotted on a log scale shows this is unlikely as the data broadly follow a power law trend in terms of *S-1*. Seeded and unseeded secondary nucleation rates for α-glycine. The secondary nucleation rate was calculated in seeded experiments at 10 different supersaturations ranging from *S*-1=0.02 to *S*-1=0.20 (red circles) and the unseeded secondary nucleation rate was determined from unseeded experiments at 8 supersaturations ranging from *S*-1=0.10 to *S*-1=0.20 (blue).

The single nucleus mechanism[9,10] proposes that primary nucleation in fact involves nucleation of a stable nucleus followed by crystal growth. Once it grows to a critical size, defined earlier (Figure 4.8.) as between 152 and 169 μm, it may act as a seed catalysing further nucleation by secondary nucleation in the 'one to many' effect. However, seed size has been previously observed to dictate nucleation rate[27] and so the distribution of potential minimum seed sizes inducing secondary nucleation can itself be the reason for the distribution of unseeded secondary nucleation rates.

4.3.6 Delay Time before Secondary Nucleation Detection

Figure 4.13. displays the supersaturation dependence of the ‘delay’ time between initial seeding and the initiation of secondary nucleation, i.e., the time at which the particle count begins to rise steeply (Figure 4.12. (a)). Delay time decreases as supersaturation increases, but it is clear from the data that it does not approach zero: there is a finite delay even at high supersatuation.

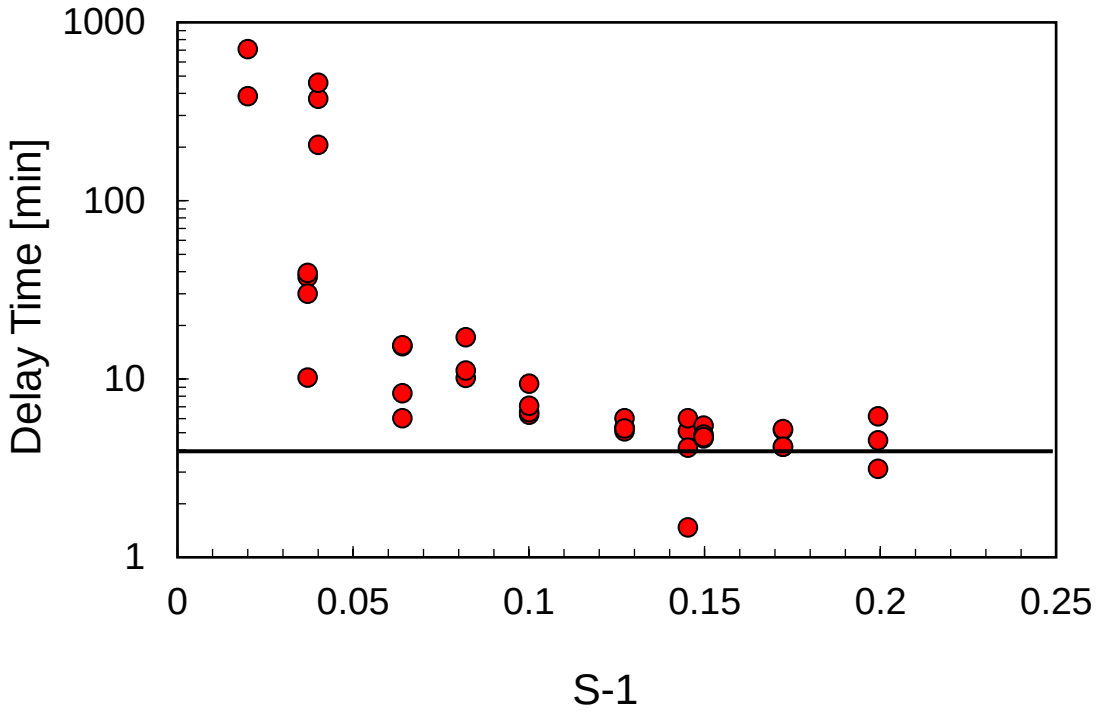

Figure 4.13. The red circles represent the delay time which is the time taken for initiation of secondary nucleation over a range of supersaturations. The black horizontal line is signifying that the delay time does not reach zero, and that there seems to be a plateau at around 4 minutes. This indicates that there is either some mechanism taking place such as activation of the seed or limitation of detection.

The delay time shown in Figure 4.13. and 4.14. suggests that there is then either a delay in the initiation of secondary nucleation from the seed or a delay in the secondary nuclei growing to a specific size to become detectable. In order to then estimate the size required to before detection, the delay time is shown against the inverse of crystal growth rate in Figure 4.14. which indicates that slower rates of crystal growth correlate with an increase in delay times. A linear fit was then passed through the data and the slope taken as the L_{min}.

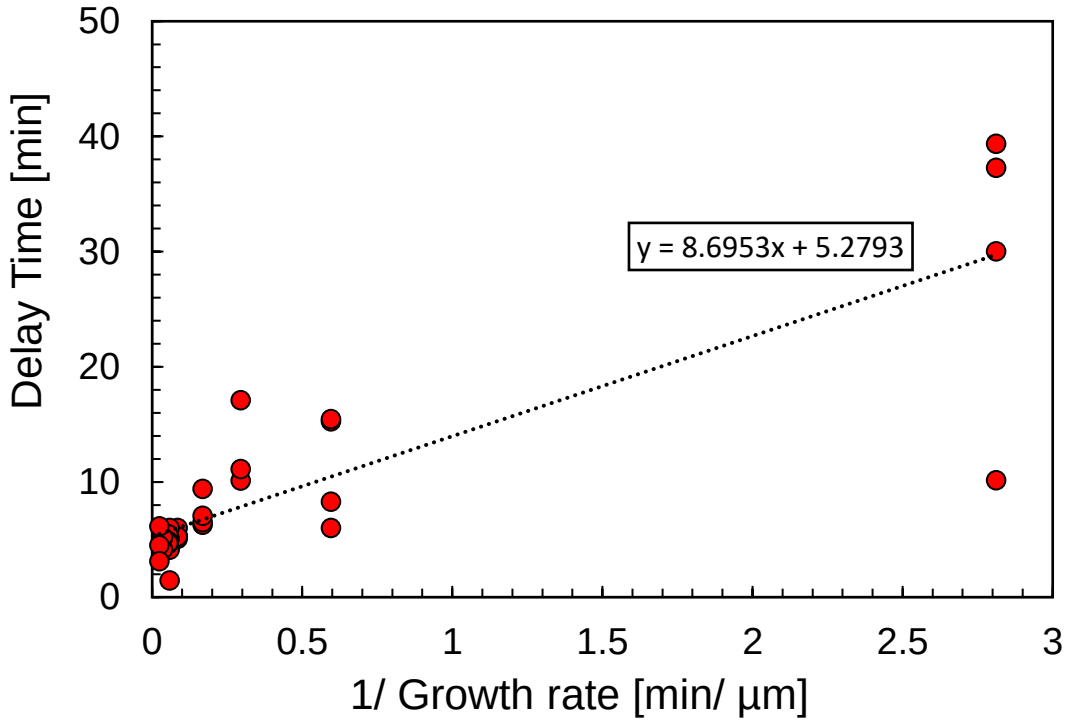

Figure 4.14 The secondary nucleation delay time (Figure 4.13.)) plotted against the inverse of the growth rate calculated from the power law fit (Figure 4.7.) for equivalent supersaturation in seeded experiments. A linear fit was passed through the data to estimate the size crystals need to grow to become detectable by the camera.

As shown the minimum size following seed addition and activation of secondary nucleation can be estimated at 9 µm. This suggests that following

seed addition, secondary nucleation takes place with the removal of small, surface layers or clusters which are swept away from the surface before growing. As the minimum size required for initiation of secondary nucleation was estimated to be in the 100s of µm range, it can be assumed that all crystals leading to the detection of secondary nucleation are generated from the seed crystal added.

It was previously proposed that commencement of secondary nucleation can be confirmed once there is an increase beyond the initial 10 crystals in focus following the addition of a seed crystal. Figure 4.14. enables an estimation that crystals begin to be detected once they reach the size of 9 µm. Assuming that this is in fact the case, then it should also be possible to see this in the raw, number weighted, particle size distribution traces.

Figure 4.15. shows example crystal size distributions at 3 selected supersaturations following commencement of secondary nucleation at a count of 10 crystals in focus. Here it can be seen that those crystals become visible to the image analysis algorithm at ~9 µm, indicating that delay observed in Figure 4.13. may not be a delay of secondary nucleation, but rather just a delay in the detection of the clusters swept away from the surface until they grow large enough to be counted. The dependence on supersaturation then becomes clear as we take into consideration the rate of growth.

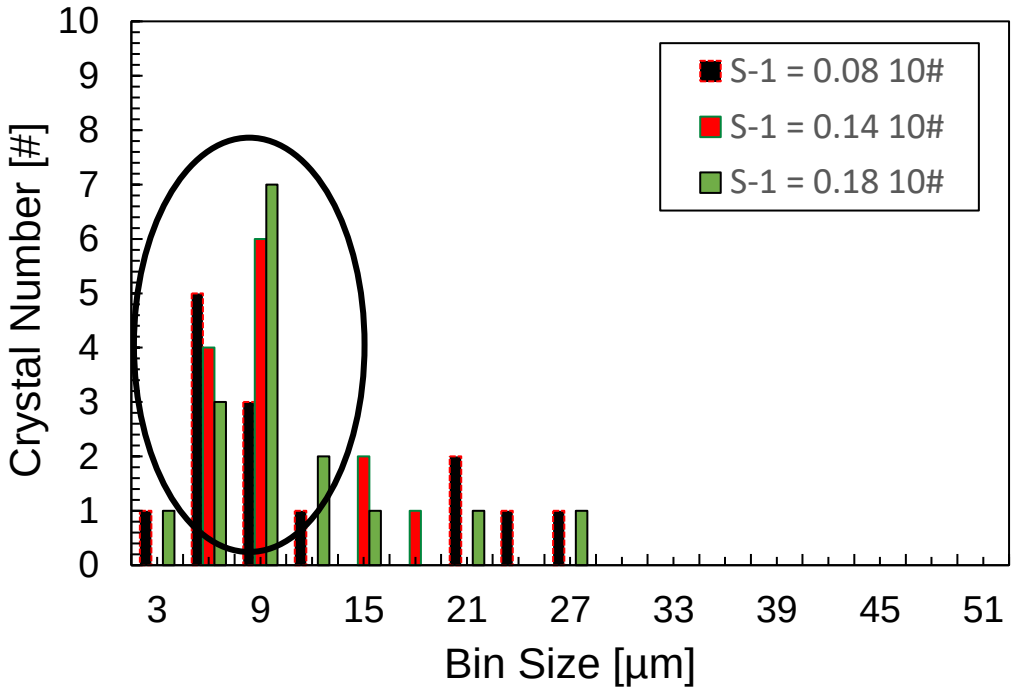

Figure 4.15. The number weighted particle size distribution at the point of confirmed initiation of secondary nucleation (>10 crystals in focus). Each bar is representative of a specific supersaturation which is indicated by the legend. The black rectangular oval highlights that most crystals are between 6 and 9 µm as secondary nucleation is firstly detected.

As shown, the predominant size of crystals in the raw traces is between 6 and 9 µm, consistent with the estaimated size based on crystal growth and delay time. It can therefore be assumed that the single crystal seed which has been added to the solution, is able to consistently generate further secondary nuclei by a surface breeding mechanism, to the degree that within minutes, secondary nucleation is both initiated and detected. It is then likely that those secondary nuclei, begin to themselves produce further nuclei once the critical threshold for L_{min} is reached at ~150 µm (Figure. 4.8.), multiplying the secondary nucleation rate.

4.3.6 Classification System

Crystal growth and secondary nucleation are often studied and presented as two conceptually separate processes or mechanisms. Our approach allows us to directly compare the growth rate and the corresponding secondary nucleation rate from the same experimental vials, based on the same imaging-based measurement and image analysis. The close relationship between growth and secondary nucleation is expected based on the power law kinetics that they both follow. This could suggest a possible mechanistic relationship where the secondary nucleation induced by fluid shear is related to growth of the crystal boundary layer in contact with the supersaturated solution, where loosely bound crystalline domains are swept from the boundary layer and serve as crystal nuclei. Figure 4.16. displays the secondary nucleation rate displayed directly against the corresponding growth rate within the proposed classification model.

In this classification system a series of regions are proposed and classified in relation to their growth and nucleation kinetics. The regions are selected and defined based on a characteristic time (τ), which could be a process specific residence time distribution and a characteristic length (L), possibly a target crystal size distribution. Therefore, how fast, and slow regions are characterised will be entirely process dependent and there is no generic approach. As an example, the definition of a fast-nucleating system for a seeded continuous process will be different to that of an unseeded batch process. In this work a characteristic time (τ) was selected of 10 minutes, at

this point, most vials had nucleated (Figure 4.13). A characteristic length was selected of 151.62 µM. This is the minimum seed size required for the initiation of secondary nucleation, estimated in Figure 4.8. (b).

As shown in Figure 4.16., the secondary nucleation rate was classified as fast, but the growth kinetics were slow. This is likely a result of the magnetic stirrer bar which often increases the nucleation rate by inducing very high localised shear on the seed crystal. Even so, both the nucleation and crystal growth kinetics increase simultaneously with supersaturation. The researcher can now begin to understand this system at this scale. If growth kinetics are too slow, supersaturation can be increased to move between regions. If the nucleation kinetics are too fast, the seed size and agitation rate can be reduced to slow it down. In this system, only as supersaturation was increased towards S-1 = 0.18 did the secondary nucleation and crystal growth relationship approach the fast-fast boundary.

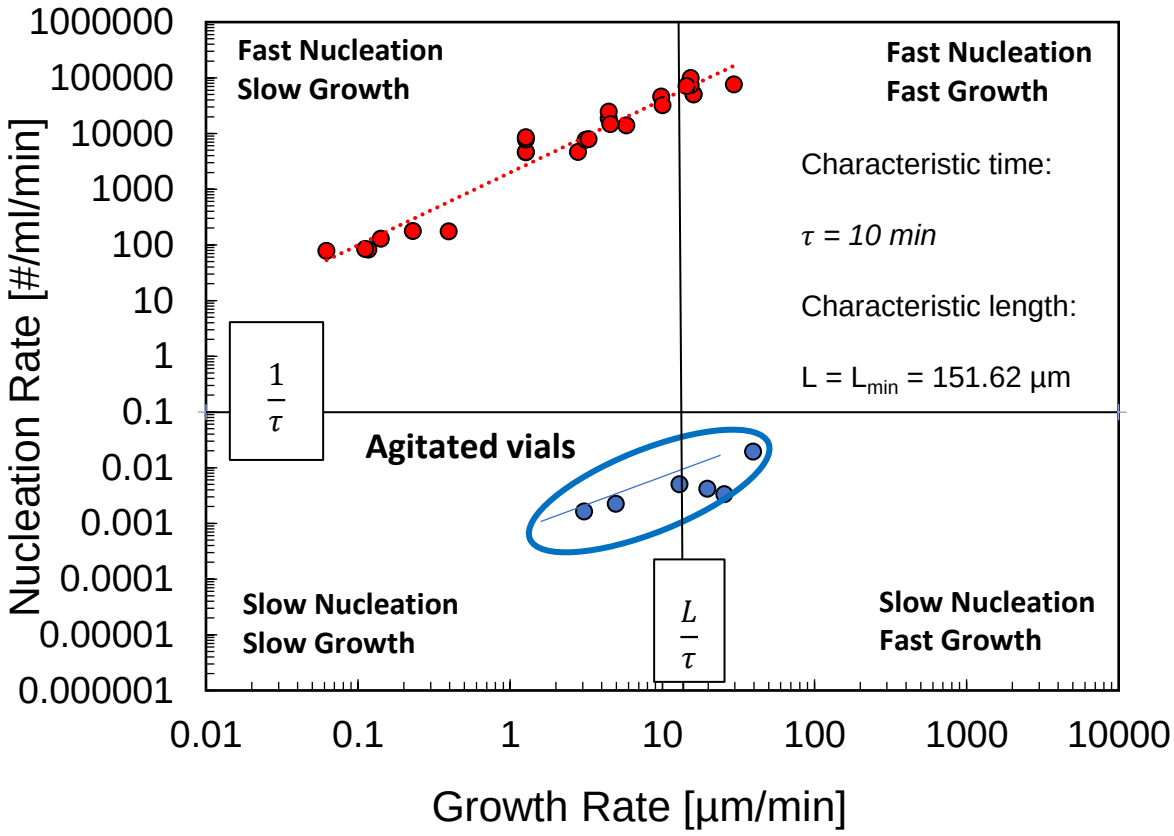

Figure 4.16. The glycine in water nucleation rates and corresponding growth kinetics have been plotted against one another. This has enabled a classification model to be drawn up which defines the kinetics into individual regions allowing the researcher to understand the kinetics in relation to the individual process selected. Secondary nucleation rates are shown in red and primary nucleation rates are shown in blue. The characteristic length and time are shown in the graph.

The primary nucleation (*J*) determined from the probability distributions showed slow nucleation behaviour with slow crystal growth rates. Therefore, to initiate nucleation, very high supersaturations will be required, but as discussed, if this system follows the 'single nucleus mechanism' then secondary nucleation will be initiated following the formation of a single crystal seed, resulting in much faster nucleation rates. This could lead to issues with

process control and CSD variations unless supersaturation could be precisely controlled.

4.4 Conclusions

This study has outlined the development and validation of a small-scale workflow enabling the rapid assessment and classification of secondary nucleation and growth kinetics of α-glycine at laboratory scales.

A comprehensive assessment of the primary nucleation kinetics was firstly completed to determine the conditions in which to seed. Small vials were then seeded to measure growth and secondary nucleation kinetics. An image analysis algorithm provided particle size distributions and counts. A MATLAB script converted the number weighted particle size distribution into volume weighted values. From this, the growth rates were calculated and compared with literature values recorded using much more time-consuming techniques. A calibration equation previously developed was applied to the particle counts to determine accurate secondary nucleation rates over a range of experimental supersaturations.

The fundamental mechanisms were then analysed, and, in this work, there was no clear dead-zone or secondary nucleation threshold when observed on a log-log plot. This highlighted that nucleation and growth kinetics follow typical power law dependencies and that the kinetics just decrease with supersaturation to very low rates. Next, a delay was observed upon addition

of a seed crystal to the supersaturated solution and detection of secondary nucleation. As the supersaturation was increased this delay time was decreased but it did not reach zero. This suggested that the surface layer of the seed may require growth and provides some mechanistic insight to the secondary nucleation behaviour where clusters are swept away from this activated boundary and undergo further growth before detection.

By assessing the secondary nucleation kinetics from unseeded vials, it was possible to confirm the single nucleus mechanism. Interestingly, the spread of nucleation rates was much larger than in seeded vials. By estimating the minimum size required for secondary nucleation to take place from induction time measurements it can be proposed that there is no clearly defined seed size to initiate secondary nucleation but instead it could be classified in the range of hundreds of micrometres. As seed size has been identified as a significant contributor to nucleation kinetics the spread of unseeded nucleation rates can be attributed to this.

Following this workflow ultimately leads the researcher to determine primary nucleation, growth and secondary nucleation kinetics from the same experimental vials using the most direct *in-situ* observation with an incorporated camera. A classification model has next been developed which considers primary nucleation, crystal growth and secondary nucleation kinetics, the most important parameters in crystallisation to enable the researcher to classify this based on their own individual process (characteristic time and crystal length). This rapid and small-scale workflow should allow more robust and optimised design of industrial crystallisation processes.

4.5 Key Points

- A rapid small-scale workflow enabling the assessment of secondary nucleation and crystal growth kinetics has been developed.
- Absence of crystal growth dead zone and secondary nucleation threshold.
- Classification system has been developed for nucleation and crystal growth kinetics.
- Glycine classified with primary nucleation slow and secondary nucleation fast with moderate growth rates up to S-1 = 0.2.

4.6 References

(1) Threlfall, T. L.; Coles, S. J. A Perspective on the Growth-Only Zone, the Secondary Nucleation Threshold and Crystal Size Distribution in Solution Crystallisation. *CrystEngComm*. 2016, pp 369–378. https://doi.org/10.1039/c5ce01608h.

(2) Agrawal, S.; Patterson, A. Secondary Nucleation: Mechanisms and Models. *Chem. Eng. Commun.* **2015**, *202* (5), 698–703.

(3) Acevedo, D.; Nagy, Z. K. Systematic Classification of Unseeded Batch Crystallization Systems for Achievable Shape and Size Analysis. *J. Cryst. Growth* **2014**, *394*, 97–105. https://doi.org/10.1016/j.jcrysgro.2014.02.024.

(4) Rathi, S.; Chavan, R. B.; Shastri, N. R. Classification of the Crystallization Tendency of Active Pharmaceutical Ingredients (APIs) and Nutraceuticals Based on Their Nucleation and Crystal Growth Behaviour in Solution State. **2020**, 70–82.

(5) Brown, C. J.; Mcglone, T.; Yerdelen, S.; Srirambhatla, V.; Mabbott, F.; Gurung, R.; Briuglia, M. L.; Ahmed, B.; Polyzois, H.; Mcginty, J.; Perciballi, F.; Fysikopoulos, D.; Macfhionnghaile, P.; Siddique, H.; Raval, V.; Harrington, T. S.; Vassileiou, A. D.; Robertson, M.; Prasad, E.; Johnston, A.; Johnston, B.; Nordon, A.; Srai, J. S.; Halbert, G.; Ter Horst, J. H.; Price, C. J.; Rielly, C. D.; Sefcik, J.; Florence, A. J. Enabling Precision Manufacturing of Active Pharmaceutical Ingredients: Workflow for Seeded Cooling Continuous Crystallisations. *Mol. Syst. Des. Eng.* **2018**, No. 3, 421–592. https://doi.org/10.1039/c7me00096k.

(6) Briuglia, M.; Sefcik, J.; ter. Horst, J. Measuring Secondary Nucleation through Single Crystal Seeding. *Cryst. growth Des.* **2019**, *19*, 421–429. https://doi.org/http://dx.doi.org/10.1021/acs.cgd.8b01515.

(7) Vesga, M. J.; McKechnie, D.; Mulheran, P. A.; Johnston, K.; Sefcik, J. Conundrum of γ Glycine Nucleation Revisited: To Stir or Not to Stir?

CrystEngComm **2019**, No. 21, 2234–2243. https://doi.org/10.1039/c8ce01829d.

(8) Rowland, D. Thermodynamic Properties of the Glycine + H2O System. *J. Phys. Chem. Ref. Data* **2018**, No. 47, 023104-1-023104–023115. https://doi.org/10.1063/1.5016677.

(9) Kadam, S. S.; Kramer, H. J. M.; Ter Horst, J. H. Combination of a Single Primary Nucleation Event and Secondary Nucleation in Crystallization Processes. *Cryst. Growth Des.* **2011**, No. 4, 1271–1277. https://doi.org/10.1021/cg101504c.

(10) Kulkarni, S. A.; Meekes, H.; Ter Horst, J. H. Polymorphism Control through a Single Nucleation Event. *Cryst. Growth Des.* **2014**, No. 14, 1493–1499. https://doi.org/10.1021/cg500059u.

(11) Brandel, C.; ter Horst, J. H. Measuring Induction Times and Crystal Nucleation Rates. *Faraday Discuss.* **2015**, No. 179, 199–214. https://doi.org/10.1039/c4fd00230j.

(12) Shi, Y.; Wang, L. Collective Vibrational Spectra of α- And γ-Glycine Studied by Terahertz and Raman Spectroscopy. *J. Phys. D. Appl. Phys.* **2005**, 3744. https://doi.org/10.1088/0022-3727/38/19/024.

(13) Shiau, L. D. Determination of the Nucleation and Growth Kinetics for Aqueous L-Glycine Solutions from the Turbidity Induction Time Data. *Crystals* **2018**, No. 403, 1–14. https://doi.org/10.3390/cryst8110403.

(14) Svoboda, V.; Venkatramanan, R.; Jaap, M.; Lue, L.; ter Horst, J. H.; Sefcik, J. Co-Crystal Phase Diagram Determination by the Solution Addition Method. *Cryst. Growth Des.* **2022**, 3380. https://doi.org/10.1021/acs.cgd.2c00169.

(15) Dowling, R.; Davey, R. J.; Curtis, R. A.; Han, G.; Poornachary, S. K.; Chow, P. S.; Tan, R. B. H. Acceleration of Crystal Growth Rates: An Unexpected Effect of Tailor-Made Additives. *Chem. Commun.* **2010**, No. 46, 5924–5926. https://doi.org/10.1039/c0cc00336k.

(16) Li, L.; Rodríguez-Hornedo, N. Growth Kinetics and Mechanism of

Glycine Crystals. *J. Cryst. Growth* **1992**. https://doi.org/10.1016/0022-0248(92)90172-F.

(17) Lung-Somarriba, B. L. M.; Moscosa-Santillan, M.; Porte, C.; Delacroix, A. Effect of Seeded Surface Area on Crystal Size Distribution in Glycine Batch Cooling Crystallization: A Seeding Methodology. *J. Cryst. Growth* **2004**, No. 270, 624–632. https://doi.org/10.1016/j.jcrysgro.2004.07.015.

(18) Sultana, M.; Jensen, K. F. Microfluidic Continuous Seeded Crystallization: Extraction of Growth Kinetics and Impact of Impurity on Morphology. *Cryst. Growth Des.* **2012**, No. 12, 6260–6266. https://doi.org/10.1021/cg301538y.

(19) Little, L. J.; Sear, R. P.; Keddie, J. L. Does the γ Polymorph of Glycine Nucleate Faster? A Quantitative Study of Nucleation from Aqueous Solution. **2015**, No. 15, 5345–5354. https://doi.org/10.1021/acs.cgd.5b00938.

(20) Dowling, R.; Davey, R. J.; Curtis, R. A.; Han, G.; Poornachary, S. K.; Chow, P. S.; Tan, R. B. H. Acceleration of Crystal Growth Rates: An Unexpected Effect of Tailor-Made Additives. *Chem. Commun.* **2010**, No. 46, 5924–5926. https://doi.org/10.1039/c0cc00336k.

(21) Caroline, A. O.; Cruz-cabeza, A. J.; Davey, R. J.; Vetter, T. Crystal Growth Cell Incorporating Automated Image Analysis Enabling Measurement of Facet Speci Fi c Crystal Growth Rates Published as Part of a Crystal Growth and Design Virtual Special Issue in Celebration of the Career of Roger. **2022**, No. 22, 2837–2848. https://doi.org/10.1021/acs.cgd.1c01019.

(22) Mullin, J. W. *Crystallisation, 4th Edition*; 2001. https://doi.org/10.1021/op0101005.

(23) Maggioni, G. M.; Mazzotti, M. Modelling the Stochastic Behaviour of Primary Nucleation. *Faraday Discuss.* **2015**, No. 179, 359–382. https://doi.org/10.1039/c4fd00255e.

(24) Coles, S. J.; Threlfall, T. L. A Perspective on a Century of Inert Seeds in

Crystallisation. *CrystEngComm* **2014**, *16*, 4355–4364. https://doi.org/10.1039/c3ce42359j.

(25) Ulrich, J.; Strege, C. Some Aspects of the Importance of Metastable Zone Width and Nucleation in Industrial Crystallizers. *J. Cryst. Growth* **2002**, No. 237–237, 3130–3135. https://doi.org/10.1016/S0022-0248(01)02284-9.

(26) Liu, Y.; Black, J. F. B.; Boon, K. F.; Cruz-Cabeza, A. J.; Davey, R. J.; Dowling, R. J.; George, N.; Hutchinson, A.; Montis, R. When Crystals Do Not Grow: The Growth Dead Zone. *Cryst. Growth Des.* **2019**, 4579–4587. https://doi.org/10.1021/acs.cgd.9b00478.

(27) Bauer, L. G.; Rosseau, R. W.; McCabe, W. L. Influnce of Crystal Size on the Rate of Contact Nucleation in Stirred Tank Crystallizers. **1974**, No. 4, 653–659.

Chapter. 5. Assessing the Effect of Fluid Shear on α-glycine Nucleation

5.1 Introduction

It is now widely accepted that secondary nucleation is a key effect in industrial crystallisation. Recent review papers[1,2,3] have summarised the literature from the past century demonstrating some level of basic understanding gradually developing over time. Although there is a large amount of literature evaluating secondary nucleation it seems that declarations are often made regarding the lack of fundamental understanding of secondary nucleation mechanisms[4,3].

Many mechanisms have been proposed for secondary nucleation i.e., nuclei[5], polycrystalline[6], and initial breeding[6] to name a few, but all are a descendent of shear or contact. Although it is likely that multiple mechanisms take place simultaneously in one form or another, there is often some contention between theories.

With the acceptance that secondary nucleation is then key in industrial crystallisation it is important that the methods followed to quantify secondary nucleation kinetics are validated and standardised across multiple crystallisation scales. It is crucial to evaluate specific conditions in a well-controlled manner and rapid computational fluid dynamics tools make understanding fluid flow properties such as shear rates, accessible under more complex flow conditions, especially for industrial crystallisation equipment. Fluid jets[7], Taylor Couette flow cells[8] and stirred tanks[9] have been used previously to measure and evaluate both primary and secondary nucleation in relation to fluid shear (Chapter 1, Section 1.4.3.2).

In this work a Couette flow cell was developed to monitor nucleation by laminar fluid shear within an approximated range of shear rates selected based on the characterisation of multiple crystalliser geometries and processing conditions using computational fluid dynamics (Chapter 1., Table 1.1.). A seed crystal was placed in the gap between two concentric cylinders, exposed to shearing fluid and a secondary nucleation rate was recorded using image analysis.

The aim of this research is to observe primary and secondary nucleation with crystal growth under laminar shear flow. This enables the observation of how secondary nucleation by fluid shear depends on experimental conditions and will hopefully help to facilitate scale-up of crystallisation processes.

5.2 Experimental

5.2.1 Couette Cell

A comprehensive overview of the Couette cell development and set-up was covered in Chapter 2.

A Couette flow cell was designed and developed to evaluate secondary nucleation in laminar fluid shear. The Couette cell is composed of two concentric cylinders where the outer cylinder is rotated to create laminar flow of the solution within the gap. A guide was printed and fixed to the stand ensuring that the inner cylinder was dropped between the outer in the same, precise location each time. Also added to the guide was a small hole, which was used to hold the seed holder in place so that the seed was held in the centre of the gap in the same location between the cylinders for each experiment. A motor was then attached to the base of the outer cylinder and the rotational rate could be controlled using the analogue display. To control the supersaturation, the inner cylinder was used as a water bath and the temperature in the gap could be controlled to ±0.5°C at the working supersaturation of 25°C.

Finally, to monitor the experiments a high-speed camera (Photron FASTCAM) was located at the side of the Couette cell and took snapshot images every 5 seconds throughout the experiment. The images were then automatically processed using an image analysis algorithm to generate a particle count and track the size of the growing seed. A diagram of the set-up is shown in Figure 5.1.

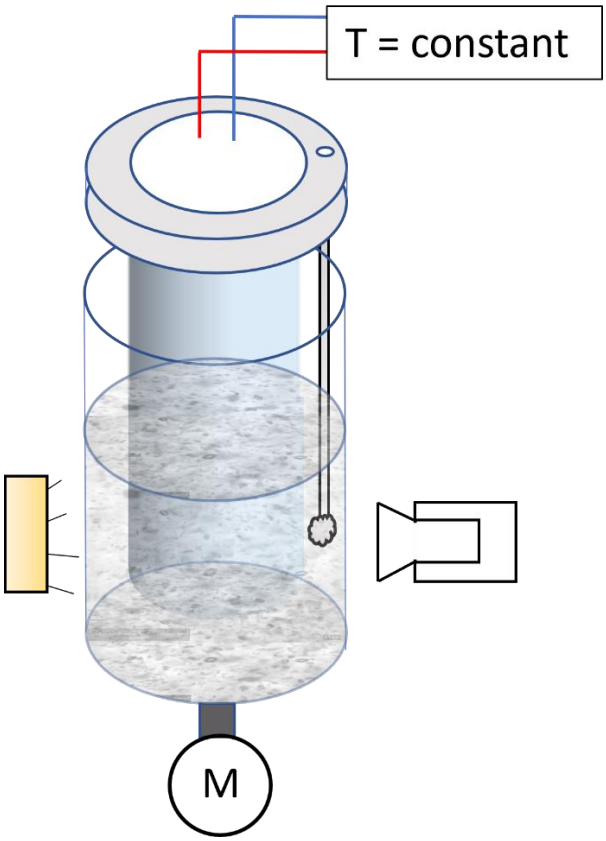

Figure 5.1. shows a schematic of the Couette flow cell. The outer cylinder rotates, and the inner cylinder remains stationary. The hollow inner cylinder is filled with re-circulated water to control the temperature of the liquid in the gap and so the supersaturation can be controlled. Using this temperature controlling technique, cooling profiles can be set where the solution is reduced to a working temperature over a given period of time. The motor at the base has an analogue display which allows the rotational rate to be precisely controlled. The seed was held in place between the two concentric cylinders and the high-speed camera took images every 5 seconds to assess the number of crystals in focus.

5.2.2.1 Couette Cell - Glycine Solution Preparation

A known quantity of glycine was firstly added to 50 mL of de-ionised water (milli-Q). The glycine solution was then heated to 60°C and stirred at 700 rpm using a magnetically agitated hot plate to achieve dissolution for one hour. The glycine solution was next transferred directly to the Couette cell and the

solution was held for an additional 30 minutes at 40°C to ensure that there was complete dissolution of any nuclei which may have formed on transfer. A temperature profile was then set, and the Couette cell was cooled to 25°C at a known rate. The solubility (C^*) of glycine in water at 25°C was known to be C^*=249.52 mg/g[10].

5.2.2.2 Calculating Shear Rates

As mentioned in Chapter 2. the Couette cell was used to assess secondary nucleation initiated exclusively by fluid shear. The seed was held in a fixed position which ensured the complete absence of any contact. The outer cylinder was rotated at a fixed rate and under the assumption that there is a linear velocity profile across the gap, the shear rate could be calculated from equation 5.1, which is a function of rotational rate and gap width. For more information, please refer to Chapter 2.

$$\dot{\gamma}_{\text{avg}} = \frac{2\pi N r_{out}}{r_{out} - r_{in}} \quad \textbf{(Eq. 5.1)}$$

Figure 5.2 shows how the seed crystal would appear between two concentric cylinders from the position looking down through the gap. As shown, the seed itself is 2 mm and the total width of the gap is 4 mm. This would leave a gap width of 1 mm between the outer rotating cylinder and the edge of the seed.

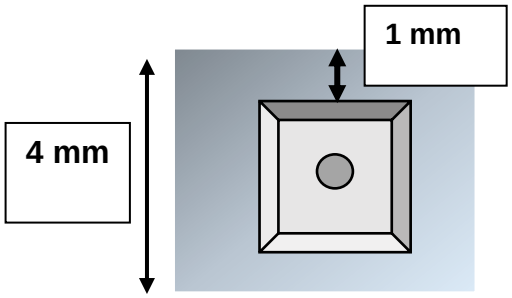

Figure 5.2. A schematic of the 'top-down' view of the seed in the gap of the Couette cell. The seed crystal sits in the centre of the gap and is 2 mm (±0.5mm) in size. The total, empty gap width is 4 mm which means that there is a 1 mm (± 0.25 mm) gap between the edge of the seed crystal and the rotating outer cylinder. The circle indicates the seed holder (capillary tube). The crystal 'seeds' were not cubic and therefore the length observed by the camera (Figure 5.3.) is likely to differ from that of the width.

Shear rates could be calculated, assuming there is no seed (L = 0) in the gap and these values are presented in Table 5.1.

For much of the work described here, there was a seed held in the gap between the two concentric cylinders. As the seed in the gap is exposed to the supersaturated solution, the seed crystal is growing during the experiment. This means that prior to detection of secondary nucleation, the gap width is shrinking (see section 5.3.6.). Therefore, calculating an exact shear rate with a seed held in place between the two cylinders proved to be challenging and, in this work, there was reluctance to present the seeded measurements in relation to shear rates and rather decided it was more appropriate to report in terms of rotational rate.

As shown in Table 5.1., the shear rates in the absence of a seed crystal range from 100 – 500 s^{-1}. From previous stirred tank estimates[11] (Table 1.1), 500 s^{-1} is likely to be close to the maximum shear experienced near to the impeller. It

may also be assumed that in the presence of a seed crystal in which the gap would be smaller, the rate of shear would be greater than those stated in Table 5.1.

Table 5.1. An overview of the rotational rates and corresponding shear rates used in the Couette cell experiments calculated using equation 5.1. The shear rate was calculated without a seed held in place. The Couette cell had the capability to run at much higher rotational rates and thus levels of shear, but this was beyond the initial scope of this project.

Rotational Rate (RPM)	**L = 0** **(Gap = 4 mm ± 0.5 mm)** **Shear Rates (s^{-1})**
100	84
200	168
300	251
400	335
600	503

Table 5.2. provides an overview of all the combinations of supersaturations and rotational rates discussed throughout this thesis chapter. The aim is to provide the reader with a clear map which can be referred to.

Table 5.2. An overview of the combinations of rotational rate and supersaturations assessed in this work for both seeded and unseeded experiments in the Couette Flow Cell.

Rotational Rate (RPM)	**Seeded – Supersaturation (*S*-1)**	**Unseeded – Supersaturation (*S-1*)**
100	0.10, 0.14 and 0.18	
200	0.10, 0.12, 0.14 and 0.18	0.18 and 0.14
300	0.10	
400	0.10, 0.14 and 0.18	
600	0.14 and 0.18	

5.2.2.3 Unseeded Experiments

A glycine solution of 50 mL was firstly prepared following the method outlined in 5.2.2.1. Once transferred to the Couette cell, the solution was kept at 40°C for 30 minutes ensuring complete dissolution of any fine nuclei which might have formed during transfer. Throughout the isothermal dissolution phase at 40°C, the outer cylinder was rotated at 50 rpm. As the cooling profile commenced, the rotation was switched off and the solution was cooled over a period of 30 minutes to a working temperature of 25°C. As the experimental operating temperature of 25°C was reached, the motor was set at a known rotational rate (RPM) and the experiment is initiated, this is time zero (T_0). Each experiment was completed under isothermal conditions. Two supersaturations

were selected (S-1 = 0.18 and 0.14) with 10 repetitions recorded at S-1 = 0.18 and 11 recorded at S-1 = 0.14. This enabled the estimation of primary nucleation kinetics (J) and growth times (t_g) from the induction time probability distributions (Chapter 4.). In previous work[12] it was discussed that 10 data points were enough to generate a probability distribution for estimation of the primary nucleation kinetics. It should be noted that more experiments would improve both the fit of the model and reduce the statistical error, perhaps improving the accuracy of the predictions.

Once rotation was initiated, images were taken every 5 seconds throughout the experiment and an induction time was recorded at the point when there was a clear and consistent inflection point in the particle count (Chapter 2, Figure 2.9.)

5.2.2.4 Seeded Experiments

Seeded experiments were initially prepared following the same solution preparation method as previously outlined (5.2.2.1 and 5.2.2.3). A known quantity of glycine was dissolved in water before transfer to the Couette Cell. An in-situ dissolution phase in the Couette cell was next completed at 40°C for 30 minutes to dissolve any fine nuclei before initiating the cooling ramp to 25°C.

A glycine seed crystal (length of 2.0 ± 0.5 mm) was glued to the base of a glass capillary tube (1.5 mm diameter). To ensure that the seed crystal was free from any contaminants in the form of micro-sized crystallites or dust, it was washed,

passing water over the surface to dissolve or remove any fine particles. This then excluded any theory of initial breeding as the source of the secondary nuclei. The seed was attached to the guide and held in place between the two concentric cylinders above the solution.

As the solution reached 25°C the seed was manually dropped into solution sitting centrally, between the two cylinders and rotation switched on. The camera observed the seed throughout the experiment taking images regularly and the seed size and number of crystals present in an image were recorded.

5.2.2.5 Assessing Crystal Growth Rates in Controlled Shear

The crystal growth kinetics were measured in the Couette cell using a novel imaging technique. From each seeded experiment, an image was taken automatically every 5 seconds and the crystal growth kinetics were recorded. Typical images are shown in Figures. 5.3 and 5.4.

Ensuring that the seed crystal was firstly placed directly into the image frame, with all edges clearly visible was essential. The edge of the crystal was then detected, and the algorithm generated a surface area (A) in micrometres squared. The surface area was converted to overall ‘length’ (L) ($L = \sqrt{A}$) in µm’s to compare with previous values from our work (Chapter 4.) and from literature. The growth rate was then recorded by plotting crystal seed size (µm) against the time (min) and passing a linear fit through the data. The slope was then taken as the growth rate. This is shown below in Figure 5.3.

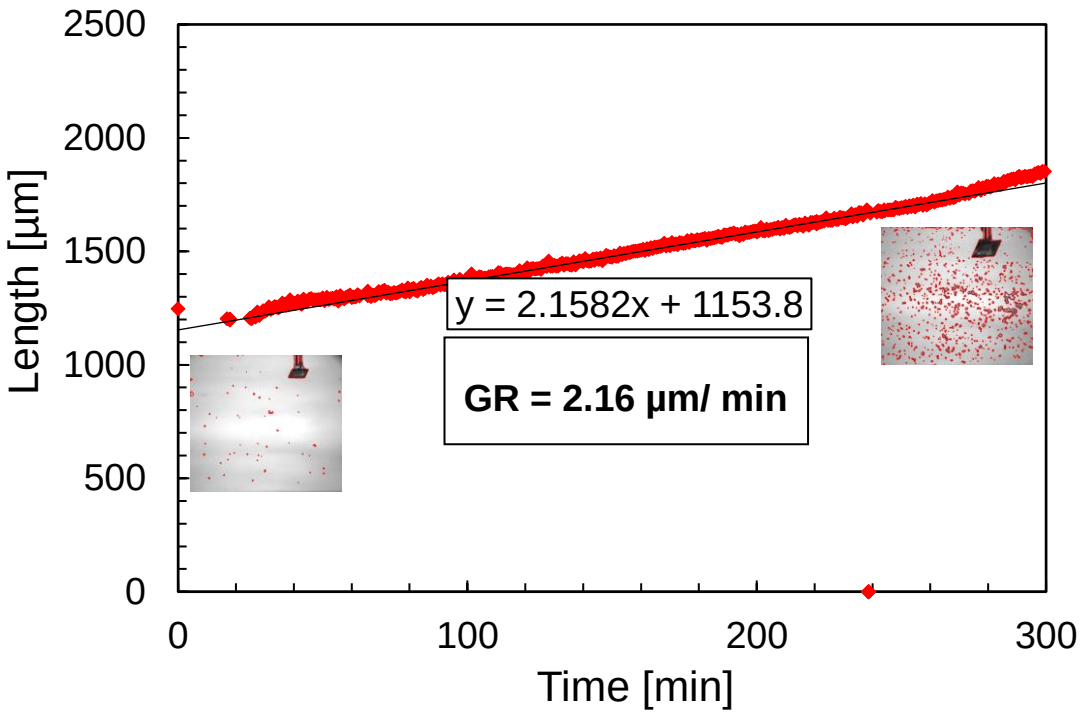

Figure 5.3. An example of a raw, crystal size (L) vs time trace used to determine the crystal growth kinetics. The edge of the crystal seed is automatically detected in each image and the size tracked for the duration of the experiment. A linear trendline is then fitted to the data and the slope taken as the growth rate.

5.2.2.6 Measuring Secondary Nucleation Kinetics in Laminar Shear

As mentioned, the high-speed camera took an image automatically every 5 seconds. The images were subsequently processed using an algorithm which automatically detected, counted, and output the number of crystals at the specific time. A calibration was then performed using 50 µm, polystyrene microspheres (EPRUI Nanoparticles & Microspheres Co) to enable the conversion of a crystal number into a crystal number density (N_p), representative of the unit volume rather than what is seen in the specific image.

The secondary nucleation rate was determined by the change in number density over time following a delay time of secondary nucleation and before the suspension density reaches a maximum (Figure. 5.16.). The secondary nucleation rate was determined over a range of experimental supersaturations including S-1 = 0.10, 0.12, 0.14 and 0.18 (Table 5.2.). Each was then exposed to a range of shear rates (Table. 5.1.).

Although it was not possible to track the particle size distribution to estimate the minimum size of crystal which could be detected (Chapter 4), the individual pixel size was known to be 21 µm and this was therefore used to estimate that the absolute minimum size that could be detected would be in the range of 20-30 µm.

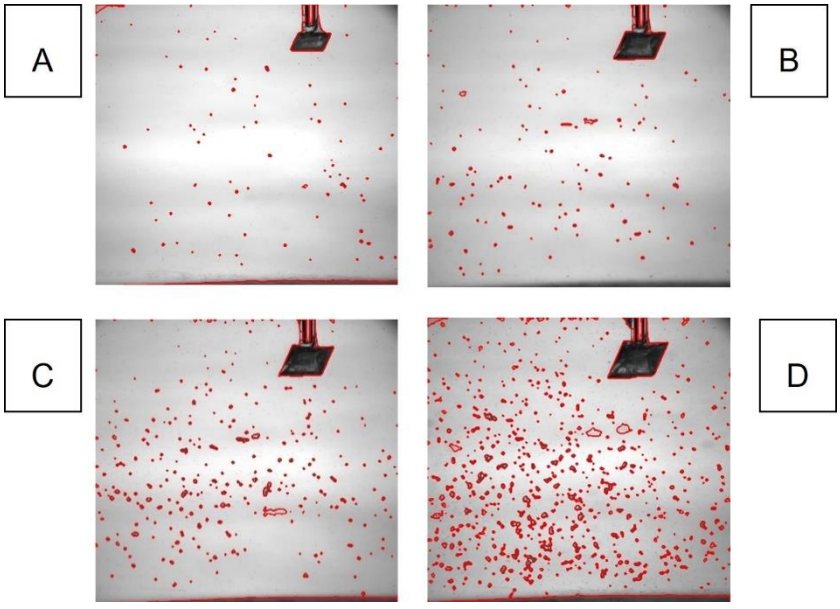

Figure 5.4. The four images displayed here represent the progression of a crystallisation experiment in the Couette flow cell. The high-speed camera monitors the seed crystal throughout the experiment and as shown, the crystal size becomes larger. The image analysis algorithm detects the number of crystals in focus and provides a number against the corresponding time. This

is then used to calculate the rate of secondary nucleation as the number of crystals in focus increases. The edge of the crystal is also detected and the change in size is automatically recorded against the corresponding time.

5.2.3 Seed on a Stick – Stirred Vessel (6 mL, 100 mL and 700 mL)

Following estimation of the secondary nucleation kinetics in the Couette cell with controlled laminar shear, more representative flow regimes were employed as a comparison. The Crystalline with overhead stirring (6 mL), EasyMax (100 mL) and OptiMax (700 mL) from Mettler Toledo were selected as the stirred tank reactors (STR's) all monitored using image analysis. The seed-on-a-stick technique was used in all three set-ups to ensure complete isolation of the mechanism fluid shear, to induce secondary nucleation.

Experiments were conducted at 6-, 100- and 700-mL volumes with agitation using overhead stirring. The Crystalline instrument was used to obtain the number of crystals in the observed volume from analysis of images taken with the instrument's 'built-in' camera. All measurements were obtained under isothermal conditions at T=25°C, i.e., matching the conditions of the induction time experiments (Chapter 4). At larger scales, using both the EasyMax and OptiMax, the PVM from Mettler Toledo was used to count the number of crystals which passed through the viewing window. Again, all experiments were conducted under isothermal conditions at T=25°C.

5.2.3.1 Solution Preparation – Stirred Vessels

Solution preparation remained the same independent of scale. A known mass of glycine was firstly dissolved in a specific volume of de-ionised water and

mixed at 60°C using a magnetically agitated hot plate. Once dissolved, the solution was directly added to the specific vessel (a pipette was used to transfer the 6 mL volume to Crystalline vials). The solution was then further dissolved in the respective stirred tank for 30 minutes, a temperature profile was set to cool to the working temperature of 25°C and all experiments were completed under isothermal conditions.

5.2.3.2 Seeded Secondary Nucleation Rates – Stirred Vessels

A schematic of the experimental set-ups used in this study is presented in Figure. 5.5. The solution was firstly prepared following the method outlined in 5.2.3.1 and once the working temperature of 25°C was reached, the seed was lowered into solution. As with previous experiments, the seed crystal of 2.0 mm (± 0.5 mm) was glued to the 'seed holder', washed and characterised before it was added to the stirred tank. For the Crystalline and EasyMax experiments, a glass capillary tube (1.5 mm diameter) was used to hold the seed in place but due to the larger dimensions of the OptiMax, a longer, specially designed and 3D-printed holder was created.

Once the seed was dropped into solution, the agitation rate was set, switched on and the experiment was initiated (T_0). For the EasyMax experiments, two rotational rates were selected of 250 and 500 RPM but for the OptiMax only one rotational rate was used of 250 RPM. In the Crystalline, to stay consistent with Chapter 4. one rotational rate of 700 RPM was employed. The shear rates

in the EasyMax and OptiMax were then estimated using the DynoChem mixing toolbox from Mettler Toledo.

To compare secondary nucleation rates with those previously presented, a calibration was completed for each experimental set-up. This excluded the Crystalline where a calibration curve had been already developed[13]. Once the suspension (number) density N_ρ was calculated, the limits of the image analysis algorithm were determined. This refers to the point where the onset of secondary nucleation can be confirmed following a critical number count and up to the point in which the maximum crystal number in focus is reached (Figure. 5.16.). Between these two limits, the secondary nucleation rate was defined by the change in suspension density over time.

The PVM was used rather than the FBRM to keep measurements consistent, utilising imaging across all scales. The same image processing algorithm was used for Couette cell experiments, the OptiMax and the EasyMax experiments. Crystalline images were automatically processed using the standard built-in, Technobis software.

A range of experimental supersaturations were evaluated with a minimum of three repetitions recorded for each set of conditions.

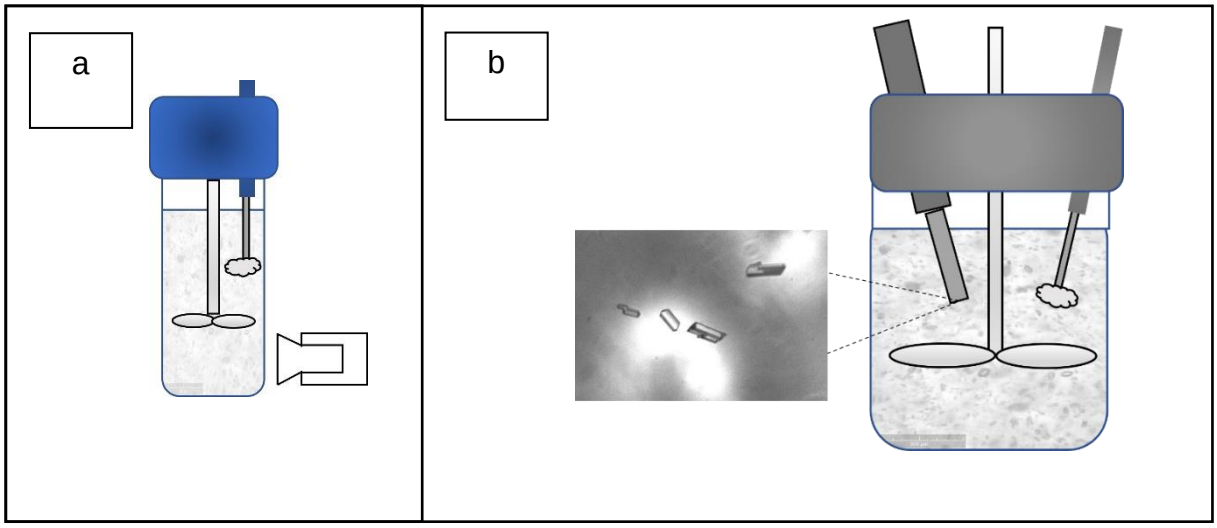

Figure. 5.5. (a) A diagram displaying the crystalline set-up with the overhead stirrer and 'seed on a stick' method. The seed was held above the rotating impeller blade and exposed to shear in order to induce secondary nucleation. (b) A schematic of the stirred tank set-up. A PVM camera was used to monitor the secondary nucleation rates in the EasyMax and OptiMax experiments. Seded experiments were completed using the seed on a stick technique in which a seed was held above the rotating impeller.

5.3 Results and Discussion

5.3.1 Couette Cell Set-up

Although the set-up used in this study was not the first Couette cell to measure nucleation under controlled shear[12,14], this set-up was developed based on challenges identified from previous literature and in this work, novel solutions were proposed. This included, controlled supersaturation with precise temperature control, outer cylinder rotation to generate laminar shear and high-resolution image analysis to quantify nucleation kinetics.

As supersaturation is the driving force for nucleation and crystal growth, controlled generation and maintenance of supersaturation is essential when

attempting to map the fundamental secondary nucleation behaviour. Some previous studies which have utilised the Couette cell set-up have conducted experiments at ‘room temperature’. In this work room temperature measurements were deemed undesirable as room temperature can often fluctuate and is difficult to control to any degree of certainty. With this, bringing the solution to room temperature is arbitrary and may take a significant amount of time depending on what temperature the solution was prepared at. It is likely that the solution will be passing through the regions of the metastable zone as it crosses the saturation boundary before reaching the desired supersaturation. In this study, a water bath technique was developed in which specific cooling profiles could be designed to quickly reach the desired temperature and prevent any primary nucleation taking place before reaching the working supersaturation.

Many previous Couette cell experiments[8] utilised an inner rotating cylinder. In this study, to achieve laminar flow across the width of the gap, the outer cylinder was rotated. It was found in literature[15] that with an outer rotating cylinder, stable laminar flow could be maintained to much higher rotational rates than the inner rotating set-ups. It is also worth noting that the seed will influence the flow regime, but this is out of the scope of this project.

To assess the flow regime within the gap in the presence of a seed crystal, a glycine suspension was created, and the crystals were tracked using the video function of the high-speed camera. From this it could then be assumed that the seed did not ‘significantly’ disrupt the laminar flow regime in the bulk of the solution and the crystals could be observed to continue their trajectory with

gradual sedimentation. By subjecting the seed to laminar flow, it is possible to assess the effect of controlled laminar shear on the kinetics of secondary nucleation. Following a review of the literature, a range of shear rates (s^{-1}) were selected which were representative of those experienced in stirred tanks, particularly levels of shear seen near the impeller. The rotational rates and corresponding unseeded shear rates selected are outlined in Table. 5.1.

Finally, previous Couette cell studies have used offline measurement devices such as microscopic observation at the end of the experiment[16] or application of webcams which may only reasonably detect cloud points due to poor resolution. In this study, a high-speed camera was used to monitor the seed crystal which could track and detect individual crystals in the micron range. This novel set-up provided direct quantitative information regarding the secondary nucleation and crystal growth rate of the crystals in the gap.

5.3.2 Couette Cell – Delay Times and Induction Times

The metastable zone width was determined experimentally using the Crystal 16 and reviewed in detail in Chapter 4. Within the metastable zone width, supersaturations were then calculated from the polythermal solubility (extrapolations) recorded in Chapter 3.

To remove any likelihood of initial breeding taking place, the seed was washed prior to addition. Initial breeding is defined by the removal of small, micro sized crystallites which are not bound by crystalline bridges to the seed crystal but rather, ‘resting’ on the surface like small specs of dust. When present, the

crystallites appear to induce secondary nucleation, but with a washing step, it can be confirmed that this would not represent a shear mechanism being observed in this work.

The delay time is defined here as the time elapsed between seed addition to the vessel and detection of nucleation. The induction time on the other hand, is the time elapsed between initiation of rotation and detection of nucleation without seed addition. The difference between the two is simply due to the presence of a seed.

Figure 5.6. shows seeded and unseeded measurements recorded in this work using the Couette flow cell, compared across multiple supersaturations at 200 RPM (unseeded shear rate of 168 s^{-1}). Also shown are unseeded literature data[12], recorded in a Couette cell with outer cylinder rotation at a relative supersaturation of S-1 = 0.4 and a rotational rate of 250 RPM. It is clear from this data that the seeded delay time is much shorter and with a narrower distribution than the corresponding unseeded induction time at the same supersaturations.

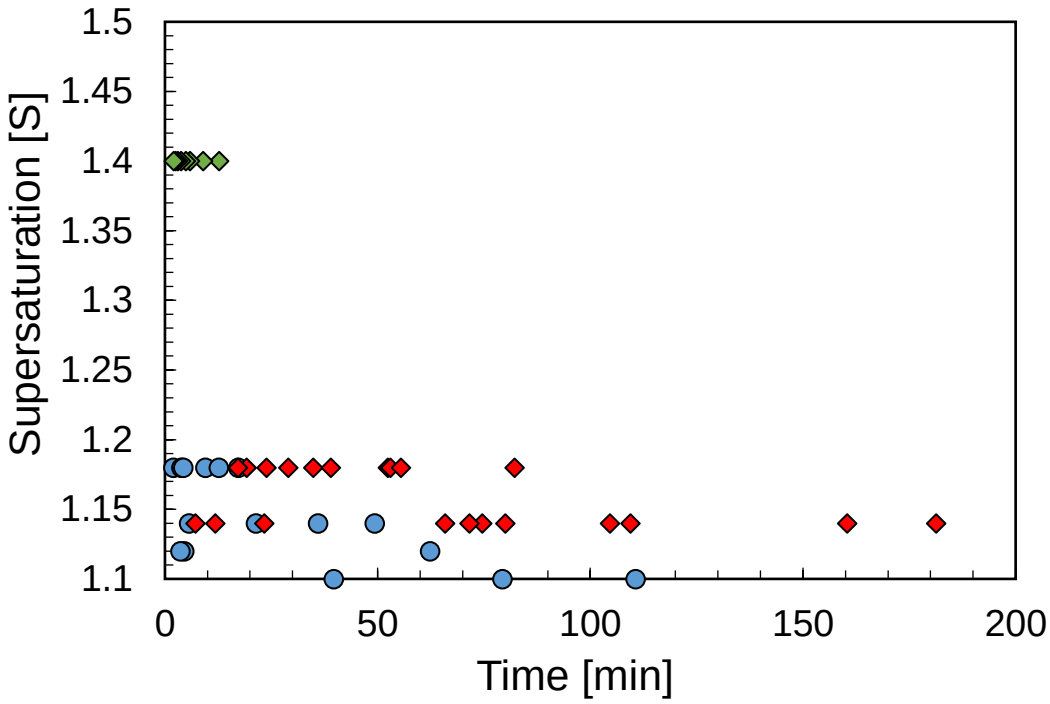

Figure. 5.6. The unseeded induction times (red diamonds) compared with seeded delay times (blue circles) in the Couette Flow Cell with literature values[12] for unseeded induction time at a supersaturation of 0.4 (green diamonds). The results from this work are presented at a rotational rate of 200 RPM (unseeded shear rate - 168 s^{-1}) to compare with literature values at 250 RPM.

There is a considerable difference between the point of detection of nucleation in seeded and unseeded experiments, even with only 'modest' rotational rates. This indicates that fluid shear alone, does undoubtedly have the potential to induce secondary nucleation in the absence of any contact-based mechanism. The three red diamonds at a supersaturation of 0.14 which are noticeably and significantly shorter than other delay times at the same supersaturation suggest that there were likely some impurities present in the solution which may have initiated nucleation much earlier than expected.

As illustrated in Figure 5.6., the literature data shows that nucleation was detected in the projected region, nucleating much earlier than the unseeded Couette cell data collected in this work at lower supersaturations.

5.3.3 Couette Cell Primary Nucleation Rates

The unseeded induction times were then replotted in the form of a probability distribution, as shown in Figure 5.7. The corresponding primary nucleation rates (J) and growth times (t_g) are then reported in Table. 5.3. As shown in Figure 5.7. the nucleation rate gets much faster with an increase in the supersaturation shown by the steepness of the slope.

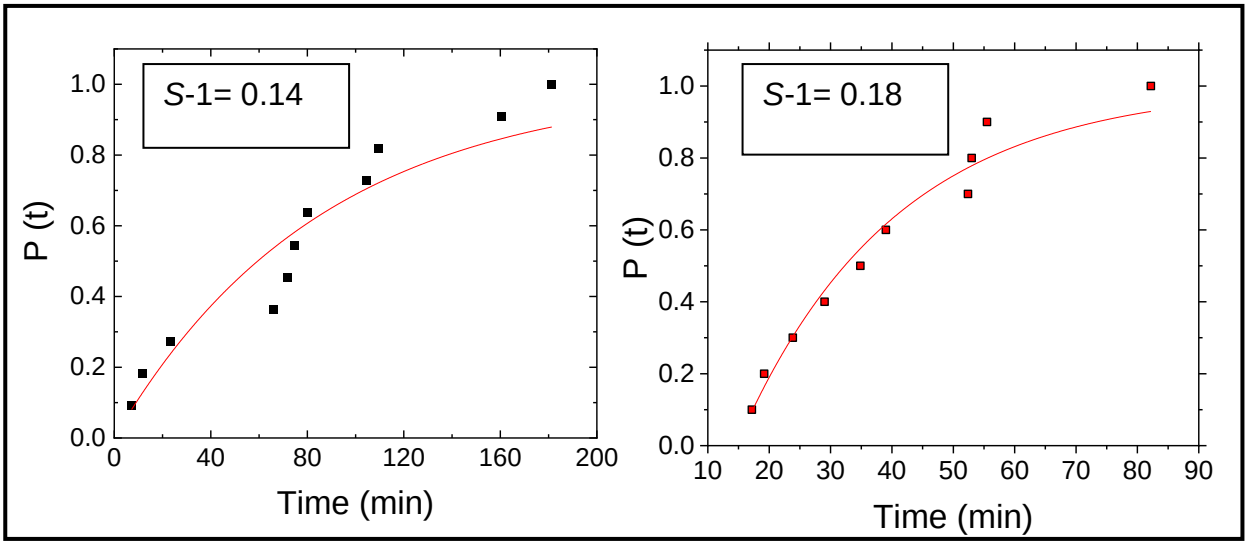

Figure. 5.7 The probability distributions from the unseeded Couette cell experiments. 11 measurements were recorded at S-1 = 0.14 and 10 at S-1 = 0.18. The primary nucleation rate and growth time could then be estimated at a shear rate of 168 s^{-1} (200 RPM).

As the growth time is a function of the time taken for the formation of a primary nucleation event, growth to a certain size and subsequently, secondary nucleation, it is expected that with a higher supersaturation there would be a shorter growth time. Interestingly, the growth time decreases with a decrease in supersaturation. This was also noticed in Figure 5.6. suggesting, once again that at some of the induction times may have been shortened due to the presence of impurities or possibly it is subject to simply, statistical variability (see also Figures 4.4 and Table 4.2).

Table 5.2. displays the J and t_g values obtained from the fit of the model and the level of experimental error. With an increase in the number of experiments, it should be possible to reduce this error and enhance the probability distribution fits and validity of the data. In this study, it was assumed that 10 repetitions were enough to generate a distribution which would put the data in a ‘ballpark’ to compare with other previous values in different experimental set-ups (Figure 5.20.).

Table 5.3. Outlines the results from the unseeded primary nucleation experiments displayed along with the corresponding supersaturation. The primary nucleation rate and growth time are displayed. The volume used was 50 mL. The nucleation rates recorded in this work are compared below with values taken from literature.

	Unseeded Primary Nucleation in Controlled Shear	
Shear Rate [s^{-1}]	168	
RPM	200	
***S*-1**	0.14	0.18
Percent nucleated (%)	100	100
***J* [#/ ml/ min]**	$2.33x10^{-4}$ (± $3x10^{-5}$)	$7.85x10^{-4}$ (± $7.1x10^{-5}$)
t_g **[min]**	0 (± 6)	15 (± 2)

5.3.4 Couette Cell Seeded Delay Times with Rotational Rate Dependence

The delay time was then evaluated in relation to variable rotational rates and supersaturation, this is shown in Figure. 5.8. Four supersaturations were selected for measurement including, *S*-1 = 0.10, 0.12, 0.14 and 0.18. Following exposure to increased rotational rates it was apparent that there was a significant reduction in the time taken for initiation of secondary nucleation but the extent to this reduction seems to depend on the supersaturation.

Interestingly, Figure. 5.8. indicates that the rotational rate has a more pronounced effect on secondary nucleation at lower supersaturations than higher supersaturations. This may be indicative of the relationship between nucleation and crystal growth which has been previously discussed in Chapter 4.

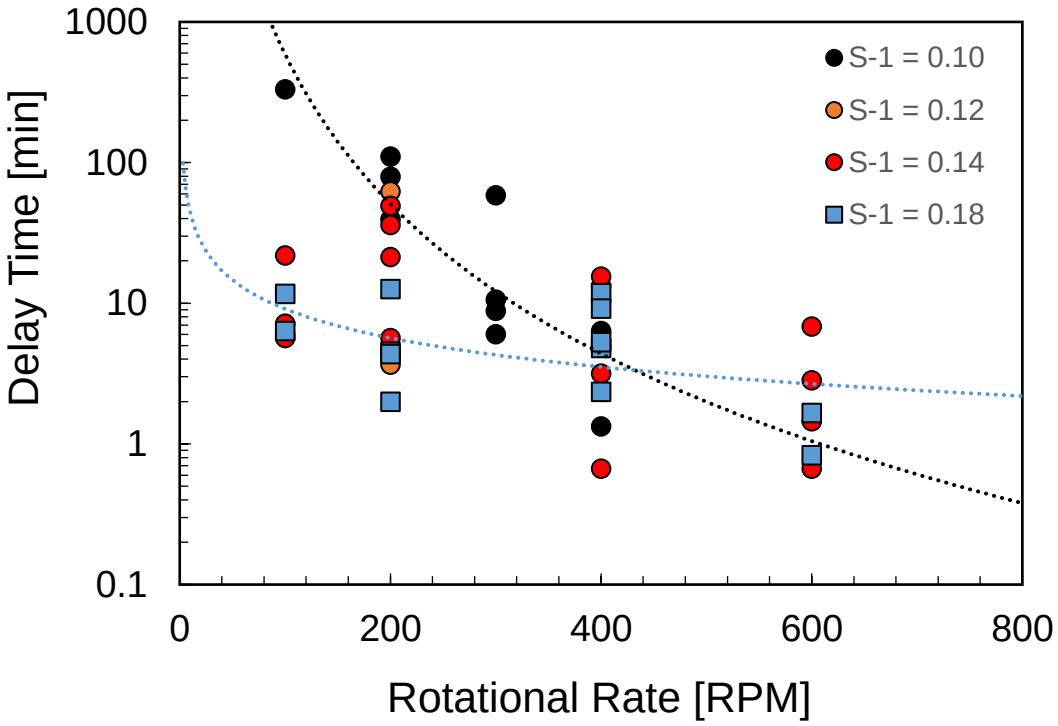

Figure. 5.8. The delay time following seed addition plotted against a corresponding rotational rate ranging from 100 to 600 RPM. Four supersaturations are shown here, *S*-1 = 0.10 (black circles), *S*-1 = 0.12 (orange circles), *S*-1 = 0.14 (red circles) and *S*-1 = 0.18 (blue squares). Both the black (*S*-1 = 0.10) and blue (*S*-1 = 0.18) lines indicate power law fits.

There is an observable decrease in the delay time with an increase in the rotational rate, much more obvious at a lower supersaturation and it seems here to display a power law relationship. Previous research, which has looked at the embryo coagulation secondary nucleation theory[17] and nuclei breeding[5]

suggests that pre-nucleation clusters attach themselves to the seed surface, use it for growth and are then dislodged easily and swiftly. This is likely to happen more quickly at higher supersaturations when the concentration of clusters is higher, and growth is quicker. A power law was fitted with the data at S-1 = 0.10 and S-1 = 0.18 although at a supersaturation of 0.18 this is not representative of what is observed. It has been previously reported in literature that in order for shear to take place and be prominent, high levels of interfacial supersaturation must be present[7]. The message conveyed here from this data suggests that shear is always active, but at lower supersaturations, the shear rate required to initiate secondary nucleation must be much greater.

5.3.5 Crystal Growth Rates in Controlled Laminar Shear

The crystal growth rates were assessed throughout the seeded Couette cell experiments by observing the change in length of the seed crystal, which was held, fixed in place in the cameras field of view (Figure. 5.3. and Figure 5.4.). The growth rates recorded in this work using the Couette cell were then compared with values from seeded Crystalline experiments (Chapter 4) and literature data[18]. This is shown below in Figure 5.9.

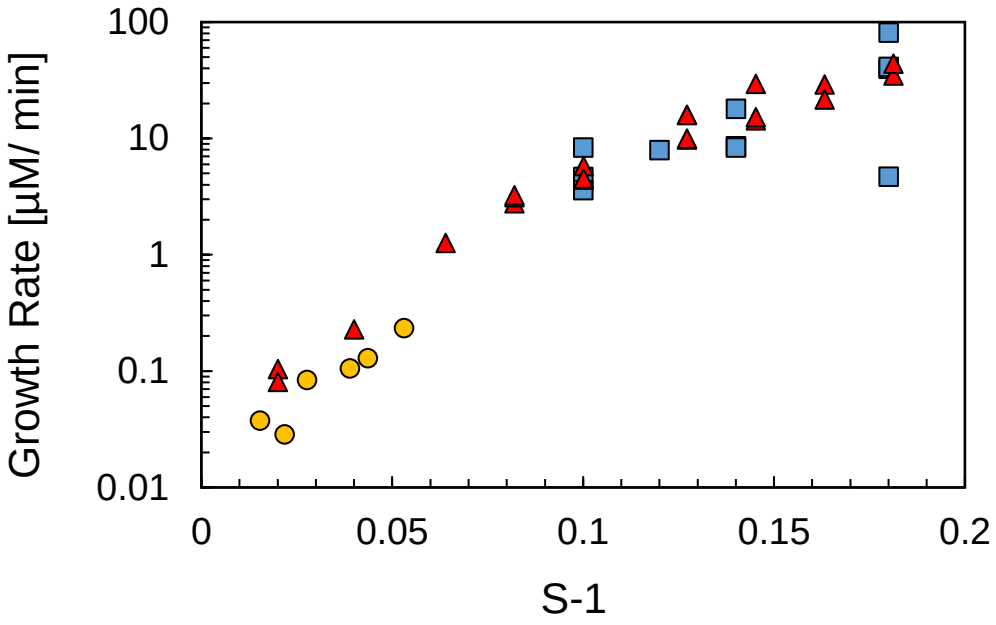

Figure. 5.9. The crystal growth rates of α-glycine in water measured using the Couette flow cell technique described in this study. In this work the change in crystal length was tracked over time under laminar shear at a rotational rate of 200 RPM. The growth rate was measured at a supersaturation of *S*-1 = 0.10, 0.12, 0.14 and 0.18. The blue squares represent the Couette cell growth rates, the red triangles represent the values recorded in Chapter 4 using the Crystalline and the yellow circles represent literature values[18].

The values recorded in the Couette cell experiments are in good agreement with the previous values tracking the distribution of crystals throughout seeded Crystalline experiments. The growth rates presented were recorded at a rotational rate of 200 RPM as there was a complete set of data, in some images the edge detection using the algorithm was not sufficient to record a true growth rate. To ensure accurate measurement, it was therefore essential that the seed was held clearly in place with all edges visible. Other measurements were carried out between 100 – 300 RPM but there was no apparent effect of rotational rate on the rate of crystal growth.

5.3.6 Couette Cell – Growing Seed in the Gap

The shear rates in the gap without seed addition were estimated in table. 5.1. As mentioned, when a crystal is placed into the gap in a supersaturated solution it will undergo crystal growth, so its size is not constant in time. As the growth rates are known, it was possible to estimate the maximum size of the seed in the gap before detection of nucleation. Figure 5.10. shows the effect of seed growth on the gap between the edge of the seed and the walls of the cylinders. The reduction in gap size during experiments made estimations on shear rates challenging.

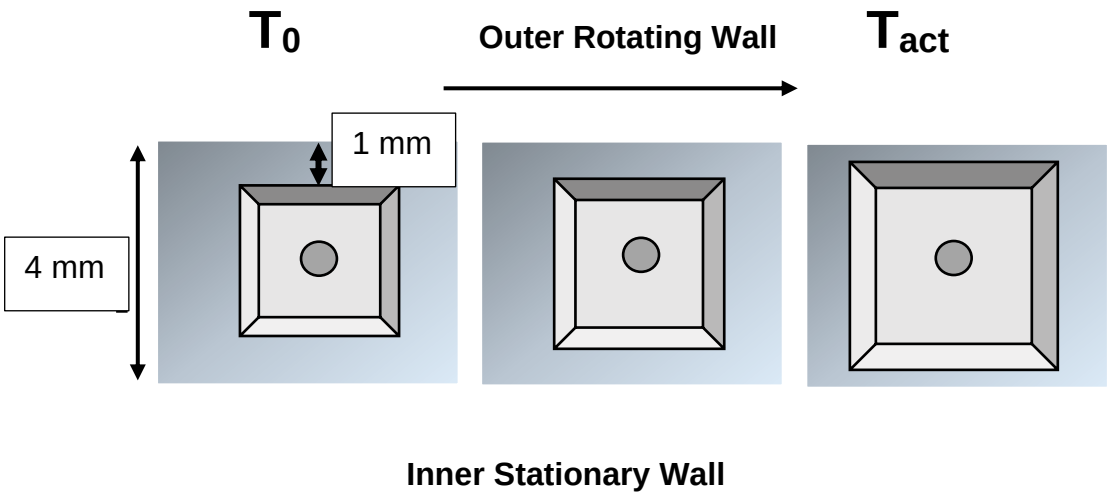

Figure. 5.10. A schematic outlining the effect of seed growth on the distance between the edge of the seed crystal and the cylinder vessel walls. As the seed grows, this distance decreases which would ultimately lead to regions of much higher shear and expected increased rates of nucleation.

Although the initial seed size of 2.0 mm (± 0.5 mm) was known, the seed held in a supersaturated solution will undergo some level of crystal growth. Therefore, the change in seed size before detection of secondary nucleation

(ΔL) could be estimated from equation 5.2. where the average delay time (t) (min) was multiplied by the crystal growth rate (G) (µm/ min) at the same supersaturation.

$$\Delta L = Gt \quad \textbf{(Eq. 5.2)}$$

Figure 5.11. shows the change of the seed size due to crystal growth at each supersaturation and corresponding rotational rate before secondary nucleation is detected. It seems that there is a decrease in the change of seed size due to crystal growth with an increase in the rotational rate.

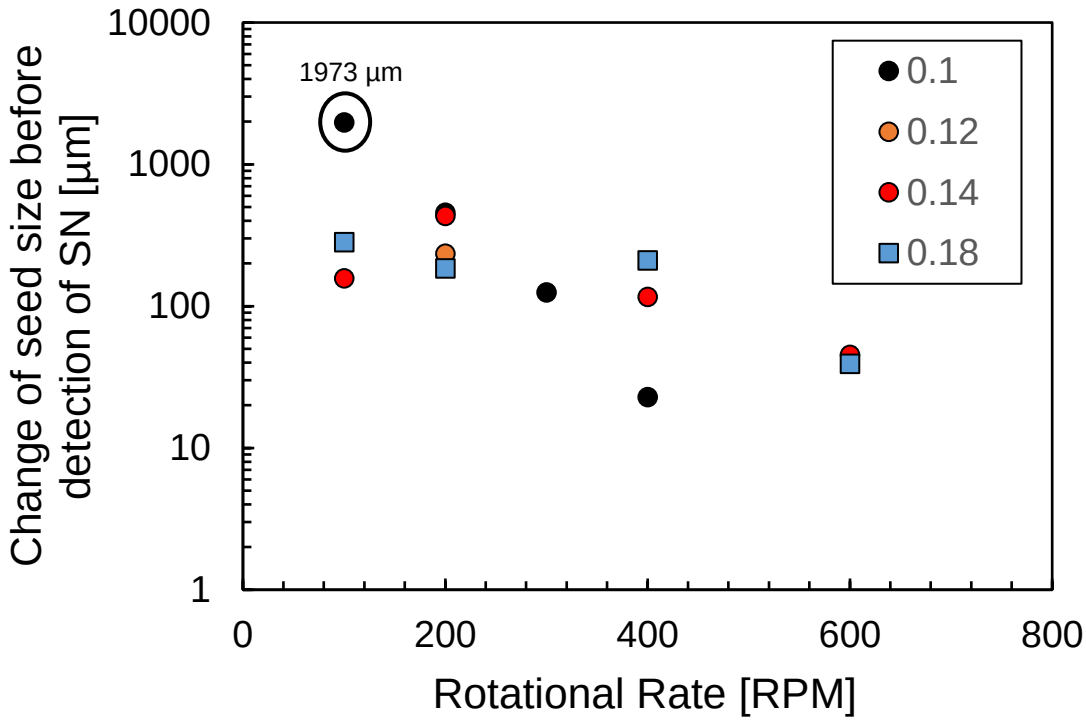

Figure. 5.11. The change in seed size before detection of secondary nucleation (ΔL) is shown vs the corresponding rotational rate (RPM). With an increase in rotational rate the seed grew less in the gap before secondary nucleation was detected. *S*-1 = 0.10 (black circles), *S*-1 = 0.12 (orange circles), *S*-1 = 0.14 (red circles) and *S*-1 = 0.18 (blue squares). Each experimental point was calculated using an average delay time (n = 1 – 5).

For supersaturations between *S*-1 = 0.10 and *S*-1 = 0.18 there seems to be a relatively similar change of the seed size, of few hundred microns before secondary nucleation was detected at all rotational rates up to 400 RPM, but significantly less change at 600 RPM as delay times were shorter. This was also shown in Figure. 5.8. when the delay time was no longer dependent on supersaturation beyond a rotational rate of 400 RPM. However, at a supersaturation of *S*-1 = 0.10 there appears to be much stronger dependence of the change of the seed size on rotational rate. It was also noted that the value at *S*-1 = 0.10 and 100 RPM seems to be an outlier as the crystal would fill almost the entire gap. This may be caused by the growth rate being overestimated for the particular seed crystal used for those conditions.

Once the average change in seed size in the gap was calculated for a particular experiment (Figure 5.11.), the actual gap width (r) between the seed surface and the outer rotating wall at the point when secondary nucleation was detected could be estimated. This was calculated by subtracting the change in seed size in one direction ($\Delta \mathrm{L}/2$) from the initial gap size of 1 mm as shown in equation 5.3.

$$\mathrm{r} = 1 - (\Delta \mathrm{L}/2) \quad \textbf{(Eq. 5.3)}$$

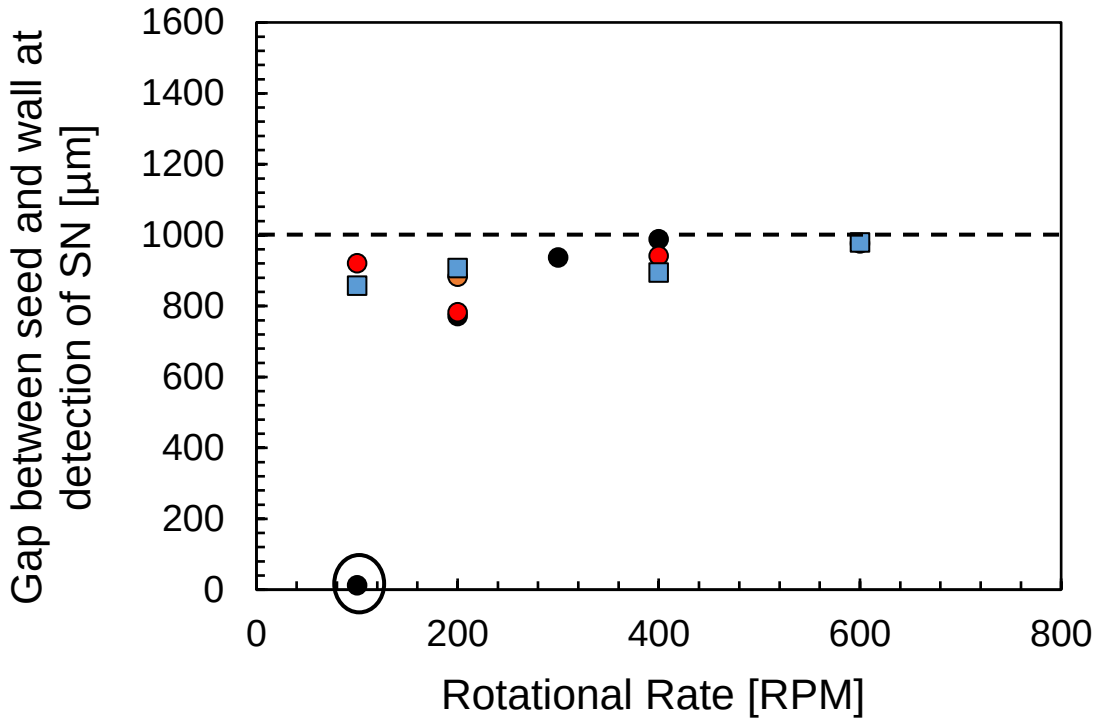

Figure. 5.12. The gap width between the seed surface and the outer rotating wall at the point of secondary nucleation detection shown vs rotational rate (RPM). *S*-1 = 0.10 (black circles), *S*-1 = 0.12 (orange circles), *S*-1 = 0.14 (red circles) and *S*-1 = 0.18 (blue squares). The horizontal dashed line represents the initial gap size of 1000 µm. The further away from the horizontal dashed line, the more the seed grew in the gap reducing the overall distance from the rotating outer wall.

Although it appears that at *S*-1 = 0.10 and 100 RPM (circled) the gap needs to completely close before secondary nucleation is detected, it is likely that initial seed size distributions (± 0.5 mm) and growth rate dispersions mean that it is likely that it does not close the gap to this extent. Growth rate dispersions have been reported previously where individual crystals within the same conditions grow at different rates[19], this was also mentioned in Chapter 4. (4.3.3). Although it is likely that at lower supersaturation the seed crystal requires a higher level of shear to initiate the removal of nuclei from the surface of the

seed. It is unlikely that this level of crystal growth in the gap is representative of what is actually happening.

At lower rotational rates (100 – 200 RPM) the seed crystal held in the gap and exposed to laminar shear seems to require more time for crystal growth before secondary nucleation is detected when compared with higher rotational rates (300 – 600 RPM).

5.3.7 Secondary Nucleation Delay Times

As with Chapter 4. the delay time was shown against the supersaturation indicating that there is a finite time, following initiation of secondary nucleation and detection.

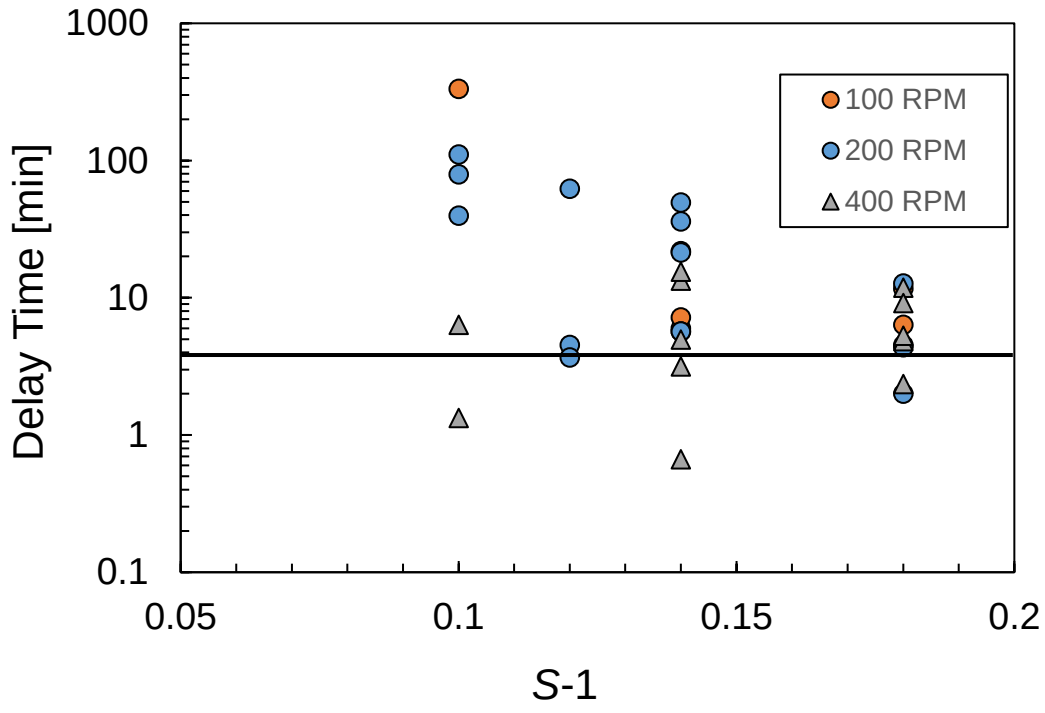

Figure 5.13. The delay time is shown at a range of supersaturations and the rotational rate (RPM) is indicated by the legend. The delay time is the time

taken for initiation of secondary nucleation and seems to decrease with an increase in both rotational rate and supersaturation.

It appears that, there is once again a finite time of 2 – 4 minutes (except for a couple of outliers at 400 RPM) even at the highest supersaturation, before secondary nucleation is detected. This is indicated by the horizontal line which is not a fit but rather a guide for the eye. From Figure 5.13. it can be seen that there is a much wider range of delay times observed at higher supersaturations compared to seeded experiments in magnetically agitated vials (see Figure 4.13.) where the crystals are well dispersed. Therefore, the changing shear rate over time with seed growth and sedimentation through the image frame are likely to play a role in detection.

Overall, it can be seen that with high rotational rates and higher rates of laminar shear, the seed requires much less time for growth before initiation and detection of secondary nucleation. This is likely representative of the higher secondary nucleation rates with higher levels of shear. The faster generation rate of further nuclei would counter the loss of crystals in the image frame occurring as a result of sedimentation. Alternatively, at lower 'initial' shear the seed may need to grow further in the gap to increase the rate of secondary nucleation with higher shear before detection.

5.3.8 Couette Cell Calibration of Suspension Density

Using the proposed Couette cell set-up, monitored with a high-speed camera, and analysed using an image analysis algorithm, the number (*N*) of crystals in

view could be automatically generated. To record a value for the secondary nucleation rate which is representative of the unit volume rather than just the number of crystals observed in the window of the camera, a calibration was completed to convert the crystal number to a suspension density N_p using polystyrene microspheres of 50 µm. Concentrated solutions of polystyrene microspheres were prepared, and a series of images were taken. The images were then processed using the algorithm and the number shown in Figure 5.14. against concentration is the average number, *N* of particles in view from a total of ~30 images at the same concentration.

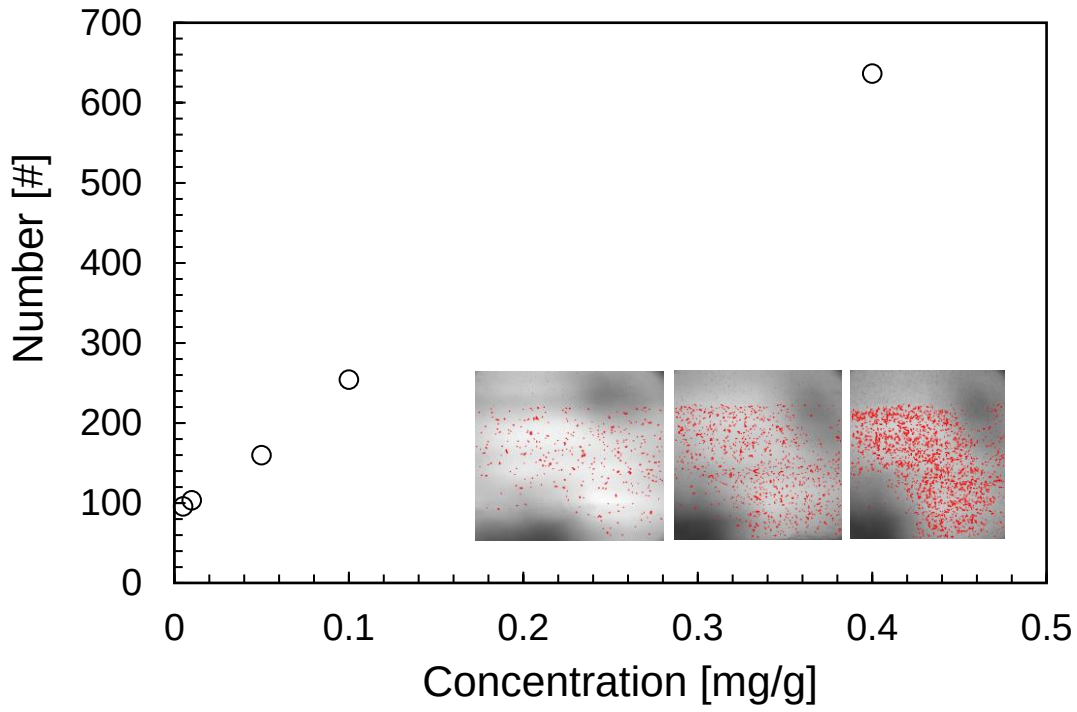

Figure. 5.14. The number of spheres in focus is shown against the corresponding concentration of 50 µm monodisperse polystyrene microspheres. Three images are shown with increasing concentrations of polystyrene microspheres and the red 'dots' are what is detected by the algorithm.

Figure 5.14. showed that there is an increase in the number of polystyrene spheres in focus with an increase in concentration showing a polynomial relationship. As the number of spheres in focus neared 600, it seemed that the image analysis algorithm struggled to accurately detect a further, continued increase in concentration, possibly due to multiple spheres overlapping. This is reflected by the fit. Figure 5.15 shows an example crystallisation experiment where crystals were detected and counted.

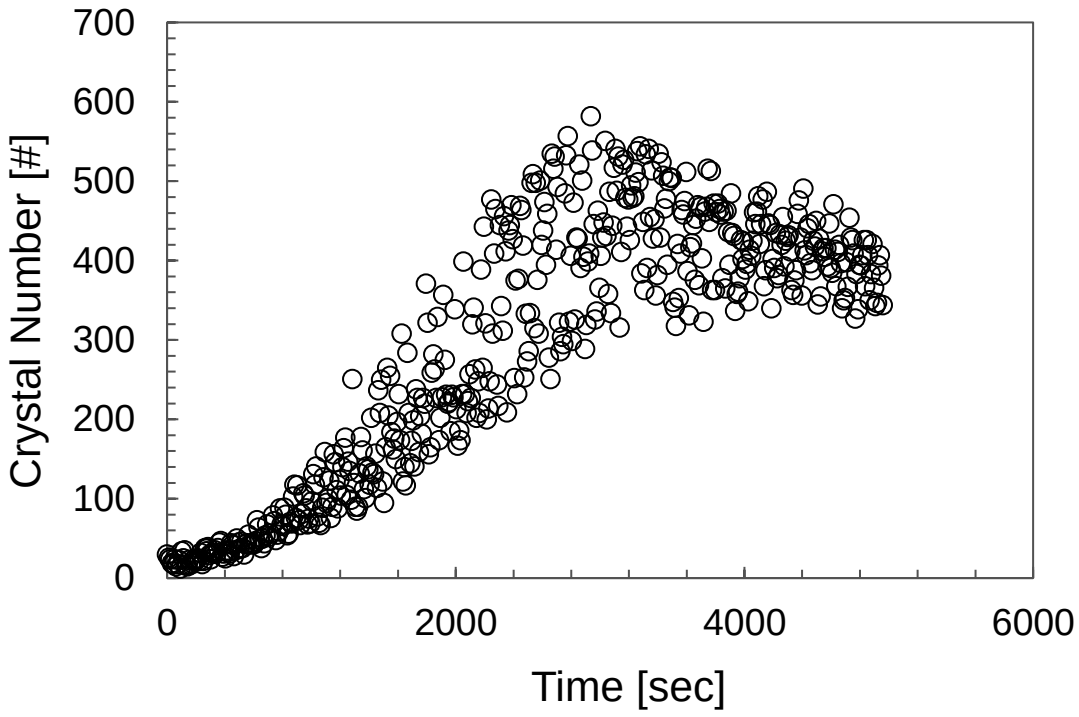

Figure. 5.15. The number of crystals in focus is shown against time in seconds. As shown, as the crystal number reaches 600, the number begins to decrease followed by the formation of a 'cloud' representative of the maximum suspension density having been reached.

As crystals are generated there seems to be a maximum 'count' reached at *N* = 600 (Chapter 2.) which is subsequently followed by a decrease in *N.* This

suggests that there is a point at which the suspension density becomes too high for the image analysis algorithm to detect individual crystals in focus. In Chapter 4. (4.2.6), upper and lower bounds were set for the determination of the secondary nucleation rate (between 10 – 160 crystals in focus using the Crystalline setup). Thus, for the Couette cell, *N* = 600 was set as the upper limit when estimating the secondary nucleation rate but setting a lower bound was not possible due to variable initial background particle counts (Chapter 2).

The polystyrene microspheres had a monodisperse size of 50 µm and a density of 1050 mg/g. The volume (V_s) of a polystyrene microsphere is calculated by equation 5.4.

$$V_s = \pi d^3/6 \quad \textbf{(Eq. 5.4)}$$

The suspension density can then be calculated by equation 5.5. where C_p represents the concentration of spheres and ρ is the density.

$$N_\rho = C_p/V_s\rho \quad \textbf{(Eq. 5.5)}$$

The suspension density (N_ρ) was then plotted against the corresponding crystal number (*N*) in focus at the same concentration. The calibration can then be used to estimate the number of crystals representative of the unknown part of the solution. This is shown in Figure 5.16.

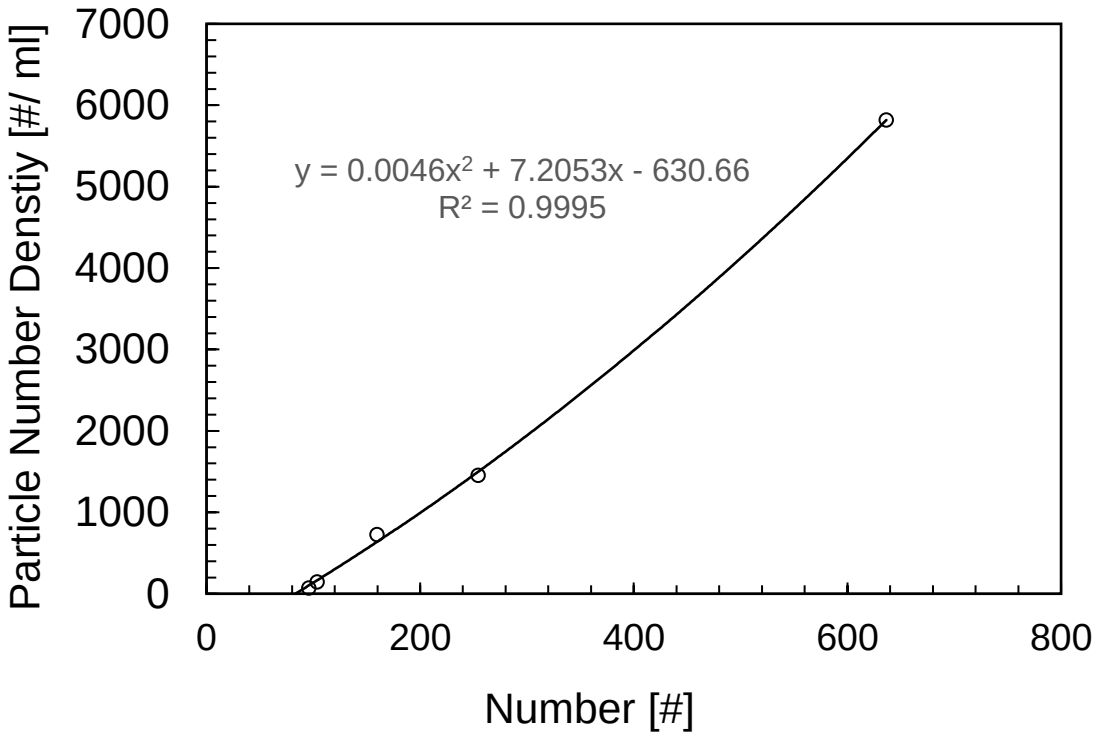

Figure. 5.16. Calibration determination by plotting the number of crystals in focus vs the number density of the monodisperse polystyrene microspheres of size 50 µm.

The calibration equation was obtained by passing a second order polynomial fit through the number density N_ρ and crystal number N plot. The equation was then used to convert the crystal number into a number density to estimate a secondary nucleation rate per unit volume. Equation 5.6. shows the calibration equation used in this work.

$$N_\rho = 0.0046N^2 + 7.2053N - 630.66 \quad \textbf{(Eq. 5.6)}$$

5.3.9 Couette Cell Secondary Nucleation Rates (*B*)

Fluid shear is often presented as a lesser secondary nucleation mechanism to contact[2], this is reflected in traditional secondary nucleation models[20]. However, there has been previous work published that showed that fluid shear is an important effect on secondary nucleation[9,21,22]. Using offline, innovative techniques such as the one presented in this work, it is possible to further develop an understanding of the mechanism's initiating and dictating the rate of secondary nucleation.

The secondary nucleation rate (*B*) was recorded in this work using image analysis where the change in number density was tracked against time. Figure 5.17. shows the secondary nucleation rate recorded at 5 different rotational rates and 4 supersaturations.

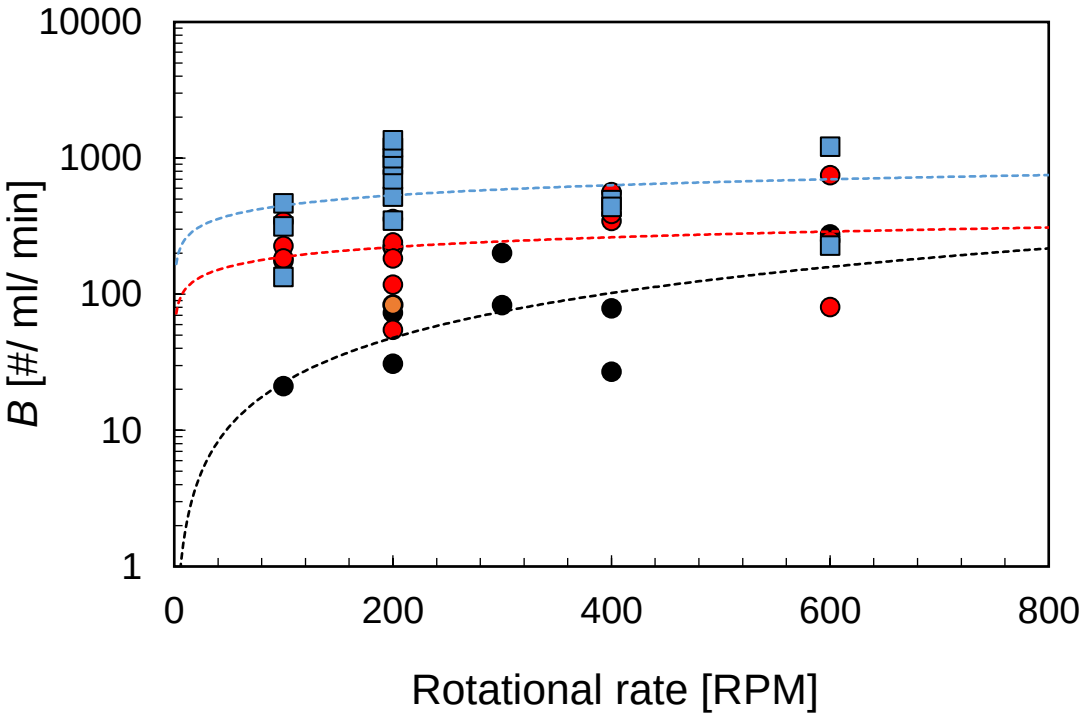

Figure 5.17. The secondary nucleation rate shown against the corresponding rotational rate across three supersaturations. *S*-1 = 0.10 (black circles), *S*-1 = 0.12 (orange circles), *S*-1 = 0.14 (red circles) and *S*-1 = 0.18 (blue squares). The data recorded at *S*-1 = 0.10, 0.14 and 0.18 were fitted with a power law.

As shown in Figure 5.17. at all 5 rotational rates, the largest rate of secondary nucleation was recorded at the greatest supersaturation of 0.18. Even at the lowest rotational rate of 100 RPM, the values recorded at *S*-1 = 0.18 were an order of magnitude higher than those at *S*-1 = 0.10. At a supersaturation of 0.10 there is clearly a dependence of the secondary rate on the rotational rate, but this relationship is less clear as the supersaturation is increased to 0.14 and 0.18. Although the reason for this behaviour cannot be clearly specified, one hypothesis relates to the secondary nucleation mechanisms (nuclei breeding, embryo coagulation secondary nucleation theory). At higher supersaturations these are more likely to result in rapid ‘coupling’, however at lower supersaturations perhaps a higher level of shear is required to remove crystallites which are more firmly bound to the surface. Figure.5.17. shows similar behaviour to that observed in the delay time plot (Figure 5.8.) where there was a stronger dependence on shear at lower supersaturation.

It may be suggested that the level of shear which was analysed in this work with a seed held in place was already at the top end of those which are seen in stirred vessels (Table. 1.1). Therefore, to analyse the effect of shear on the secondary nucleation rate, perhaps it would be more appropriate to start experiments at lower rotational rates (or increased gap) to really develop an understanding of the behaviour. In all of the experiments conducted in this

work, secondary nucleation was observed and so there is option to work at lower rotational rates.

The final consideration, as mentioned previously, is the role of sedimentation on the secondary nucleation rate. It is known that the rate of nuclei generation must be greater than the rate of sedimentation in order to generate an estimated secondary nucleation rate. In future work it would be interesting to take this further and quantify the sedimentation rate in order to develop a further, more accurate rate of secondary nucleation.

5.3.10 Stirred Vessel – Seed on a Stick

The EasyMax set-up was used to estimate the significance of shear in a stirred tank with a seed held, fixed in place in solution. The seed was previously washed and characterised to ensure that initial breeding was prevented. The seed, held at the base of a capillary tube was then exposed to two rotational rates, the first of 250 RPM and the second of 500 RPM. Using the DynoChem mixing toolbox[23], predictions as to the vessel averaged turbulent shear rate were made.

Figure 5.18. displays the secondary nucleation kinetics at the two rotational rates and the data is fitted with a power law. To guide the reader, two dashed horizontal lines are shown at the same supersaturation to show the difference in resulting secondary nucleation rates.

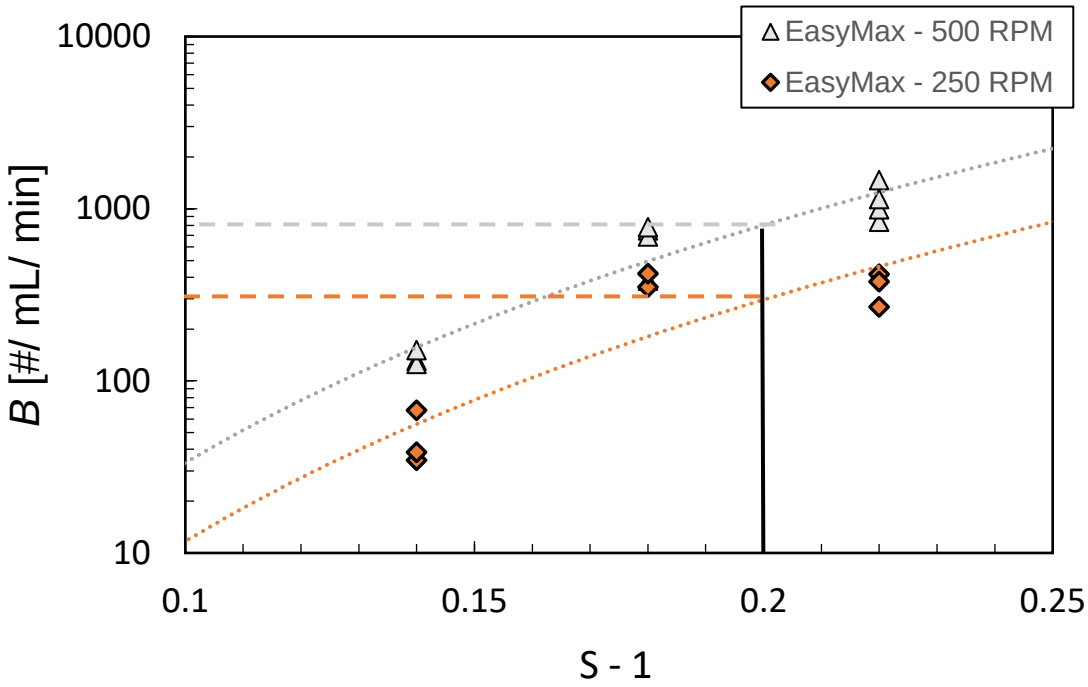

Figure. 5.18. The secondary nucleation rates are displayed above from the EasyMax set-up at 100 mL from Mettler Toledo. The orange diamonds represent the rotational rate of 250 RPM (average shear rate of 90 s^{-1}) and the grey triangles represent a rotational rate of 500 RPM (average shear rate 250 s^{-1}). The seed crystal was held in place using the 'seed on a stick' method preventing any collision with the impeller.

As shown in Figure 5.18, the secondary nucleation kinetics at a higher shear rate of 250 s^{-1} are much greater than the secondary nucleation kinetics at the lower rate of shear (90 s^{-1}). Assuming that all secondary nuclei formed are generated from the initial seed crystal, then it is clear that the level of shear results in a significant increase in the rate of secondary nucleation. In this set-up the seed was held in the same location for each experiment and the impeller type was kept constant. Of course, to improve the validity of the shear estimations, further CFD simulations may provide more quantifiable

information regarding the shear exerted on the surface of the seed crystal which may be different from that of the vessel averaged shear. The conditions could then be replicated offline in the Couette cell.

Figure 5.19., shows the secondary nucleation kinetics using the ‘seed on a stick’ technique in two further stirred tank experimental set-ups (Figure 5.5.) The Crystalline set-up was used with a volume of 6 mL and the OptiMax was used with a volume of 700 mL. A seed crystal was glued to the base of a ‘holder’ and placed into each reactor. Due to the size differences between vessels, it becomes challenging to compare nucleation rates without any quantifiable shear rate knowledge at the seed surface. The EasyMax at a shear rate of 250 s^{-1} (vessel averaged at 500 RPM) was selected to compare with the OptiMax with a vessel averaged shear rate of 210 s^{-1} and a rotational rate of 250 RPM. The shear rates were selected as an attempt to keep as much consistency as possible, but it is likely that the shear rates within the Crystalline, due to the proximity of the seed to the impeller are much higher. Predictions regarding the shear rate distributions in Crystalline vials can be found in literature[24].

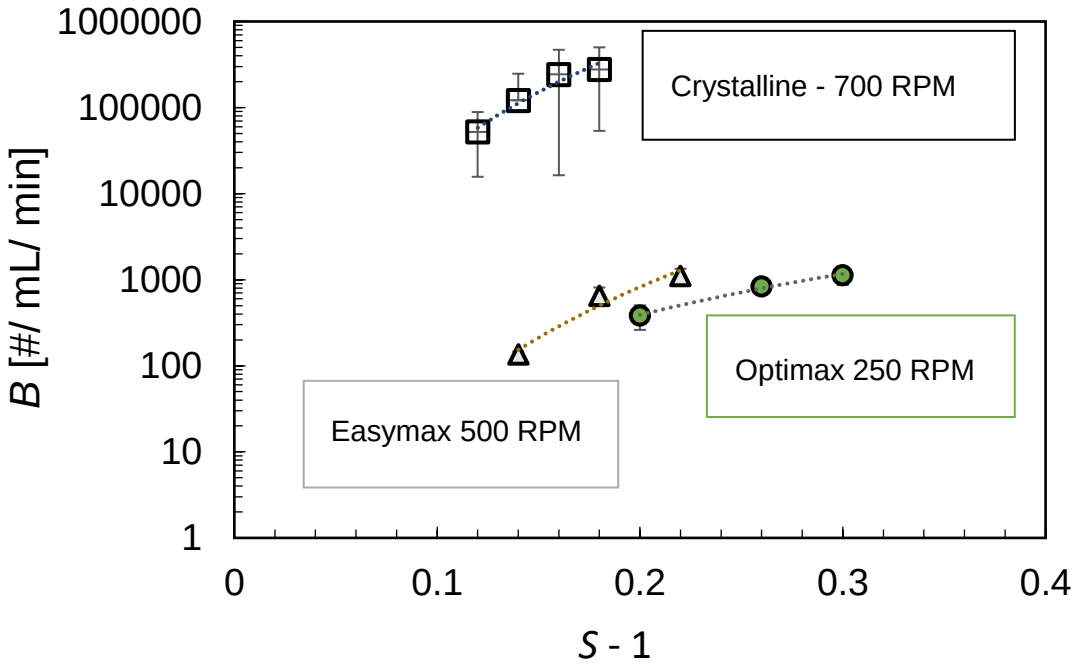

Figure. 5.19. Secondary nucleation rates were assessed using a range of different experimental techniques and volumes. All three displayed above were using the 'seed on a stick' method in which a seed crystal was held in place near to the rotating impeller. The crystalline (6 mL – open squares), Easymax (100 mL - grey triangles) and Optimax (700 mL – green circles).

Previously, in unseeded stirred vessels with volumes of 85 – 680 mL, with an increase in volume it was shown that nucleation was detected earlier, induction time distributions became narrower but the resulting primary nucleation kinetics were similar across all scales[25]. In this work, Figure 5.19. shows similar behaviour to what was shown in literature possibly validating their conclusion which was that the single nucleation mechanism controls isothermal crystallisations[25]. There is a clear increase in the secondary nucleation kinetics with a decrease in the volume although this may be due to the location of the seed crystal. Assuming that all secondary nuclei generated

originate from a single nucleus (the seed added), the dependence of secondary nucleation on the proximity to the impeller can be evaluated. This is of course, in more clear terms, the exposure of the seed crystal to the degree of shear. Another alternative which must be considered when interpreting the data is the camera used, it may also be possible that the location of the camera, the resolution and the algorithm used to detect secondary nucleation all influence the generated rate. The Couette cell, EasyMax and OptiMax all used the same image processing algorithm but employed different cameras with various resolutions. The crystalline nucleation kinetics were quantified using the in-built camera and standard algorithm.

5.3.10 Shear Induced Secondary Nucleation Kinetics

The results from the stirred vessel, ‘seed on a stick’ secondary nucleation measurements were then compared directly with the Couette cell data and presented in Figure 5.20. To show a more complete dataset the secondary nucleation kinetics from the seeded magnetically agitated vials (Chapter 4.) were also so displayed. As shown the results from the Couette cell produce secondary nucleation kinetics comparable with those recorded using the lab-scale stirred tank reactors but are multiple orders of magnitude lower than the small-scale Crystalline set-ups where the seed was always near to the impellers.

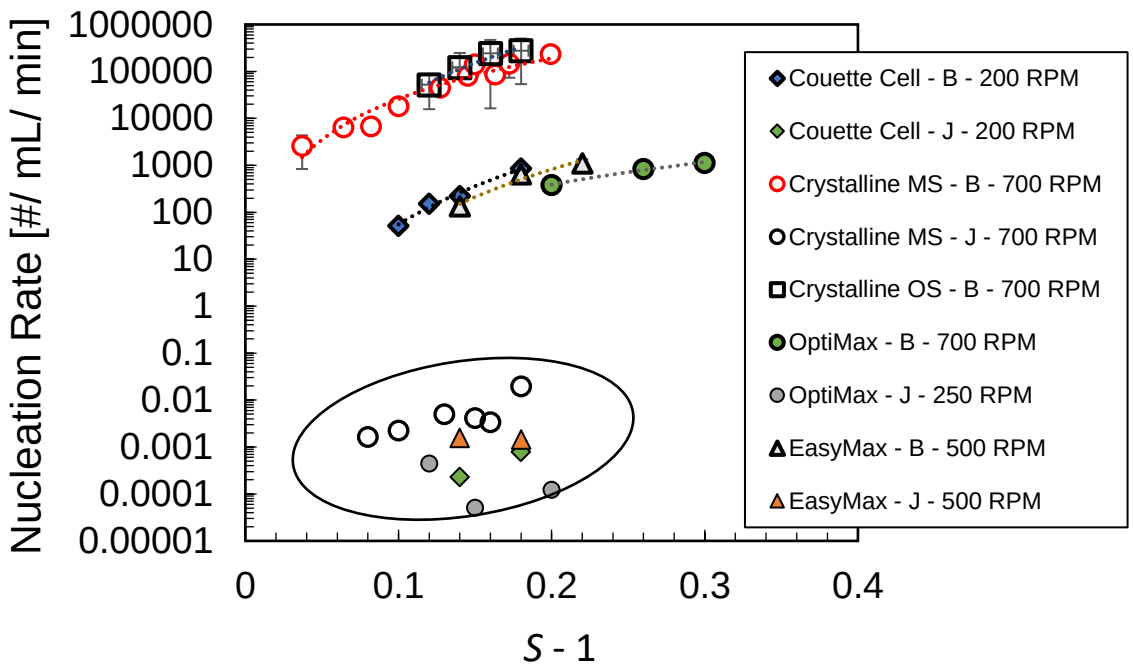

Figure. 5.20. Comparison of multiple different experimental methods to assess shear. The Couette cell was used with a seed held in place by attachment to the base of a capillary tube. The stirred tanks utilised a seed held in place within the vicinity of the rotating impeller. The crystalline overhead stirrer had a seed held in place near to the impeller and the magnetically agitated Crystalline vials had a seed 'dropped' in freely. Error bars are used to show the distribution of values, an average of (minimum) three repeats are shown. Circled are all the primary nucleation (*J*) values many orders of magnitude lower than secondary nucleation kinetics (*B*).

The shear rate distributions in small, agitated vials has been estimated in literature[24] finding that there was an average shear of ~100 s^{-1} agreeing with previous estimations[26]. They also found that in both magnetically agitated vials and over-head stirred, there was peak shear at 700 – 1000 s^{-1} near the impeller tip. Of course, in an industrial process where the contents are well-mixed, seeds will be theoretically well distributed throughout the entire crystallisation vessel. In this process however, the seed was either dropped into the small

magnetically agitated vial (discussed in Chapter 4) or held just above the rotating impeller as shown in Figure. 5.5. The similarities between secondary nucleation rates and estimated shear rates both for magnetically agitated and overhead stirred Crystalline vials suggest that the dominant secondary nucleation mechanism in both is shear induced at relatively high shear rates rather than contact. In previous work, it was shown that the squeeze film effect[27] prevents high energy collisions between particles and a wall when using a fluid jet. This is counter to much of the literature which focuses on contact based secondary nucleation. It is likely that this boundary layer near the impeller results in rapid generation of secondary nuclei and it is plausible that only larger crystals with high Stokes numbers[27] will contact the impeller with intensities significantly lower than often portrayed. At the larger scale, a seed was held, fixed in place in a stirred tank, but the distance from the impeller was much greater than in the Crystalline experiments. As expected, due to the increased distance between the crystal seed and the impeller, where shear rates are lower, the secondary nucleation rates were recorded multiple orders of magnitude below those in the Crystalline.

The Couette cell proposed in this work does have the potential to replicate estimated shear rate distributions which may be from simulations of stirred vessels or empirical predictions. Interestingly the Couette cell with consistent shear rates likely towards the maximum level of those seen in the stirred tank have resulted in secondary nucleation rates which are in a similar range. This may indicate that laminar shear is less effective than similar magnitude of fluid shear in turbulent flow conditions present in stirred tanks. In this set-up with

laminar flow, particle tracking proved to be challenging due to sedimentation which was not accounted for in the evaluation of the particle number density measurement. This may have resulted in lower-than-expected secondary nucleation rates as the sedimentation rate will offset the increase in particle number due to secondary nuclei generation, meaning that not all the crystals will be accounted for. With an overhead stirrer where crystals are well-mixed, this will not be the case. With that said, even with a reduced secondary nucleation rate due to sedimentation, the secondary nucleation rates in the Couette cell under laminar fluid shear are many orders of magnitude higher than primary nucleation rates. From the data presented here, it is shown that secondary nucleation can be quantified under laminar shear and that shear may be the dominant secondary nucleation mechanism in stirred tanks.

Further experimental and computational evaluation of the relationship between secondary nucleation, crystal growth and fluid shear is required to develop a better understanding of nuclei breeding[5], which is a mechanism which may describe what is seen here. It is possible that this is sped up by the increased rate of growth of the clusters using the surface of the seed with increased supersaturation.

Conclusions

A Couette flow cell set-up was designed and developed which could achieve a relatively controlled level of laminar shear on the surface of a seed crystal. Experiments were conducted to evaluate the effect of a range of rotational

rates and thus shear rates on the kinetics of secondary nucleation. It was found that under the same experimental conditions, the addition of a seed crystal with complete absence of any contact other than shearing of solution, resulted in a much shorter time taken for nucleation to be detected than those experiments conducted without a seed crystal. The secondary nucleation rates were then assessed, and it was seen that there was a significant dependence of secondary nucleation on rotational rate at low supersaturations (S-1 = 0.10), but this dependency was less clear as the supersaturation was increased.

Secondary nucleation rates were then measured in stirred crystallisation vessels using the ‘seed on a stick’ method. It was noticed that at lower vessel volumes where the seed was held in closer proximity to the impeller, the secondary nucleation rates were orders of magnitude higher than those nucleation kinetics at larger scales where the seed was held far from the impeller.

The nucleation kinetics from all experiments were finally compared and it was found that the Couette cell generated secondary nucleation rates comparable with the EasyMax and OptiMax but lower than those from the Crystalline vials.

Key Points

- A Couette flow cell was designed, developed, and validated.
- Novel imaging set-up integrated to track and count the number of crystals in focus enabling quantification of secondary nucleation and crystal growth kinetics.
- Seeded delay times and unseeded induction times measured with laminar fluid shear validating the significance of shear induced secondary nucleation.
- Secondary nucleation rates from Couette cell compared with those from characterised stirred vessels using the ‘seed on a stick’ technique.

References

(1) Xu, S.; Hou, Z.; Chuai, X.; Wang, Y. Overview of Secondary Nucleation: From Fundamentals to Application. *Ind. Eng. Chem. Res.* **2020**, No. 59, 18335–18356. https://doi.org/10.1021/acs.iecr.0c03304.

(2) Agrawal, S. G.; Paterson, A. H. J. Secondary Nucleation : Mechanisms and Models Secondary Nucleation : Mechanisms and Models. *Chem. Eng. Commun.* **2015**, *202* (5), 698–706. https://doi.org/10.1080/00986445.2014.969369.

(3) Zhang, D.; Wang, X.; Ulrich, J.; Tang, W.; Xu, S.; Li, Z.; Rohani, S.; Gong, J. Control of Crystal Properties in a Mixed-Suspension Mixed-Product Removal Crystallizer: General Methods and the Effects of Secondary Nucleation. *Cryst. Growth Des.* **2019**, No. 19, 3070–3084. https://doi.org/10.1021/acs.cgd.8b01530.

(4) Garside, J.; Rusli, I. T.; Larson, M. A. Origin and Size Distribution of Secondary Nuclei. *AIChE J.* **1979**, *25* (1), 57–64. https://doi.org/10.1002/aic.690250107.

(5) Anwar, J.; Khan, S.; Lindfors, L. Secondary Crystal Nucleation: Nuclei Breeding Factory Uncovered. *Angew. Chemie - Int. Ed.* **2015**, No. 54, 14681–14684. https://doi.org/10.1002/anie.201501216.

(6) Lewis, A.; Seckler, M.; Kramer, H.; Van Rosmalen, G. M. *Industrial Crystallisation. Fundamentals and Applications*; Cambridge University Press, 2015.

(7) Tai, C. Y.; Tai, C. Der; Chang, M. H. Effect of Interfacial Supersaturation on Secondary Nucleation. *J. Taiwan Inst. Chem. Eng.* **2009**, No. 40, 439–442. https://doi.org/10.1016/j.jtice.2009.01.006.

(8) Wang, M. -L; Huang, H. -T; Estrin, J. Secondary Nucleation of Citric Acid Due to Fluid Forces in a Couette Flow Crystallizer. *AIChE J.* **1981**, *27* (2), 312–315. https://doi.org/10.1002/aic.690270222.

(9) Yousuf, M.; Frawley, P. J. Secondary Nucleation from Nuclei Breeding

and Its Quantitative Link with Fluid Shear Stress in Mixing: A Potential Approach for Precise Scale-up in Industrial Crystallization. *Org. Process Res. Dev.* **2019**, No. 23, 926–934. https://doi.org/10.1021/acs.oprd.9b00029.

(10) Rowland, D. Thermodynamic Properties of the Glycine + H2O System. *J. Phys. Chem. Ref. Data* **2018**, No. 47, 023104-1-023104–023115. https://doi.org/10.1063/1.5016677.

(11) Marchisio, D. L.; Soos, M.; Sefcik, J.; Morbidelli, M. Role of Turbulent Shear Rate Distribution in Aggregation and Breakage Processes. *AIChE J.* **2006**, *52* (1), 158–173. https://doi.org/10.1002/aic.10614.

(12) Forsyth, C.; Mulheran, P. A.; Forsyth, C.; Haw, M. D.; Burns, I. S.; Sefcik, J. Influence of Controlled Fluid Shear on Nucleation Rates in Glycine Aqueous Solutions. *Cryst. Growth Des.* **2015**, No. 15, 94–102. https://doi.org/10.1021/cg5008878.

(13) Briuglia, M.; Sefcik, J.; ter. Horst, J. Measuring Secondary Nucleation through Single Crystal Seeding. *Cryst. growth Des.* **2019**, *19*, 421–429. https://doi.org/http://dx.doi.org/10.1021/acs.cgd.8b01515.

(14) Liu, J.; Svärd, M.; Rasmuson, Å. C. Influence of Agitation and Fluid Shear on Nucleation of M-Hydroxybenzoic Acid Polymorphs. *Cryst. Growth Des.* **2014**, No. 14, 5521–5531. https://doi.org/10.1021/cg500698v.

(15) Swinney, H. L. Flow Regimes in a Circular Couette System with Independently Rotating Cylinders. *J. Fluid Mech.* **1986**, *164*, 155–183. https://doi.org/10.1017/S0022112086002513.

(16) Wang, M. -L; Huang, H. -T; Estrin, J. Secondary Nucleation of Citric Acid Due to Fluid Forces in a Couette Flow Crystallizer. *AIChE J.* **1981**, *27* (2), 312–315. https://doi.org/10.1002/aic.690270222.

(17) Qian, R. Y.; Botsaris, G. D. A New Mechanism for Nuclei Formation in Suspension Crystallizers: The Role of Interparticle Forces. *Chem. Eng. Sci.* **1997**, No. 20, 3429 3440,. https://doi.org/10.1016/S0009-

2509(97)89691-1.

(18) Li, L.; Rodríguez-Hornedo, N. Growth Kinetics and Mechanism of Glycine Crystals. *J. Cryst. Growth* **1992**. https://doi.org/10.1016/0022-0248(92)90172-F.

(19) Ulrich, J. *Growth Rate Dispersion-A Review*; 1989.

(20) Mersmann, A.; Sangl, R.; Kind, M.; Pohlisch, J. Attrition and Secondary Nucleation in Crystallizers. *11* **1988**, *1*, 80–88.

(21) Yousuf, M.; Frawley, P. J. Experimental Evaluation of Fluid Shear Stress Impact on Secondary Nucleation in a Solution Crystallization of Paracetamol. *Cryst. Growth Des.* **2018**, No. 18, 6843–6852. https://doi.org/10.1021/acs.cgd.8b01074.

(22) Sung, C. Y.; Estrin, J.; Youngquist, G. R. Secondary Nucleation of Magnesium Sulfate by Fluid Shear. *AIChE J.* **1973**, *19* (5), 957–962. https://doi.org/10.1002/aic.690190511.

(23) Dynochem® Mixing and Heat Transfer https://www.scale-up.com/Dynochem.

(24) Achermann, R.; Adams, R.; Prasser, H.; Mazzotti, M. Characterization of a Small-Scale Crystallizer Using CFD Simulations and X-Ray CT Measurements. *Chem. Eng. Sci.* **2022**, No. 256, 1–12. https://doi.org/10.1016/j.ces.2022.117697.

(25) Steendam, R. R. E.; Keshavarz, L.; Blijlevens, M. A. R.; De Souza, B.; Croker, D. M.; Frawley, P. J. Effects of Scale-Up on the Mechanism and Kinetics of Crystal Nucleation. *Cryst. Growth Des.* **2018**, No. 18, 5547–5555. https://doi.org/10.1021/acs.cgd.8b00857.

(26) Nappo, V.; Sullivan, R.; Davey, R.; Kuhn, S.; Gavriilidis, A.; Mazzei, L. Effect of Shear Rate on Primary Nucleation of Para-Amino Benzoic Acid in Solution under Different Fluid Dynamic Conditions. *Chem. Eng. Res. Des.* **2018**, *136*, 48–56. https://doi.org/10.1016/j.cherd.2018.04.039.

(27) Souza, B. De; Cogoni, G.; Tyrrell, R.; Frawley, P. J. Evidence of Crystal

Nuclei Breeding in Laboratory Scale Seeded Batch Isothermal Crystallization Experiments. **2016**, No. 16, 3443–3453. https://doi.org/10.1021/acs.cgd.6b00407.

Chapter. 6. Conclusions and Future Work

6.1.1 Conclusions

The work outlined in this thesis has investigated some of the challenges which are faced in developing industrial crystallisation processes. Specifically, this thesis has aimed to develop a better understanding of secondary nucleation phenomena. It is hoped that the results of this work can provide novel insights and facilitate more efficient process development and optimisation.

6.1.2 Solubility

Solubility is the most important physical property of a crystallisation system as it is needed to select the required supersaturation, the driving force for crystal nucleation and growth. Previously, experimental measurements of glycine solubility in water have produced inconsistent values, especially at elevated temperatures. Here, three experimental techniques were critically evaluated, polythermal temperature cycling, isothermal equilibration and finally, solute addition. When using the polythermal temperature cycling approach, it was found that there is an obvious dependence of the solubility recorded on the heating rate selected. Therefore, the best practice would be to select multiple heating rates and extrapolate to the zero-heating rate which would correspond to the theoretical equilibrium solubility. This investigation revealed that each technique had strengths and challenges demonstrating that the set of conditions and circumstances i.e., suspension density and temperature of measurement, should dictate the selection of an appropriate methodology to follow.

6.1.3 Nucleation and Crystal Growth Workflow

Following a review of the literature, there seemed to be a lack of well-established experimental techniques used to measure and quantify secondary nucleation. Chapter 4 covered the development of a small-scale workflow, from which a considerable amount of both mechanistic and kinetic data could be extracted from experiments using a single vial. This ultimately resulted in the development of a classification system based on nucleation and crystal growth rates estimated from these small scale measurements.

Firstly, an assessment of the primary nucleation kinetics was completed, starting with the metastable zone. As expected an increase in the rate of heating resulting in a wider metastable zone width. As the metastable zone width is kinetically rather than thermodynamically driven, it was not possible to use the same, extrapolation technique as with the solubility to estimate the 'true' metastable limit. From the probability distributions of induction times obtained under isothermal condition within the metastable zone, primary nucleation kinetics were estimated. It was found that for rapid screening approaches, a relatively small number of experiments was sufficient to generate a reasonable estimate of the primary nucleation rate *J,* but to improve the accuracy of *J* the number of experiments would need to be increased.

The crystal growth rates were estimated from both unseeded and seeded vials by tracking the change in crystal size distribution over time, producing relatively similar results. The results were then compared with values from literature obtained by observing single crystal growth under a microscope and were in relatively good agreement. The crystal growth rate vs relative

supersaturation was plotted on a log-log scale and showed that there was no ‘dead-zone’ as previously thought. Instead, a typical power law relationship was observed where the crystal growth rates continued to decrease with decreasing supersaturation to very low but non-zero values. This implies that when discussing potential dead-zones the data should be shown on a log-log scale as to clearly reveal whether there is a power law relationship a opposed to a zone where values actually reach ‘zero’.

The secondary nucleation kinetics were estimated from both unseeded and seeded vials and again the data showed the absence of a secondary nucleation threshold when plotted on a log-log scale. The similarity in secondary nucleation kinetics from seeded and unseeded vials indicated that the underlying mechanism is the same once secondary nucleation was initiated providing evidence for the ‘single nucleus mechanism’, where firstly a seed is formed via primary nucleation before initiating secondary nucleation. The minimum size required (L_{min}) to initiate secondary nucleation was then determined using the growth time (t_g) or the minimum induction time plotted against the inverse of crystal growth rate, and it was found that seeds with the minimum size of 100 – 200 µm are required before proliferation.

Following seed addition to seeded vials there was a significant time delay, however this delay did not reach zero with increasing supersaturation and seemed to plateau at around 4 minutes beyond S = 1.15. It was hypothesised that some adjustment of the surface layer of the seed crystal may be required at any supersaturation and further that secondary nuclei must grow to some minimum observable size before they become detectable. The delay time was

plotted against the inverse of crystal growth rate and the minimum observable size L_{min} was estimated from the linear fit to be around ~10 µm. The number weighted crystal size distribution traces were then analysed at the point of detection of secondary nucleation (>10 particles (#) in focus) and indicated that the mode of crystal size distribution were also around 10 µm. This would be consistent with the surface breeding mechanism, where small crystal nuclei are being constantly swept away from the surface of a growing seed crystal and only once these nuclei grow to 10 µm they are detected.

Finally, a classification diagram for crystal growth and nucleation was introduced with four regions ranging from slow nucleation and slow crystal growth to fast nucleation and fast crystal growth. The boundaries between the regions can be set based on a characteristic residence time and a characteristic crystal size. The nucleation rates are then plotted vs the corresponding crystal growth rates at the same crystallisation conditions. These classification diagrams provide quantitative insights into interdependence of the nucleation and growth kinetics and options for controlling relative rates of nucleation and growth e.g. agitation or seed load, to facilitate development and optimisation of crystallisation processes.

6.1.4 Couette Cell – Shear Experiments

There is still a lack of fundamental understanding of the mechanisms involved in secondary nucleation and how secondary nucleation can be measured. Chapter 4 enabled the assessment of some fundamental mechanistic insight

into secondary nucleation behaviour. To take this work further, Chapter 5 outlined the design and development of a Couette flow cell used in the evaluation of secondary nucleation under controlled laminar fluid shear. Shear rates were quantified in the gap (without a seed), taking into account the gap width and rotational rate. The seed was then held in the centre of the gap between the stationary inner cylinder and outer, rotating cylinder. By using the 'seed on a stick' technique, any mechanical contact with the seed was completely avoided. The direct comparison of the unseeded induction time and seeded delay time under the same experimental conditions revealed that the time taken for detection of nucleation was significantly reduced in the presence of the seed across all supersaturations. As mentioned in Chapter 4, there was a time delay in secondary nucleation becoming detectable, even at the highest supersaturation and it was assumed that this was due to the limitations of detection of nuclei swept away from the growing seed crystal surface. There was a clear increase in the dependence of delay times on rotational rate at lower supersaturation when compared with higher supersaturation. The secondary nucleation rates showed the same dependence on effective shear with low supersaturations resulting in considerably lower secondary nucleation rates at lower rotational rates than at rotational rates. However, at high supersaturations, this dependence was much less pronounced. Here it can be assumed that at high supersaturations ($> S\text{-}1 = 0.14$), nuclei are swept away from the surface even at low rotational rates but at low supersaturations nuclei take a much longer time to become stable and then detectable once removed, resulting in longer delay times.

The ‘seed on a stick’ technique was then applied to stirred tank reactors including small scale (6 mL) and lab-scale (100 and 700 mL) vessels. The EasyMax and OptiMax, vessels were also characterised using the DynoChem mixing toolbox to estimate the shear rate averages before selecting appropriate rotational rates to compare across different vessels. The secondary nucleation kinetics estimated using the Couette cell were of the same order of magnitude as those produced using the lab-scale stirred tanks although they were some orders of magnitude lower than those recorded in the small-scale Crystalline vials. It is likely that due to the proximity of the seed to the impeller in the small-scale experiments, the level of shear is much higher than those experienced in the lab scale stirred tank reactors and Couette cell.

6.1.5 Concluding Remarks

This work has developed several novel experimental techniques and workflows for quantitative assessment of solubility, primary and secondary nucleation and crystal growth. A novel set-up was also designed and built to measure secondary nucleation kinetics under well controlled laminar shear. This work has expanded our knowledge of crystallisation and provided a new perspective on some well-established theories such as the secondary nucleation threshold, growth only zone and provided further evidence for the single nucleus mechanism. It was unequivocally demonstrated that secondary nucleation can be induced by fluid shear under laminar flow conditions and when compared with stirred tank reactors with turbulent low conditions, the

secondary nucleation rates were in a similar range, suggesting that the dominant secondary nucleation mechanism may in fact be fluid shear.

6.2 Future Outlook

To translate this work into a practical approach for process design and scale-up, understanding the fluid dynamics in crystallisation vessels is of paramount importance. Although computational fluid dynamics was outside the scope of this work, it will be crucial for determining shear rate distributions across multiple scales, understanding the change in flow regimes in the presence of suspended crystals and how the crystals travel in suspension depending on their size and density. This should help to develop the rational approach for the selection of crystallisation conditions in conjunction with experimental workflows and improved understanding of the fundamentals of secondary nucleation such as those described in this work.

Some more, chapter specific future investigations to take this work further are suggested below.

1. A critical evaluation of techniques commonly used to measure solubility was completed in Chapter. 3 aiming to provide a rationale for selection of appropriate methodologies in early stages of solvent screening. Using the solute addition technique, it was possible to measure solubility under challenging processing conditions such as high temperature. To improve thermodynamic models, such as those briefly

mentioned in Chapter. 3, a quick measurement of the triple point using the solute addition technique may enable ‘anchoring’ of the model and improve the fit, saving time and resources early in the drug development process. Therefore, the next stage of this work should be a complete evaluation of the glycine in water phase diagram measuring the boiling point elevation and triple point to boost the performance and accuracy of thermodynamic models. The methodology outlined in Chapter. 3 should be used to characterise the thermodynamic properties of other systems.

2. In Chapter. 4 a workflow was developed in which one small (3 mL) vial could produce both nucleation and growth kinetics and one set of experiments (8 vials) could result in the classification of a crystallising system. This provided a real opportunity to reduce material consumption in early-stage development and to standardise characterisation procedures to reduce uncertainties across different campaigns. As the aim of this workflow was to rapidly estimate, ‘ball-park’ nucleation kinetics the seed size was not well controlled (2.5 (±1.0) mm). This may be one factor which ultimately led to a large distribution of secondary nucleation rates at the same supersaturation and rotational rate. Future researchers may then want to reduce this variability and improve the precision of the secondary nucleation rates by controlling the seed size to a much greater degree.

3. In Chapter. 4, well accepted boundaries within the metastable zone including the secondary nucleation threshold and growth only region were probed in small, agitated vials with magnetic agitation. It was acknowledged that the absence of secondary nucleation threshold and growth dead zone when plotted on a log scale is specifically for this system, recorded under the outlined, given processing conditions where shear rates are likely to be constant and in the 1000(s) s^{-1}. More work should therefore be completed measuring these boundaries and observing how processing conditions influence the combination of secondary nucleation and growth, such as whether there are conditions where the nucleation and growth rates do in fact reach zero or whether they always follow power law kinetics. Of particular importance is that similar measurements are caried out in other systems to explore the generality or otherwise of secondary nucleation and growth phenomenology.

   It would be interesting to probe the relationship between crystal growth and secondary nucleation further, for instance, is there a point at which the growth mechanism shifts resulting in higher levels of secondary nucleation and an observed secondary nucleation threshold on a linear scale?

4. The idea of a minimum size (L_{min}) required for the initiation of secondary nucleation was determined and a methodology to estimate this size was presented based on growth time/ minimum induction time and crystal

growth rates. To validate this prediction, more work needs to be carried out on other systems and an investigation should be launched in relation to why this may occur. For example, is the L_{min} related to the stokes number and could it be, that when the stokes number increases through a ‘critical value’ the seed enters the high shearing region near the impeller initiating secondary nucleation?

5. With new tools developed to measure the role of fluid shear in secondary nucleation, such as the Couette cell methodology, and a new perspective on the mechanisms which lead to crystal proliferation from a seed, can more advanced modelling be used to compliment what was discovered in this work? For example, at high supersaturation the rate of secondary nucleation did not seem to significantly increase with increased shear. Could the nuclei breeding mechanism be limited by the availability of sites for nuclei to attach to the surface? This is undoubtedly a speculation, but it may be possible that at high supersaturation the surface of the seed become saturated with nuclei inducing a rate limiting effect in which nuclei may be required to be dislodged before additional nuclei can join and use the surface for growth.

6. In Chapter. 5, a Couette cell was developed to induce laminar shear flow under well controlled experimental conditions to evaluate secondary nucleation on a seed held in a fixed location. Computational

fluid dynamic (CFD) tools should now be used to characterise the Couette cell and estimate the shear rate at the surface of the seed under different conditions such as rotational rates and seed sizes. The same CFD characterisation methodology should then be completed for the various ‘seed on a stick’ set-ups where simulations may be used to estimate shear rates at precise locations (close to and further away from the impeller). The shear rates from the more complex flow regimes (e.g., turbulence) experienced in stirred tanks can theoretically be replicated in the Couette cell and the secondary nucleation kinetics quantified providing the knowledge to make more informed decisions in scale-up.